



Ministry of Higher Education and
Scientific Research



University SAAD DAHLEB BLIDA 1

Institute of Aeronautics and Space Studies

Thesis for obtaining the Master's degree in Aeronautics

Option: Space propulsion

Theme:

**Numerical Simulation of Methane Turbulent Premixed
Combustion with Hydrogen Addition**

Proposed and supervised by:

Dr A. NECHE (IAES)

Dr R. ALLOUCHE (IAES)

Realized by:

OUARMIM Alaa Eddine

AMRATE Soheib

**COLLEGE YEAR
2022-2023**

Acknowledgements

We want to express our gratitude to the Almighty God for giving us the favor of finishing our studies.

We want to thank our promoters Mr. R. ALLOUCHE, and Mr. A. NECHE for their support, and for their help as we prepared for this work,

Special thanks to Mr. R. RENANE for all the guidance he provided during the preparation of this work,

Without forgetting, we would like to thank all of the AES instructors who contributed to our education and anyone else who helps to streamline operations at this institution.

Finally, we want to thank everyone in our family, our dear friends, and our coworkers.

ملخص

تبحث هذه المذكرة في آثار إضافة الهيدروجين على لهب الميثان / الهواء من خلال محاكاة عددية باستخدام ANSYS Fluent. تتضمن الدراسة مراجعة شاملة لعمليات الاحتراق، والنمذجة الرياضية لظواهر الاحتراق، ومحاكاة عددية لعملية الاحتراق. أظهرت نتائج المحاكاة أن إضافة الهيدروجين إلى لهب الميثان / الهواء يؤدي إلى تغييرات كبيرة في عملية الاحتراق، بما في ذلك زيادة درجة حرارة اللهب، وسرعة اللهب، ومعدل إطلاق الحرارة. تساهم نتائج هذه الدراسة في فهم عملية الاحتراق ولها آثار مهمة على تصميم أنظمة الاحتراق وتحسينها. يتضمن العمل المستقبلي التحقق التجريبي والمزيد من التحقيقات لآثار إضافة الهيدروجين على مخاليط الوقود المؤكسدة الأخرى.

Abstract

This dissertation investigates the effects of hydrogen addition on methane/air flames through a numerical simulation using ANSYS Fluent. The study involves a comprehensive review of combustion processes, mathematical modeling of combustion phenomena, and a numerical simulation of the combustion process. The simulation results showed that the addition of hydrogen to methane/air flames leads to significant changes in the combustion process, including an increase in flame temperature, flame speed, and heat release rate. The findings of this study contribute to the understanding of the combustion process and have important implications for the design and optimization of combustion systems. Future work involves experimental validation and further investigations of the effects of hydrogen addition on other fuel-oxidant mixtures.

Résumé

Cette mémoire étudie les effets de l'ajout d'hydrogène sur les flammes méthane/air à travers une simulation numérique utilisant ANSYS Fluent. L'étude comprend un examen complet des processus de combustion, une modélisation mathématique des phénomènes de combustion et une simulation numérique du processus de combustion. Les résultats de la simulation ont montré que l'ajout d'hydrogène aux flammes méthane/air entraîne des changements significatifs dans le processus de combustion, notamment une augmentation de la température de la flamme, de la vitesse de la flamme et du taux de dégagement de chaleur. Les résultats de cette étude contribuent à la compréhension du processus de combustion et ont des implications importantes pour la conception et l'optimisation des systèmes de combustion. Les travaux futurs impliquent une validation expérimentale et des investigations supplémentaires sur les effets de l'ajout d'hydrogène sur d'autres mélanges combustible-oxydant.

Summary

List of figures.....	7
List of tables.....	10
Symbols:	11
Problematic.....	13
GENERAL INTRODUCTION	1
1 CHAPTER 1: LITERATURE REVIEW	5
1.1 Combustion History:.....	6
1.2 Combustion fundamentals:	7
1.2.1 Combustion definition:.....	7
1.2.2 Chemical Kinetics:.....	9
1.2.3 Damköhler Number (Da):	12
1.2.4 Types of Combustion:	13
1.2.5 Flame Structures:	15
1.2.6 Flame Regime:.....	15
1.2.7 Oxidation and reduction:.....	17
1.3 Fuels:.....	18
1.3.1 Fuel properties:.....	19
1.4 Methane and hydrogen combustion:.....	20
1.5 Numerical methods for simulating combustion:	22
1.6 Previous studies on hydrogen addition to methane/air flames:	24
2 CHAPTER 2: MATHEMATICAL MODEL & METHODOLOGY	27
2.1 Problem Formulation and Assumptions:.....	28
2.2 Mathematical Model and Governing Equations:	29
2.3 Turbulence Modeling:	36
2.4 Numerical Methods and Software Used:	38
2.4.1 Computational Fluid Dynamics (CFD):	38
2.4.2 Software Used:.....	39
2.4.3 Numerical Methods:.....	39
3 CHAPTER 3: PROBLEM SET-UP AND SOLUTION.....	41
3.1 Introduction:.....	42
3.2 Combustion Chamber geometry:	43

3.3	Meshing:.....	46
3.3.1	Description of Meshing Parameters and their Selection Criteria:.....	47
3.3.2	Splited geomety:.....	49
3.3.3	mesh sensitivity study:.....	50
3.3.4	Solver configuration:.....	52
3.3.5	Periodic setup:.....	53
4	CHAPTER 4: RESULTS AND DISCUSSION	56
4.1	Introduction:.....	56
4.2	Kerosene/Air Flame Simulation Results:.....	56
4.2.1	Temperature contour:.....	56
4.2.2	Velocity contour:.....	61
4.2.3	Species variation:.....	62
4.3	Methane/Air Flame Simulation Results:.....	69
4.3.1	Effect of Preheat Temperature on Combustion Performance and Characteristics:.....	69
4.3.2	Effect of operating pressure on Combustion Performance and Characteristics:.....	73
4.4	Effects of Hydrogen Addition on Combustion:.....	82
4.4.1	Temperature Contours:.....	82
4.4.2	Velocity contour:.....	85
4.4.3	CO2 Masse Fraction contours:.....	87
4.5	Comparison and validation of results:.....	90
	CONCLUSION.....	94
	OUTLOOK.....	97
	APPENDIX.....	99
	REFERENCES:.....	119

List of figures

Figure 1.1 Combustion flames.....	8
Figure 1.2 Combustion Elements.....	8
Figure 1.3 Combustion stages in CI engine [19]	9
Figure 1.4 Concentration & temperature profile. (a) premixed, (b) diffusion flame [27].....	14
Figure 1.5 Diesel engine flame [28]	14
Figure 1.6 Flame structure phases [29]	15
Figure 1.7 Flame regime diagram by Borghi modified by Peter [27].	16
Figure 1.8 Different flame regimes and its characteristics [27]	17
Figure 1.9 Dependence of methane flame speed on temperature, pressure, and equivalence ratio under different combustion conditions [49].....	20
Figure 1.10 Effect of hydrogen addition on the flame speed of methane/air mixture [50].	21
Figure 3.1 Flowchart diagram of numerical modeling using ANSYS Fluent [64].....	42
Figure 3.2 Representation of combustion chamber geometry.....	44
Figure 3.3 Representation of combustion chamber geometry (2).....	44
Figure 3.4 splitted geometry.....	45
Figure 3.5 Boundary zones	45
Figure 3.6 boundary zones (2).....	46
Figure 3.7 Skewness and Orthogonal Quality mesh metrics spectrum [65].....	47
Figure 3.8 Meshed geometry	48
Figure 3.9 Skewness metrics for the generated mesh.....	48
Figure 3.10 Element quality metrics for the generated mesh.....	49
Figure 3.11 Meshed Splited geometry	49
Figure 3.12 Skewness metrics for the generated mesh	50
Figure 3.13 Element quality metrics for the generated mesh.....	50
Figure 3.14 Temperature Variation at Combustion Chamber Outlet for Different Mesh.....	51
Figure 3.15 Periodic setup	55
Figure 4.1 Longitudinal temperature contour for kerosene combustion at different regimes. A: 7% power, B: 30% power, C: 85% power and D: 100% power settings.	57
Figure 4.2 Longitudinal temperature variation chart for kerosene combustion at different regimes. A: 7% power, B: 30% power, C: 85% power and D: 100% power settings.	58
Figure 4.3 TIT contour for kerosene combustion at different regimes. A: 7% power, B: 30% power, C: 85% power and D: 100% power settings.....	59
Figure 4.4 TIT variation chart for kerosene combustion at different regimes. A: 7% power, B: 30% power, C: 85% power and D: 100% power settings.	60
Figure 4.5 Longitudinal velocity contour for kerosene combustion at different regimes. A: 7% power, B: 30% power, C: 85% power and D: 100% power settings.	61
Figure 4.6 Longitudinal velocity variation chart for kerosene combustion at different regimes. A: 7% power, B: 30% power, C: 85% power and D: 100% power settings.....	62
Figure 4.7 Longitudinal NO masse fraction contour for kerosene combustion at different regimes. A: 7% power, B: 30% power, C: 85% power and D: 100% power settings.....	63

Figure 4.8 Longitudinal NO masse fraction variation chart for kerosene combustion at different regimes. A: 7% power, B: 30% power, C: 85% power and D: 100% power settings.	64
Figure 4.9 Longitudinal Co ₂ masse fraction contour for kerosene combustion at different regimes. A: 7% power, B: 30% power, C: 85% power and D: 100% power settings.	65
Figure 4.10 Longitudinal Co ₂ masse fraction variation chart for kerosene combustion at different regimes. A: 7% power, B: 30% power, C: 85% power and D: 100% power settings.	66
Figure 4.11 Longitudinal Co masse fraction contour for kerosene combustion at different regimes. A: 7% power, B: 30% power, C: 85% power and D: 100% power settings.	67
Figure 4.12 Longitudinal Co masse fraction variation chart for kerosene combustion at different regimes. A: 7% power, B: 30% power, C: 85% power and D: 100% power settings.	68
Figure 4.13 Masse fraction variation for reactants at 85% power, POP= 1850144 Pa, T= 776.55 k for kerosene/air flame	69
Figure 4.14 Longitudinal temperature contour for methane combustion at 85% rpm with different initial Temperature (A) T= 300 k, (B) T= 350 k, (C) T= 400 k, (D) T= 450 k.....	70
Figure 4.15 variation of TIT (temperature inlet turbine) for methane combustion at 85% rpm with different initial Temperature (A) T= 300 k, (B) T= 350 k, (C) T= 400 k, (D) T= 450 k.....	71
Figure 4.16 Longitudinal velocity contour for methane combustion at 85% rpm with different initial Temperature (A) T= 300 k, (B) T= 350 k, (C) T= 400 k, (D) T= 450 k.....	73
Figure 4.17 Longitudinal temperature contour for methane combustion at 85% rpm with different initial operating pressure (A) P= 1 atm, (B) P= 3 atm, (C) P= 5 atm	75
Figure 4.18 Transversal contour of Temperature inlet turbine (TIT) variation at P= 3 atm for methane/air flame	76
Figure 4.19 TIT variation chart for methane combustion at 85% rpm with different initial operating pressure (A) P= 1 atm, (B) P= 3 atm, (C) P= 5 atm	76
Figure 4.20 Longitudinal velocity contour for methane combustion at 85% rpm with different initial operating pressure (A) P= 1 atm, (B) P= 3 atm, (C) P= 5 atm	78
Figure 4.21 Velocity Variation chart at Different Operating Pressures for methane/air flame	79
Figure 4.22 Mass fraction variation for different Species at POP= 1 atm, T= 300 k for methane/air flame	80
Figure 4.23 The Longitudinal contour of turbulence intensity at 1 atm Operating Pressure for methane/air flame	81
Figure 4.24 Longitudinal temperature contour for methane/hydrogen combustion at 85% rpm with 3 atm operating pressure (A) 0% H ₂ , (B) 5% H ₂ , (C) 25% H ₂	83
Figure 4.25 TIT contour for methane/hydrogen combustion at 85% rpm with 3 atm operating pressure (A) 0% H ₂ , (B) 5% H ₂ , (C) 25% H ₂	84
Figure 4.26 TIT variation chart for methane/hydrogen combustion at 85% rpm with 3 atm operating pressure (A) 0% H ₂ , (B) 5% H ₂ , (C) 25% H ₂	85
Figure 4.27 Longitudinal Velocity contour for methane/hydrogen combustion at 85% rpm with 3 atm initial operating pressure (A) 0% H ₂ , (B) 5% H ₂ , (C) 25% H ₂	86
Figure 4.28 Longitudinal Velocity variation chart for methane/hydrogen combustion at 85% rpm with 3 atm initial operating pressure (A) 0% H ₂ , (B) 5% H ₂ , (C) 25% H ₂	87
Figure 4.29 Longitudinal co ₂ masse fraction contour for methane/hydrogen combustion at 85% rpm with 3 atm initial operating pressure (A) 0% H ₂ , (B) 5% H ₂ , (C) 25% H ₂	88

Figure 4.30 Co ₂ masse fraction variation chart for methane/hydrogen combustion at 85% rpm with 3 atm initial operating pressure (A) 0% H ₂ , (B) 5% H ₂ , (C) 25% H ₂	89
Figure 4.31 Maximum temperature variation at different power settings	90
Figure 4.32 Maximum velocity variation at different power settings	91
Figure 4.33 Maximum Species masse fraction variation at different power settings	92
Figure A.1 Conversion process.....	103
Figure A.2 Converted Chemkin files	104
Figure A.3 Creating New Project.....	104
Figure A.4 Diagram view and set-up.....	105
Figure A.5 Pre-Processing data entry	106
Figure A.6 PSR configuration	106
Figure A.7 Species data entry.....	107
Figure A.8 Ansys Reaction Workbench selection	107
Figure A.9 Choosing Start Mechanism Reduction.....	107
Figure A.10 Chemkin project entry.....	108
Figure A.11 Defining tolerances	109
Figure A.12 Selecting conditions	109
Figure A.13 Running reduction	110
Figure A.14 Resulted reduced mechanism	110
Figure B.1 Residuals-100% power settings	111
Figure B.2 Residuals – 5 % H ₂	111
Figure B.3 Residuals – 35 % H ₂	112
Figure C.1 Longitudinal density contour for kerosene combustion at different regimes. A: 7% power, B: 30% power, C: 85% power and D: 100% power settings.	113
Figure C.2 Longitudinal N ₂ masse fraction contour for kerosene combustion at different regimes. A: 7% power, B: 30% power, C: 85% power and D: 100% power settings.....	114
Figure C.3 Longitudinal C ₁₂ H ₂₃ masse fraction contour for kerosene combustion at different regimes. A: 7% power, B: 30% power, C: 85% power and D: 100% power settings.	115
Figure D.1 Chemkin import step 1	116
Figure D.2 Chemkin import step 2.....	116
Figure D.3 Patch step 1	117
Figure D.4 Patch step 2	117
Figure D.5 Patch step 3	118
Figure D.6 Patch step 4	118

List of tables

Table 1.1 Fuels properties.....	19
Table 1.2 Advantages and disadvantages of different numerical methods	23
Table 3.1 Different meshes	51
Table 4.1 The Preheat temperatures effects on maximum temperatures for methane/air combustion	70
Table 4.2 variations in velocity resulting from changes in the preheat temperature of methane/air flames	72
Table 4.3 the effect of operating pressure on the maximum temperature for methane/air flames	74
Table 4.4 the maximum velocity values obtained for methane/air flames at different operating pressures	77
Table A.1 Flow variables for 7% engine power setting, operating pressure 357171 Pa and inlet temperature 492.6 K.....	100
Table A.2 Flow variables for 30% engine power setting, operating pressure 852447 Pa and inlet temperature 635.36 K.....	100
Table A.3 Flow variables for 85% engine power setting, operating pressure 1850144 Pa and inlet temperature 776.55 K.....	100
Table A.4 Flow variables for 100% engine power setting, operating pressure 1943008 Pa and inlet temperature 784.39K.....	101
Table A.5 Flow variables for Preheat temperature effect study, the operating pressure 101325 Pa and four different preheat temperatures are considered: 300 K, 350 K, 400 K, and 450 K.....	101
Table A.6 Flow variables for operating pressure effect study, the inlet temperature 300 K and three different operating pressure are considered: 1 atm,3 atm, 5 atm.....	102
Table A.7 Flow variables for methane/air/hydrogen study, the inlet temperature 300 K and the operating pressure is 3 atm.....	102
Table A.8 CH ₄ , H ₂ masse fractions variation for different hydrogen percentages.....	102

Symbols:

A: the pre-exponential factor;

B: model constant;

$C_{1\varepsilon}$, $C_{2\varepsilon}$, $C_{3\varepsilon}$: constants;

C_{D1} , C_{D2} : model constants;

Da: the Damköhler number;

C_p : the specific heat at constant pressure;

D_f : the diffusivity of the mixture fraction;

D_i : the diffusivity of species i;

D_k : the diffusion coefficient of species k;

D_ξ : the diffusivity of the progress variable;

Ea: the activation energy;

e: the specific internal energy;

f: the mixture fraction;

Gk: the turbulent kinetic energy generation term;

Gb: the generation of turbulence kinetic energy due to buoyancy;

γ_λ : intermittency factor;

g: the gravitational acceleration vector;

H: the enthalpy of the reaction;

h: the enthalpy per unit mass;

I: the identity tensor;

J_j : the diffusion flux of species j;

k: the rate constant;

K: the thermal conductivity;

Ka: the Karlovitz number;

L: the characteristic length scale;

μ : the molecular viscosity of the fluid;

μ_t : the turbulent viscosity coefficient;

μ_t : the eddy viscosity;

ν_i : the stoichiometric coefficient of species i in the chemical reaction;

ν_i^0 : the initial stoichiometric coefficient of species i;

p: the pressure;

P_k : the production of turbulence kinetic energy due to mean velocity gradients;

POP: Operation Pressure;

q: the heat flux vector;

Q: the heat release rate per unit volume;

r : stoichiometric oxygen requirement of the reaction;
 R : the gas constant;
 R_i : the rate of formation or consumption of species i ;
 R_k : the source term for species k due to chemical reactions;
 S : the modulus of the mean rate-of-strain-tensor;
 S_{ij} : is the symmetric part of the velocity gradient tensor.
 S_ε : any additional source or sink term for turbulent dissipation rate;
 S_h : heat of chemical reactions and other source-defined heat sources;
 S_k : user-defined source term;
 Sc_t : turbulent Schmidt number;
 σ_k : the turbulent Prandtl number for k ;
 T : the temperature;
 TIT : Turbine Inlet Temperature;
 $\tau_{EDM,k}$: characteristic time for turbulent mixing;
 $\tau_{kin,k}$: characteristic time for the chemical reaction;
 t : time;
 $t_{1/2}$: the half-life of the reaction;
 u : the velocity vector;
 V_{Dj} : the diffusion velocity of species j ;
 W_i : the mass reaction rate of species i ;
 x_i : the position in the i -direction;
 Y : the mass fraction of the fuel species;
 Y_i : the mass fraction of species i ;
 Y_i^0 : the initial mass fraction of species i ;
 Y_k : the mass fraction of species k ;
 \tilde{Y}_{fuel} : mean mass fraction of fuel;
 Y_M : contribution of fluctuating dilatation in compressible turbulence to the overall dissipation rate;
 Y_k^* : fine-structure state of species k ;
 Y_k^0 : surrounding state of species k ;
 \tilde{Y}_k : mass fraction of species k as cell average;
 ∇ : the gradient operator;
 Π : the viscous dissipation term;
 \square : the Temperature exponent;
 ξ : the progress variable;
 ε : the turbulent dissipation rate;
 $\overline{\Omega}_y$: is the mean rate-of-rotation tensor;
 ρ : the density;
 τ : the stress tensor;

Problematic

The combustion of fossil fuels, such as kerosene, in various applications, including gas turbines and internal combustion engines, has been a significant source of energy for decades. However, with increasing concerns about environmental pollution and the need to reduce greenhouse gas emissions, there is a growing demand to explore cleaner and more efficient alternatives to traditional fossil fuel combustion.

One promising alternative is the utilization of methane as a fuel source in combination with hydrogen supplementation. Methane, the primary component of natural gas, offers several advantages such as abundant availability and lower carbon content compared to kerosene. Additionally, hydrogen, known for its high reactivity and low pollutant emissions, can enhance the combustion process and promote cleaner energy conversion.

The objective of this research is to investigate the feasibility of replacing kerosene/air combustion with methane/air combustion, supplemented with varying percentages of hydrogen. By studying the combustion characteristics, including temperature profiles, velocity distribution, and species mass fractions, we aim to assess the performance, efficiency, and environmental impact of these alternative fuel compositions.

GENERAL INTRODUCTION

The increasing demand for sustainable and clean energy sources has led to a renewed interest in hydrogen as a fuel for various applications, including power generation, transportation, and aerospace industries [1]. Hydrogen has the highest energy content per unit mass of any fuel and produces only water vapor as a byproduct, making it a clean and environmentally friendly alternative to traditional fossil fuels. However, the widespread use of hydrogen as a fuel is currently limited by various technical and economic challenges, including storage, distribution, and combustion issues [2, 3].

In the aerospace industry, the combustion of hydrocarbon fuels such as kerosene is a major contributor to greenhouse gas emissions and air pollution [4]. Therefore, there is a growing interest in exploring alternative fuel options, such as methane, which can potentially reduce emissions and improve combustion efficiency [5]. Methane is a low-cost and abundant fuel, and its combustion produces less carbon dioxide and nitrogen oxide emissions compared to kerosene [6].

However, the use of methane as a fuel also has some challenges, including its lower energy density and its tendency to produce soot during combustion [7]. To address these challenges, the addition of hydrogen to methane/air flames has been proposed as a potential solution to enhance combustion efficiency and reduce emissions [8].

Therefore, the aim of this study is to investigate the effect of hydrogen addition on methane/air flames using numerical simulations. The study will focus on a 3D turbojet combustion chamber and will use ANSYS Fluent solver to simulate the combustion process. The results of this study can provide valuable insights into the optimization of hydrogen-enriched methane combustion, which can contribute to the development of more sustainable and efficient aerospace propulsion systems.

The primary goal of this study is to investigate the effect of hydrogen addition on methane/air combustion in a 3D turbojet combustion chamber. To achieve this goal, the following specific objectives have been identified:

- Simulate the combustion of kerosene/air flames using the ANSYS Fluent solver with a detailed chemical mechanism and compare the results with a previous study [9].
- Simulate the combustion of methane/air flames using the ANSYS Fluent solver with a general chemical mechanism and compare the results with the kerosene/air flame simulations.
- Investigate the effect of hydrogen addition on the combustion characteristics of methane/air flames by adding hydrogen at different rates.
- Evaluate the performance of the hydrogen-enriched methane combustion in terms of combustion efficiency, and emissions.

This study aims to answer the following research questions:

- How does the combustion of methane/air flames compare with kerosene/air flames in a 3D turbojet combustion chamber?
- What is the effect of hydrogen addition on the combustion characteristics of methane/air flames?
- How does the combustion efficiency, and emissions of hydrogen-enriched methane combustion compare with that of pure methane combustion?

The answers to these research questions will provide insights into the feasibility of using hydrogen-enriched methane combustion as a replacement for kerosene combustion, and the potential benefits of hydrogen addition for enhancing the combustion efficiency and reducing emissions.

This thesis is organized into four chapters;

- Chapter 1 contains the literature review on the combustion characteristics of methane/air flames, the effect of hydrogen addition on combustion, and numerical simulation techniques for turbulent combustion.
- Chapter 2 describes the methodology and mathematical models used for the numerical simulations, including the computational domain and boundary conditions, the chemical mechanism, and the turbulence model.
- Chapter 3, describes the setup and solution of computational fluid dynamics simulation that models combustion in the combustion chamber of a model aircraft engine.
- Chapter 4 presents the simulation results of kerosene, methane, and hydrogen-enriched methane combustion, including the effect of hydrogen addition on the combustion characteristics, such as temperature distribution, species concentrations, and reaction rates. The performance of hydrogen-enriched methane combustion will also be evaluated in various terms.
- Finally, the conclusion provides a summary of the main findings of this study and their implications for the use of hydrogen-enriched methane combustion as a replacement for kerosene combustion in a 3D turbojet combustion chamber. The limitations of the study and recommendations for future research will also be discussed.

The organization of this thesis aims to provide a clear and logical presentation of the research methodology, results, and conclusions. The chapter-by-chapter structure also facilitates easy navigation of the thesis for readers interested in specific aspects of the research.

CHAPTER 1
LITERATURE
REVIEW

1.1 Combustion History:

Combustion of gaseous fuels has been a topic of interest for several decades due to their widespread applications in various industries, including power generation, transportation, and aerospace. The combustion process involves a complex interplay between chemical reactions and fluid mechanics, which is still not completely understood. Over the years, researchers have developed several models and simulations to better understand the combustion process and improve its efficiency.

Historically, the study of combustion can be traced back to the 17th century when Robert Boyle and Robert Hooke conducted experiments on combustion and the properties of gases. Later in the 18th century, Antoine Lavoisier proposed the concept of oxidation, which laid the foundation for the modern understanding of combustion [10].

In the 19th century, the development of the internal combustion engine and the emergence of gas lighting and heating systems led to an increased interest in the combustion of gaseous fuels [11]. In the early 20th century, Fritz Haber and Carl Bosch developed the Haber-Bosch process for the production of ammonia from hydrogen and nitrogen gas, which is still widely used today [12].

With the advent of computational fluid dynamics (CFD) in the latter half of the 20th century, researchers were able to develop more sophisticated models for simulating the combustion process. These models include zero-dimensional (0-D) models, which assume a well-mixed reactor with uniform composition, and one-dimensional (1-D) models, which include axial variations in composition and flow [13]. However, these models are limited in their ability to capture the complex fluid dynamics and chemical reactions that occur in turbulent combustion.

To overcome these limitations, researchers have developed more advanced models such as large eddy simulation (LES) and direct numerical simulation (DNS) [14]. These models require significant computational resources and are not yet widely used in industrial applications.

Finally, the study of combustion has a rich history and continues to be an active area of research. Advances in modeling and simulation techniques have improved our understanding of the combustion process and have led to the development of more efficient and environmentally friendly combustion systems.

1.2 Combustion fundamentals:

1.2.1 Combustion definition:

Combustion, also known as burning, is a chemical process that occurs when a fuel substance reacts with an oxidizing agent, typically oxygen, resulting in the production of heat, light, and various byproducts [15]. The process involves breaking the chemical bonds in the fuel molecules, releasing energy that is then used to break the bonds in the oxygen molecules, leading to the formation of new molecules, such as carbon dioxide, water vapor, and various other combustion byproducts, depending on the specific fuel and oxidizer involved [16].



Figure 1.1 Combustion flames

The three key elements of combustion are fuel, oxidizer, and heat [17]. The fuel is the material that reacts with the oxidizer to produce energy. The oxidizer provides the oxygen that is needed for the combustion reaction to occur, and heat is required to initiate and sustain the reaction, which can come from an external source or can be generated by the combustion itself [18].

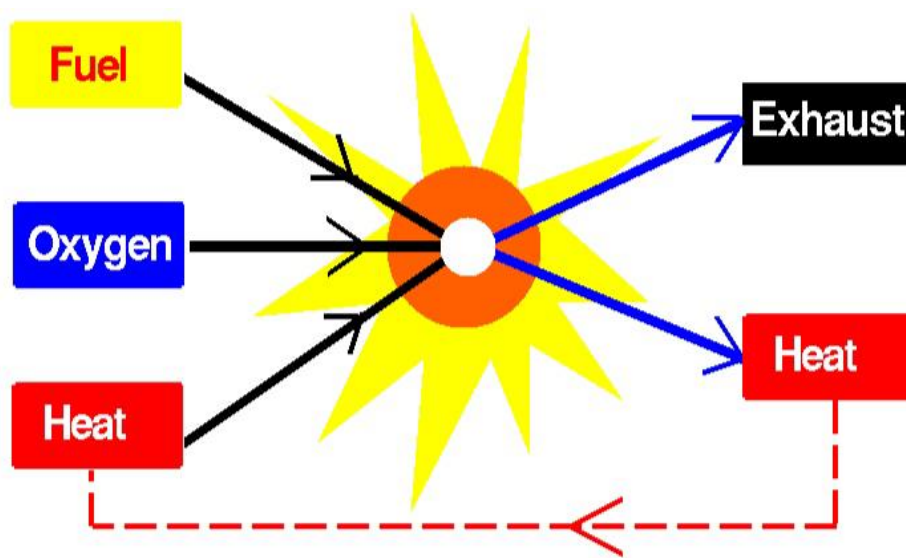


Figure 1.2 Combustion Elements [69]

The combustion process can be divided into three stages: ignition, flame propagation, and combustion completion [16]. During ignition, the heat energy initiates the reaction between the fuel and the oxidizer, forming a flame that propagates through the mixture, leading to the release of energy. The combustion completion stage occurs when the fuel is completely consumed, and the reaction stops [17].

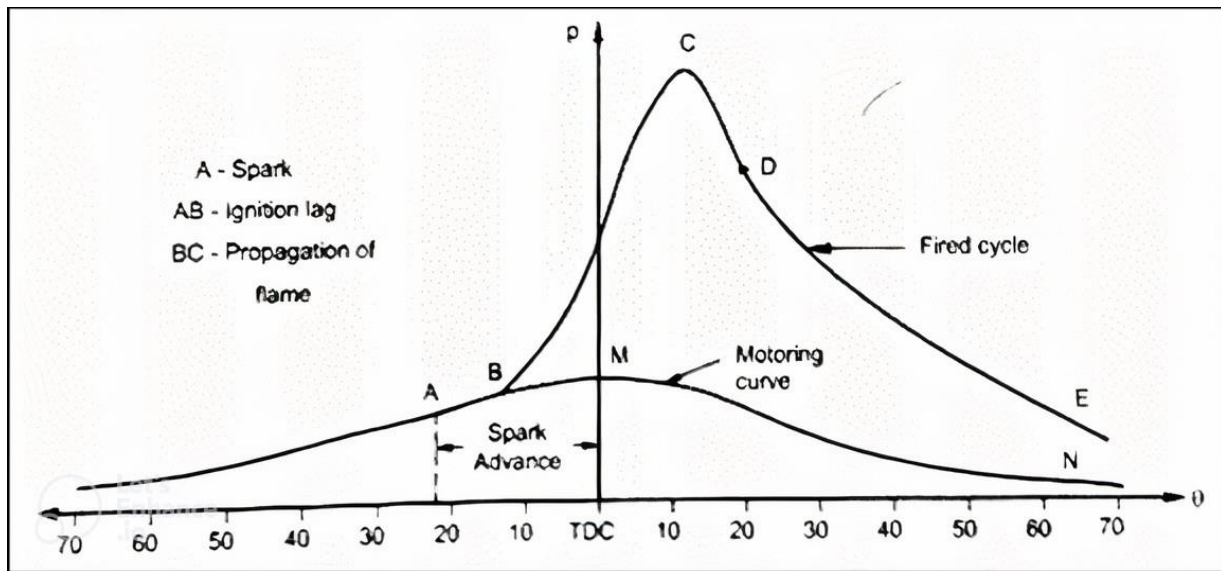


Figure 1.3 Combustion stages in CI engine [19]

The efficiency and rate of combustion depend on various factors, including the type of fuel and oxidizer, the amount of oxygen available, the temperature and pressure of the environment, and the stoichiometric ratio of fuel and oxidizer [16]. The stoichiometric ratio is the ideal proportion of fuel and oxidizer required for complete combustion to occur [17]. Combustion can occur in various forms, including rapid combustion, slow combustion, and spontaneous combustion [20].

1.2.2 Chemical Kinetics:

Chemical kinetics is the study of chemical reactions and their rates. The rate of these reactions depends on various factors, such as temperature, pressure, and reactant

concentrations. The reaction rate is typically modeled using reaction mechanisms, which describe the elementary steps involved in the reaction.

The rate of a chemical reaction is defined as the change in concentration of a reactant or product per unit time, and is typically expressed in units of moles per liter per second (mol/L/s). The rate of a reaction can be influenced by several factors, including the concentrations of reactants and products, temperature, pressure, and the presence of a catalyst [21].

The rate of a chemical reaction can be determined experimentally by measuring changes in the concentrations of reactants and products over time. The rate law for a reaction is an equation that relates the rate of the reaction to the concentrations of the reactants. The general form of a rate law is:

$$\mathbf{Rate} = k [\mathbf{A}]^m [\mathbf{B}]^n \quad 1.1$$

- Where **Rate** is the rate of the reaction, **k** is the rate constant (which depends on the temperature and the presence of a catalyst), **[A]** and **[B]** are the concentrations of the reactants, and **m** and **n** are the reaction orders with respect to A and B, respectively [22].

The rate constant is a proportionality constant that relates the rate of the reaction to the concentrations of the reactants. It can be determined experimentally by measuring the rate of the reaction at different concentrations of the reactants and then using the data to calculate the rate constant.

The reaction order with respect to a particular reactant is the power to which its concentration is raised in the rate law. For example, if the rate law is:

$$\text{Rate} = k [A]^2[B]^3$$

➤ Then the reaction is second order with respect to A and third order with respect to B.

In addition to the rate law, chemical kinetics also involves the investigation of reaction mechanisms, which are the series of individual chemical steps that lead to the overall reaction. The rate-determining step is the slowest step in the mechanism and determines the overall rate of the reaction [23].

➤ Some other important equations related to chemical kinetics include:

- **The Arrhenius equation, which relates the rate constant to temperature [24]:**

$$k = AT^\beta e^{(-Ea/RT)} \quad 1.2$$

- **The rate expression for a first-order reaction [25]:**

$$\text{Rate} = k [A] \quad 1.3$$

- **The half-life equation for a first-order reaction:**

$$t_{(1/2)} = \frac{\ln(2)}{k} \quad 1.4$$

- The rate expression for a second-order reaction:

$$Rate = k [A]^2 \quad 1.5$$

- Integrated rate law for a second-order reaction:

$$\frac{1}{[A]_t} = kt + \frac{1}{[A]_0} \quad 1.6$$

➤ where:

- A is the pre-exponential factor;
- β is Temperature exponent. It describes the dependence of the rate constant on temperature.
- Ea is the activation energy;
- $t_{(1/2)}$ is the half-life of the reaction;
- $[A]_t$ is the concentration of A at time t;
- $[A]_0$ is the initial concentration of A.

1.2.3 Damköhler Number (Da):

The Damköhler numbers (Da) are dimensionless numbers used in chemical engineering to relate the chemical reaction timescale (reaction rate) to the transport phenomena rate occurring in a system. It is named after German chemist Gerhard Damköhler. The Karlovitz number (Ka) is related to the Damköhler number by [26]:

$$Da = 1/Ka \quad 1.7$$

In its most commonly used form, the Damköhler number relates the reaction timescale to the convection time scale, volumetric flow rate, through the reactor for continuous (plug flow or stirred tank) or semibatch chemical processes:

$$Da = \frac{\textit{reaction rate}}{\textit{convective mass transport rate}} \quad 1.8$$

The value of Da provides a quick estimate of the degree of conversion that can be achieved. As a rule of thumb, when Da is less than 0.1 a conversion of less than 10% is achieved, and when Da is greater than 10 a conversion of more than 90% is expected.

1.2.4 Types of Combustion:

There are three types of combustion: diffusion flames, premixed flames, and partially premixed flames.

- a. **Diffusion flames:** Diffusion flames (non-premixed flames) occur when fuel and oxidant are mixed in the combustion chamber, leading to a flame front that propagates through the mixture. Examples of diffusion flames are: Bunsen burners, torches, and candle flames.

- b. **Premixed flames:** Premixed flames occur when the fuel and oxidant are mixed prior to entering the combustion chamber, resulting in a pre-existing flame front that propagates through the mixture. Examples of premixed flames are: Gasoline engine, Gas turbine engine, Gas grill flame, and Blowtorch flame.

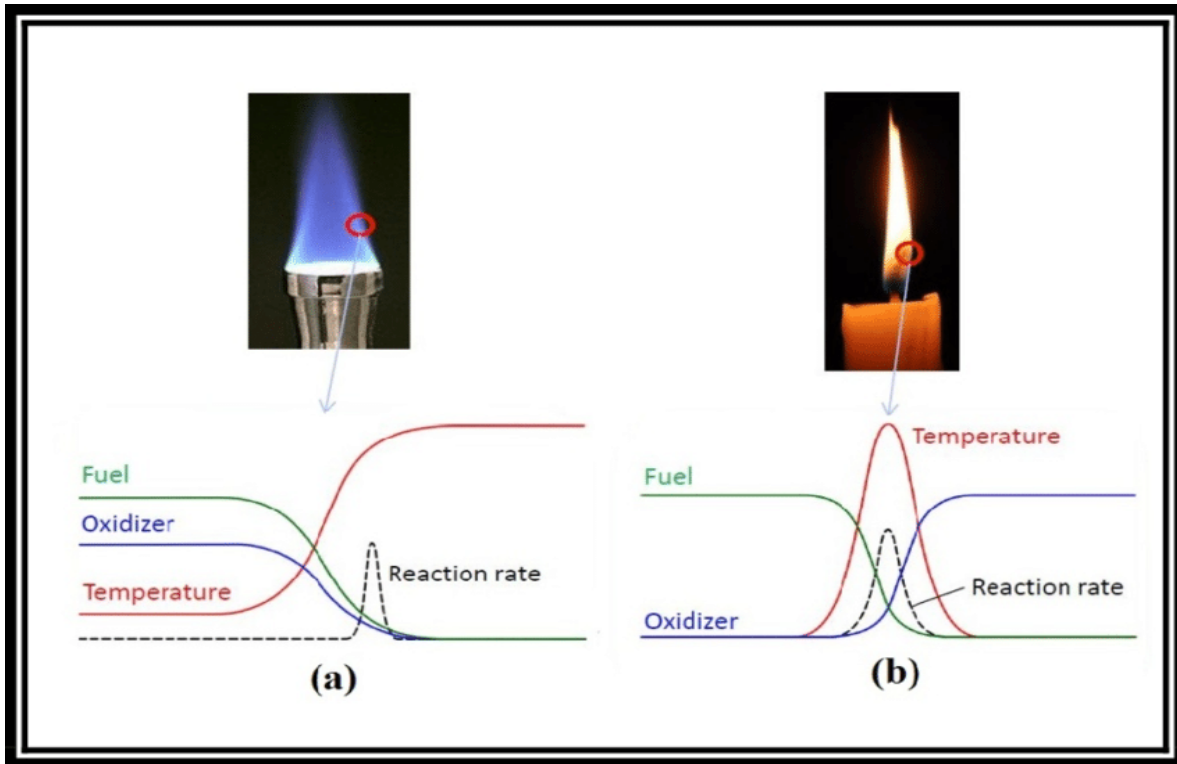


Figure 1.4 Concentration & temperature profile. (a) premixed, (b) diffusion flame [27].

- c. **Partially premixed flames:** Partially premixed flames occur when there is a combination of premixed and diffusion combustion, resulting in a flame front that is partially premixed and partially diffusive. Examples of partially premixed flames are: Diesel engine and industrial burners.



Figure 1.5 Diesel engine flame [28]

1.2.5 Flame Structures:

Flame structure refers to the spatial distribution of temperature, species concentration, and velocity within a flame. The flame structure depends on the type of combustion and the characteristics of the fuel and oxidant. In general, the flame structure consists of a reaction zone where the fuel and oxidant react, a preheat zone where the reactants are heated to their ignition temperature, and a post-flame zone where the reaction products are cooled.

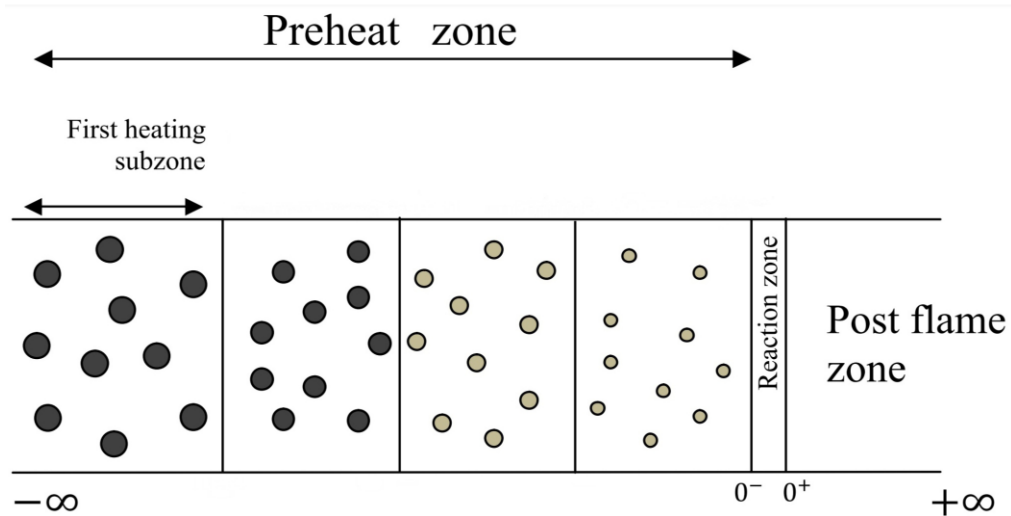


Figure 1.6 Flame structure phases [29]

1.2.6 Flame Regime:

Flame regime refers to the characteristic behavior and structure of a turbulent premixed flame under specific conditions. It describes the overall appearance, stability, and interaction of the flame with the surrounding flow and affects important flame properties such as flame speed, flame shape, and flame stabilization mechanisms.

The flame regime is typically determined by several factors, including the flow conditions, fuel-air mixture, turbulence intensity, and the geometry of the combustion system. These factors influence the interaction between turbulence and combustion, leading to different flame structures and behaviors.

Different flame regimes can be identified based on experimental observations, numerical simulations, or theoretical analyses. Some commonly recognized flame regimes include laminar flames, cellular flames, turbulent flames with wrinkled structures, and flamelet regimes. Each regime exhibits distinct characteristics, such as flame shape, propagation speed, flame stability, and the presence of turbulence-generated eddies or flame surface wrinkling.

The most popular classifications of turbulent flames are proposed by Borghi which is known as flame regime diagram. This diagram (figure 8) was modified by Peter. The diagram is characterized by dimensionless parameters (Re_T , Da , Ka), turbulent parameters (u' , L_T) and flame parameters (s_L , δ_L). This diagram also assumed that the mass diffusivity and the thermal diffusivity is equal. Therefore, the Schmidt number is unity. Figure 8 shows a pictorial representation of different flame regimes [27].

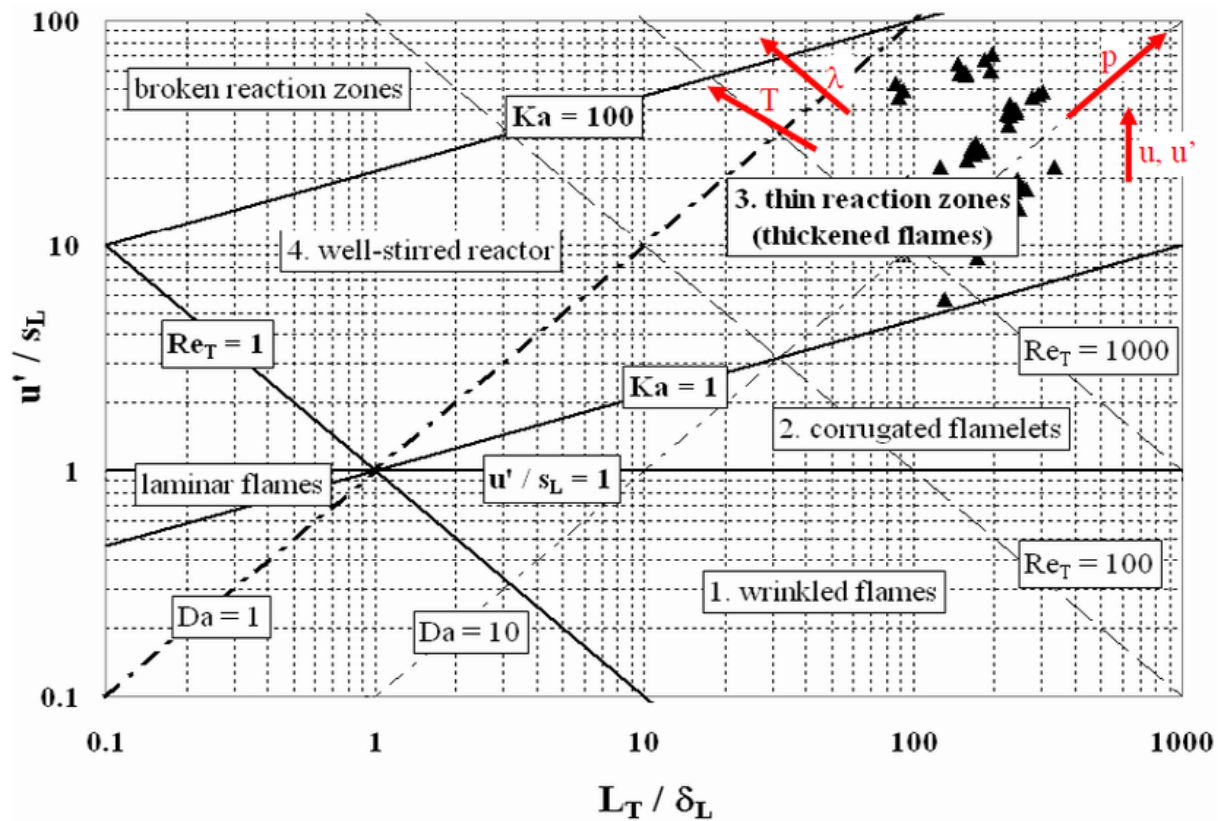


Figure 1.7 Flame regime diagram by Borghi modified by Peter [27].




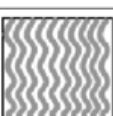
flame regime	Re_T	Da	Ka	u'/s_L	δ_L/η	graphical illustration of the flame front
wrinkled flame	> 1	> 1	< 1	< 1	< 1	
corrugated flame	> 1	> 1	< 1	> 1	< 1	
thickened flame (thin reaction zones)	$\gg 1$	≥ 1	> 1	$\gg 1$	> 1	
distributed flame (well-stirred reactor)	> 1	< 1	> 1	> 1	> 1	

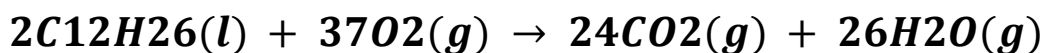
Figure 1.8 Different flame regimes and its characteristics [27]

1.2.7 Oxidation and reduction:

The chemical reactions involved in combustion include oxidation and reduction reactions. In an oxidation reaction, oxygen combines with a substance to produce energy and waste products. In a reduction reaction, a substance gains electrons and becomes reduced, while another substance loses electrons and becomes oxidized. These reactions are fundamental to the process of combustion and are essential to understanding how fuel and oxidant interact in a combustion chamber.

Redox reactions, also known as oxidation-reduction reactions, are chemical reactions in which there is a transfer of electrons between the reactants. In a redox reaction, one substance is oxidized, which means it loses electrons, and another substance is reduced, which means it gains electrons.

- For example, we consider the reaction between kerosene ($C_{12}H_{26}$) and oxygen (O_2) [30]:



In this reaction, kerosene is oxidized, while oxygen is reduced. The carbon atoms in kerosene go from a -26 oxidation state to a +4 oxidation state in carbon dioxide (CO₂), while the oxygen atoms in O₂ go from a 0 oxidation state to a -2 oxidation state in water (H₂O).

1.3 Fuels:

Fuels can be classified into different types based on their origin and properties. The three main types of fuels are fossil fuels, biofuels, and hydrogen fuel.

- **Fossil fuels:** Fossil fuels are derived from organic matter that has been buried under the earth's surface for millions of years. They include coal, oil, and natural gas. These fuels have high energy density, making them a popular choice for powering vehicles, machines, and power plants. However, they also have significant environmental impacts, such as air pollution and greenhouse gas emissions.
- **Biofuels:** Biofuels are derived from renewable organic sources, such as plants and animals. They include ethanol, biodiesel, and biogas. These fuels have lower energy density compared to fossil fuels, but they are renewable and have lower greenhouse gas emissions. However, the production of biofuels can also have significant environmental impacts, such as deforestation and the use of pesticides.
- **Hydrogen fuel:** Hydrogen fuel is produced by splitting water molecules into hydrogen and oxygen using an electrolysis process. It has high energy density and zero greenhouse gas emissions when used in fuel cells. However, the production of hydrogen fuel can still have environmental impacts, depending on the source of electricity used for the electrolysis process.

Fuels can also be found in several matter states, so we find solid, liquid, and gaseous fuels;

1.3.1 Fuel properties:

The properties of fuels are important to understand in order to design efficient and effective combustion systems. For example, the ignition temperature, heat of combustion, and volatility can affect the efficiency of combustion and the formation of pollutants. Here are some key properties of hydrogen, methane, and kerosene at ambient conditions:

Table 1.1 Fuels properties

Fuel	Hydrogen	Methane	kerosene
Chemical Formula	H ₂	CH ₄	C ₁₂ H ₂₃ - C ₁₅ H ₂₇ [37]
Molecular Weight	2.016 g/mol [31]	16.04 g/mol [35]	170 - 215 g/mol [38]
Boiling Point	-252.87 °C [31]	-161.5 °C [35]	175-325°C [39]
Melting Point	-259.16 °C [31]	-182.5 °C [35]	-26 to -48°C [39]
Density	0.0899 g/L [31]	0.717 kg/m ³ [40]	0.78-0.85 g/cm ³ [40]
Solubility	1.9 mg/L [32]	28.7 mg/L [35]	Insoluble [41]
Heat Of Combustion	141.8 kJ/mol [33]	890.4 kJ/mol [36]	43.1 MJ/kg [42]
Heat Of Formation	0 kJ/mol [33]	-74.9 kJ/mol [35]	-385.76 kJ/mol [43]
Heat Of vaporization	0.449 kJ/mol [33]	8.18 kJ/mol [35]	42.7 kJ/mol [44]
Specific Heat Capacity	28.8 J/(mol·K) [33]	P=cte: [35] 35.7 J/(mol·K) V=cte: [35] 20.7 J/(mol·K)	2.01 kJ/(kg·K) [45]
Thermal Conductivity	0.1805 W/(m·K) [33]	0.0314 W/(m·K) [36]	0.15 W/(m·K) [45]
Auto-ignition temperature	584.85 °C [47]	540 °C [48]	210 °C [39]

1.4 Methane and hydrogen combustion:

Methane and hydrogen are two commonly studied fuels due to their special properties. The combustion of methane and hydrogen produces carbon dioxide and water vapor as the primary byproducts, making them attractive options for reducing greenhouse gas emissions.

Studies have shown that methane flames can have different types of flame structures, including laminar and turbulent flames. Laminar flames are characterized by smooth flame fronts with low flame speeds, while turbulent flames have a wrinkled flame front and higher flame speeds. The propagation of methane flames is influenced by several factors, including the fuel-air mixture, temperature, pressure, and flow rate.

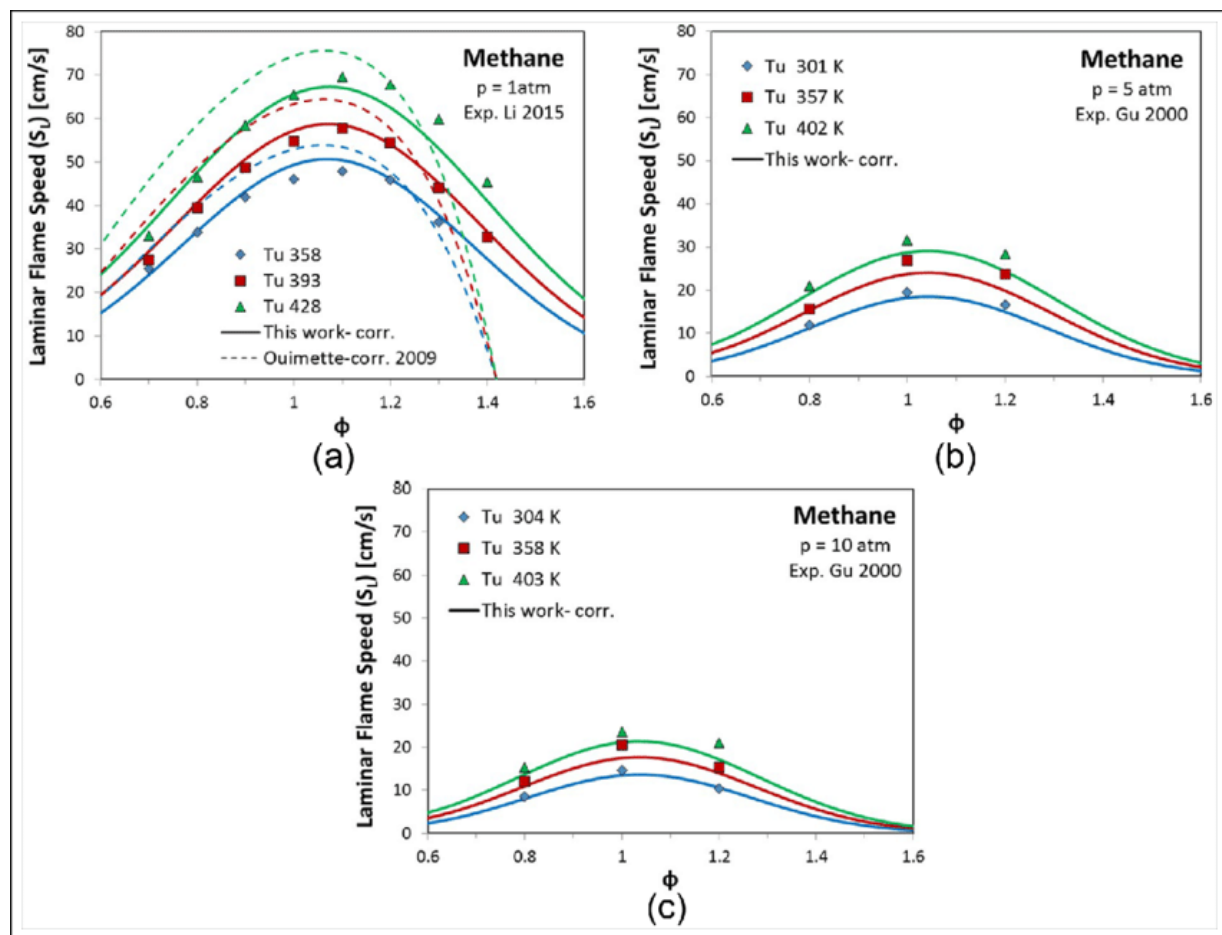


Figure 1.9 Dependence of methane flame speed on temperature, pressure, and equivalence ratio under different combustion conditions [49].

The addition of hydrogen to methane/air flames has been studied as a potential method for improving the combustion efficiency and reducing emissions. Studies have shown that adding hydrogen to methane/air flames can change the flame structure and propagation characteristics. The addition of hydrogen can increase the flame speed, widen the flammability range, and reduce the lean flammability limit. The combustion efficiency of the mixture can also be improved by adding hydrogen, as hydrogen has a higher combustion efficiency compared to methane.

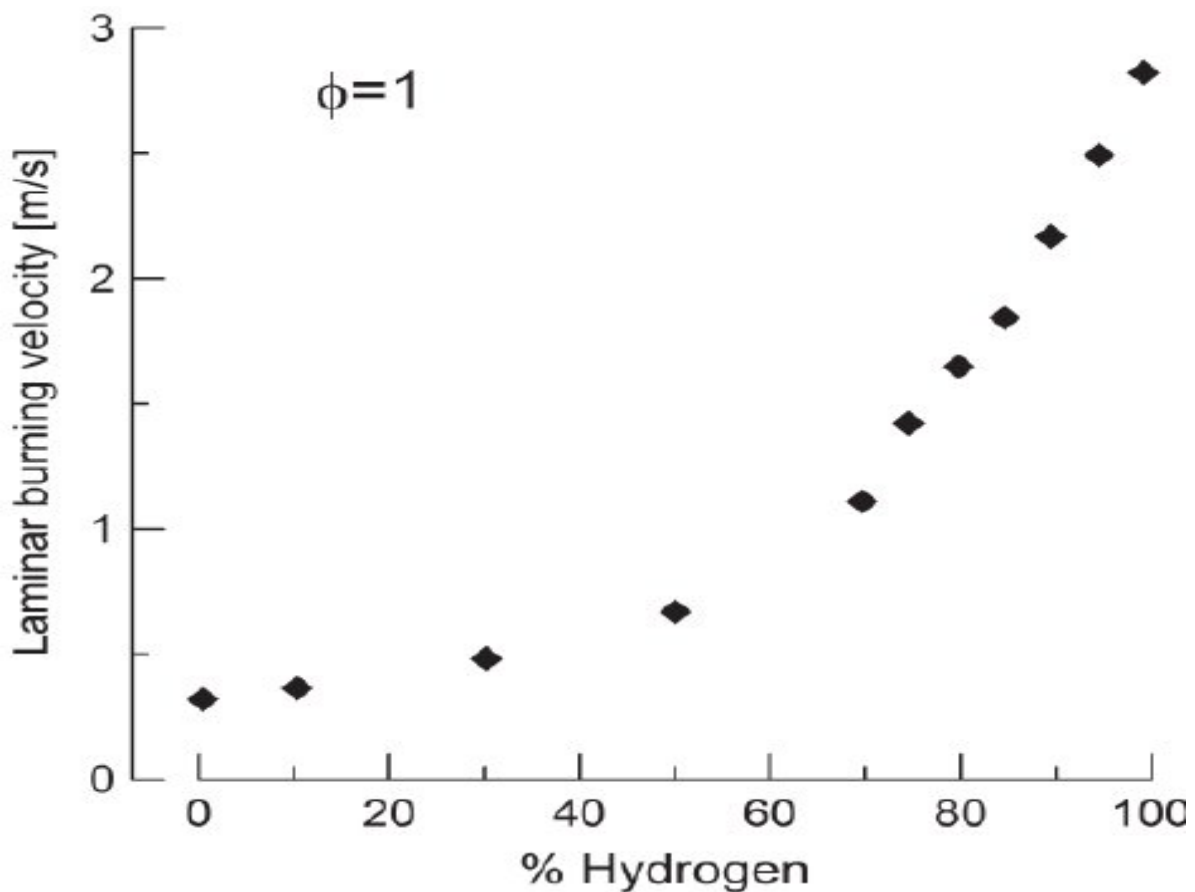
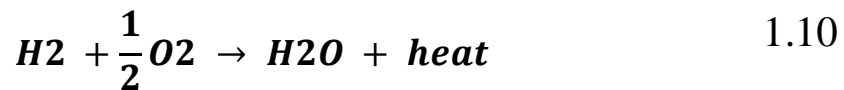


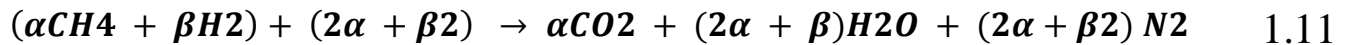
Figure 1.10 Effect of hydrogen addition on the flame speed of methane/air mixture [50].

- **Combustion Chemistry of Methane and Hydrogen:**

The combustion of methane and hydrogen involves the reaction of the fuel with oxygen (O₂) in the presence of heat to produce carbon dioxide (CO₂), water (H₂O), and heat. The combustion reaction can be represented by the following equations [51, 52]:



The general Methane/Hydrogen combustion equation is written as [53]:



The combustion of methane and hydrogen is an exothermic reaction, which means that it releases energy in the form of heat. The amount of heat released during combustion is proportional to the amount of fuel burned, and can be calculated using the heat of combustion equation [54];

$$\Delta H_{\text{combustion}} = \sum n \Delta H_{f(\text{products})} - \sum m \Delta H_{f(\text{reactants})} \quad 1.12$$

1.5 Numerical methods for simulating combustion:

Numerical simulations have become an important tool for investigating combustion processes, as they are cost-effective and more time-efficient, and are required to solve the governing equations that describe the combustion process, such as the conservation of mass, momentum, energy, and species, and the most commonly used numerical methods for combustion simulations are the finite volume method (FVM), finite element method

(FEM), and finite difference method (FDM), each with its own advantages and disadvantages.

Table 1.2 Advantages and disadvantages of different numerical methods [70]

Method	Advantages	Disadvantages
Finite Volume Method	<ul style="list-style-type: none"> - Natural choice for CFD problems due to its ability to handle conservation laws effectively. - Efficient flux evaluation at cell boundaries for robust handling of nonlinear conservation laws. - Supports local mesh refinement for improved accuracy in specific regions. - Well-established and widely used in CFD applications. 	<ul style="list-style-type: none"> - Limited capability to increase the order of approximation functions for higher accuracy. - Functions approximating the solution cannot be easily made of higher order.
Finite Difference Method	<ul style="list-style-type: none"> - Easy to increase the element order for higher-order accuracy. - Efficient implementation on regular grids, suitable for large-scale simulations. - Well-suited for simulations requiring high accuracy with boundary-fitted meshes. 	<ul style="list-style-type: none"> - Limited capability in handling curved boundaries and defining boundary conditions. - Difficulty in handling material discontinuities. - Lack of local grid refinement or adaptive mesh refinement.
Finite Element Method	<ul style="list-style-type: none"> - General and versatile method applicable to multi-physics analysis. - Ability to increase the accuracy by increasing the order of the elements and locally refining the mesh. - Supports adaptive mesh refinement for improved accuracy in specific regions of interest. - Enables mixed formulations, allowing the combination of different functions for approximating different physics fields. - Handles curved and irregular geometries naturally. 	<ul style="list-style-type: none"> - Requires mathematical expertise for implementation. - More advanced mathematics compared to other methods. - More complex implementation compared to finite-difference and finite-volume methods. - May be challenging or impossible to handle with other methods.

In addition to the numerical method used, the accuracy of the simulation also depends on the numerical schemes used to discretize the governing equations, the treatment of boundary conditions, and the time integration scheme used. These factors should be carefully considered when selecting a numerical method for simulating combustion.

In this thesis, the FVM is used as the numerical method for simulating combustion due to its ability to handle complex geometries and boundary conditions, and its accuracy in capturing the turbulent flow features.

1.6 Previous studies on hydrogen addition to methane/air flames:

Several studies have been conducted to investigate the effects of hydrogen addition on methane/air flames. These studies provide valuable insights into the influence of hydrogen on flame characteristics, stability, burning velocity, and pollutant emissions. Here, we summarize key findings from selected studies, highlighting the scientists, dates, and references.

- **Effects of hydrogen addition on propagation characteristics of premixed methane/air flames:**

In a study by Minggao Yu, Kai Zheng, Ligang Zheng, Tingxiang Chu, and Pinkun Guo. (2015), an experimental study has been conducted to investigate the effects of hydrogen addition on the fundamental propagation characteristics of methane/air premixed flames at different equivalence ratios in a venting duct [55]. The experiments revealed that increasing hydrogen concentration resulted in higher laminar burning velocities, extended flammability limits, enhanced reactivity and increased burn temperature. The study provided detailed flame structure analyses, presenting valuable insights into the interaction between hydrogen and methane in premixed flames.

In a related research, researchers conducted an experimental study to the effects of hydrogen addition on laminar premixed methanol–air flames [56]. This study, conducted

by Peng Xiao, Han Wu, Ziyu Wang, Saifei Zhang, Chia-fon Lee, Ziman Wang, and Fushui Liu (2019), investigated the flame stability limits and observed that the laminar flame speed (LFS) and burning velocity (LBV) both increase when more hydrogen is added into the methanol–air mixtures.

- **Kinetic Effects of Hydrogen Addition on the Thermal Characteristics of Methane–Air Premixed Flames:**

A numerical investigation was implemented to evaluate the kinetic effects of hydrogen addition on the thermal characteristics of lean and stoichiometric premixed methane–air flames was the focus of a study by Qingfang Li, Ge Hu, Shiyong Liao, Qian Cheng, Chi Zhang, and Chun Yuan (2014) [57]. On the basis of the detailed kinetic reaction mechanism GRI-Mech 3.0. The flame temperature profiles and the distributions of reactive species were predicted as a function of flame height by solving a freely propagating laminar premixed flame model. Some global properties of the premixed flame, i.e., the flame temperature gradient, the inner layer flame temperature, and the heat release rate, were estimated. Results showed that hydrogen enrichment in methane–air flames led to increases in the peak flame temperature, the peak temperature gradient, and the peak heat release rate, but a decrease in the inner layer flame temperature.

- **Effects of hydrogen addition on laminar and turbulent premixed methane and iso-octane–air flames:**

An experimental study conducted by C. Mandilas, M.P. Ormsby, C.G.W. Sheppard, and R. Woolley. (2007), examined the influence of hydrogen addition to methane and iso-octane–air premixtures has been investigated under both laminar and turbulent conditions [58]. Five percent by mass of hydrogen was added to base fuel. Measurements were performed at 5 bar and the equivalence ratio was varied from the lean ignition limit to either the rich ignition or sooting/buoyancy limit. The study found that the laminar burning velocity, u_l , increased for fuel lean and stoichiometric methane/hydrogen mixtures compared to pure methane. Interestingly, a doubling in u_l was observed at the lean limit.

- **Numerical simulation of methane-hydrogen-air premixed combustion in turbulence:**

In a numerical simulation study by Yue Wang, Xin Zhang, and Yanfei Li. (2023), which focuses on the 3D modeling of turbulent premixed combustion in a turbulence constant volume combustion chamber (CVCC) [59]. The study utilizes the realizable k- ϵ model for turbulence and the premixed combustion model. The simulations specifically investigate methane-hydrogen-air combustion under varying conditions. The initial conditions include a temperature of 298 K, pressure of 1 bar, and a gas equivalence ratio of 1.

The effects of turbulence intensity (0 m/s, 0.7 m/s, 1.3 m/s, 2.0 m/s) and hydrogen fraction ($R(H_2) = 0\%, 10\%, 30\%, 50\%$) on flame characteristics are analyzed. It is observed that during spherical flame combustion and propagation, the rate of pressure increase initially rises and then decreases. Both turbulence intensity and hydrogen fraction exhibit similar effects on the flame propagation process. Increasing turbulence intensity leads to a higher flame propagation rate. At a flame radius of 30 mm, a turbulence intensity of 2.0 m/s results in a flame propagation velocity approximately 2.7 times that of laminar flow. Consequently, both the maximum combustion pressure and the maximum pressure rise rate show a monotonically increasing trend.

Furthermore, an increase in hydrogen fraction significantly enhances the flame propagation rate. When the hydrogen fraction is 50%, the maximum velocity reaches 4.82 m/s, which is approximately 1.5 times that of pure methane. Higher hydrogen fractions also lead to a faster occurrence of the maximum pressure, with the maximum pressure reaching about 9 bar at an $R(H_2)$ of 50%, which is 2.25 times that of pure methane combustion.

CHAPTER 2
MATHEMATICAL
MODEL &
METHODOLOGY

2.1 Problem Formulation and Assumptions:

As mentioned earlier in the first chapter, the objective of this study is to investigate the effect of hydrogen addition on methane/air flames under turbulent conditions. Specifically, the study aims to determine the optimal hydrogen concentration for improving combustion efficiency and reducing emissions in a practical combustion system.

The boundaries of the simulation include the reactor geometry, boundary conditions, and initial conditions. The reactor geometry consists of a cylindrical combustion chamber with a centrally located fuel injector and a flat inlet surface for air. The boundary conditions are defined as follows: the fuel inlet velocity, the temperature and pressure at the inlet, and the concentration of each species in the inlet stream. The initial conditions are the temperature, pressure, and concentration of species at the start of the simulation.

❖ Assumptions:

- A. The combustion process is assumed to be homogeneous, and it occurs in a well-mixed reactor.
- B. The simulation is carried out under steady-state conditions, with a constant fuel flow rate.
- C. The effects of radiation and gravity are neglected in the simulations, as they are assumed to be negligible under the conditions considered.
- D. The simulations are carried out using the Reynolds-averaged Navier-Stokes (RANS) equations, which assume that the turbulence is statistically steady and can be modeled using a turbulence closure model.

- E. The realizable k-epsilon turbulence model is used to model turbulence, which is based on the assumption that the turbulent kinetic energy and its dissipation rate are the most important variables for describing turbulent flow.
- F. The combustion process is modeled using the eddy dissipation (EC) and the eddy dissipation concept (EDC) models.
- G. A Reduced chemical mechanism (CHEMKIN) consisting of 26 reactions was employed to describe the chemical kinetics of the kerosene/air, in addition to a 4-step mechanism for methane/hydrogen/air combustion system.
- H. The simulations are performed in a 3D domain with periodic and non-periodic boundary conditions in the streamwise direction.

These assumptions provide a framework for the numerical simulations and allow for the investigation of the effect of hydrogen addition on methane/air flames under turbulent conditions.

2.2 Mathematical Model and Governing Equations:

➤ The governing equations for the simulation are expressed as follows:

- **Continuity equation:** The continuity equation is a fundamental principle in fluid dynamics that express the conservation of mass within a fluid flow, it was formulated by French mathematician and physicist Augustin-Louis Cauchy in the 19th century, it states that the rate at which mass enters or leaves a control volume must be balanced by the rate of change of mass within the volume.

➤ Mathematically, the continuity equation is represented as [60]:

$$\frac{\partial \rho}{\partial t} + \frac{\partial(\rho u_i)}{\partial x_i} = 0 \quad 2.1$$

- S_m is the mass added to the continuous phase from a dispersed second phase due to vaporization of liquid droplets or any user defined source term.
- **Momentum equation:** In fluid dynamics, the momentum equation is commonly expressed in its differential form, known as the Navier-Stokes equation. The equation relates the acceleration of fluid particles to the pressure gradient, viscous forces, and external forces acting on the fluid. It can be written as :

$$\frac{\partial(\rho u_j)}{\partial t} + \frac{\partial(\rho u_j u_i)}{\partial x_i} = -\frac{\partial p}{\partial x_i} + \frac{\partial \tau_{ij}}{\partial x_j} \quad 2.2$$

➤ with:

$$\tau_{ij} = 2\mu S_{ij} + \beta \frac{\partial u_k}{\partial x_k} \delta_{ij} \quad 2.3$$

- The τ_{ij} equation refers to the stress tensor equation in the context of the Navier-Stokes equations or the Reynolds-averaged Navier-Stokes (RANS) equations. The stress tensor, denoted by τ_{ij} , represents the viscous stresses within a fluid.

- **Energy equation:** The energy equation, or the conservation of energy equation, is a fundamental principle in thermodynamics and fluid dynamics. It is based on the first law of thermodynamics ($\Delta U = Q - W$) and has been developed and derived by multiple scientists over the years.

The equation used in this simulation is a partial differential equation and is often solved numerically to model heat transfer and energy conservation in various physical systems;

$$\frac{\partial \rho}{\partial t} \left[\rho \left(e + \frac{1}{2} u_i u_i \right) \right] \frac{\partial}{\partial x_i} \left[\rho u_j \left(h + \frac{1}{2} u_i u_i \right) \right] = \frac{\partial u_i \tau_{ij}}{\partial x_j} - \frac{\partial q_j}{\partial x_j} \quad 2.4$$

➤ With:

$$e = h - \frac{p}{\rho} + \frac{u^2}{2} \quad 2.5$$

$$h = \sum_j Y_j h_j + \frac{p}{\rho} \quad 2.6$$

$$h_j = \int_{T_{ref}}^T C_{p,j} dt \quad 2.7$$

➤ where:

- S_{ij} is the symmetric part of the velocity gradient tensor.

- **Equation of state:** Or the enclosure equation;

$$P = \rho r T \quad 2.8$$

- **Species transport equation:** describes the transport and conservation of mass for individual chemical species within a fluid system, the general form can be written as [61]:

$$\frac{\partial(\rho Y_i)}{\partial t} + \nabla \cdot (\rho Y_i u) = -\nabla \cdot J_i + R_i + S_i \quad 2.9$$

- R_i is the net rate production of species.

- ANSYS Fluent models mass diffusion J_i in turbulent flows by the equation:

$$J_i = -\left(\rho D_{i,m} + \frac{\mu_t}{Sc_t}\right) \nabla Y_i - D_{T,i} \frac{\nabla T}{T} \quad 2.10$$

- Sc_t is the turbulent Schmidt number.

- **The eddy dissipation model (EDM):**

Based on the idea proposed by Spalding that the reaction rate will be determined by the mixing process or the rate of eddy breakdown, Magnussen and Hjertager proposed the eddy dissipation model (EDM) that relates the reaction rate with the mean mass fraction of reacting chemical species [62]:

$$\tilde{\omega}_{EDM} = A \frac{\tilde{\epsilon}}{\tilde{k}} \min \left\{ \tilde{Y}_{fuel}, \frac{1}{r} \tilde{Y}_{O_2}, B \frac{1}{1+r} \tilde{Y}_{pr} \right\} \quad 2.11$$

- Where r is the stoichiometric oxygen requirement of the reaction and \tilde{Y}_{fuel} is the mean mass fraction of fuel, A and B are model constants that can adopt different values for fitting purposes.

This formulation of mean reaction rate provides good predictions in many practical cases where fast chemistry assumption is justified. However, the EDM fails in the prediction of flames, where the reactions in the near burner zone are kinetically controlled. Therefore, an inclusion of chemical kinetics into the mean reaction rate formulation becomes necessary. Among different options, the series process approach, proposed by Azevedo. It is based on the assumption that total reaction time can be represented as a sum of the characteristic time for turbulent mixing, $\tau_{EDM,k}$, and of the characteristic time for the chemical reaction $\tau_{kin,k}$:

$$\tau_{total} = \tau_{EDM,k} + \tau_{kin,k} \quad 2.12$$

Because the characteristic times are the reciprocal values of the respective reaction rates $\tau = 1/\omega$ for the mean reaction rate can be obtained:

$$\tilde{\omega} = \frac{\tilde{\omega}_{EDM,k}, \tilde{\omega}_{kin,k}}{\tilde{\omega}_{EDM,k} + \tilde{\omega}_{kin,k}} \quad 2.13$$

- Which in fact the harmonic mean value;

- **Eddy dissipation concept (EDC) model:**

In contrast to EDM, the EDC model provides an empirical expression for the mean reaction rate based on the assumption that chemical reaction occurs in the regions where

the dissipation of turbulence energy takes place. In flows of moderate to intensive turbulence, these areas are concentrated in isolated regions, occupying only a small fraction of the flow. These regions consist of “fine structures” whose characteristic dimensions are of the order of Kolmogorov’s length scale in two dimensions, but not in the third. The fine structures are not evenly distributed in time and space. They appear intermittently. Magnussen’s model is based on the following main elements:

- A cascade model that describes the energy transfer from larger to smaller scales in turbulent flow.
- An energy transfer model that expresses the characteristic quantities for the lowest level of scales as functions of scales from the large-scale level.
- The large-scale levels are related to the mean flow by a turbulence model or resolved directly by LES.
- The fine structures are assumed to be a steady-state homogeneous reactor; the chemical reactions occur there.

In the EDC model, the fluid state is determined by the fine structure state, the surrounding state, and the fraction of fine structures. The ratio between the mass in the smaller eddies and the total mass in the surroundings is:

$$\gamma_\lambda = \left(\frac{3C_{D2}}{4C_{D1}^2} \right)^{1/4} \left(\frac{\mathbf{v} \cdot \tilde{\epsilon}}{\widetilde{k^2}} \right)^{1/4} \quad 2.14$$

Where C_{D1} and C_{D2} are model constants. Actually, γ_λ is a kind of intermittency factor, providing the possibility to find the fine structures or fine-structure regions in a

given location. The time scale for the mass transfer between the fine structures and the surroundings is estimated as:

$$\tau^* = \left(\frac{C_{D2}}{3}\right)^{1/2} \left(\frac{v^*}{\tilde{\epsilon}}\right)^{1/2} = \frac{1}{m^*} \quad 2.15$$

Where m^* is the mass flow over the boundaries of a fine structure. Assuming all fine structures to be perfectly stirred reactors (PSRs), the mass exchange between the fine structures and the surroundings m^* can be linked to $\frac{\gamma_\lambda^2}{\tau^*}$. This gives the following expression for the mean reaction rate:

$$\widetilde{\omega}_k = \frac{\gamma_\lambda^2}{\tau^*} (Y_k^0 - Y_k^*) \quad 2.16$$

- The mass averaged mean state can be found from the fine-structure state Y_k^* and the surrounding state Y_k^0 as:

$$\tilde{Y} = \gamma_\lambda^2 Y^* + (1 - \gamma_\lambda^2) Y^0 \quad 2.17$$

- Thus, the mean reaction rate can be represented as a function of the mean state values:

$$\widetilde{\omega}_k = \frac{\gamma_\lambda^2}{\tau^*} (\tilde{Y}_k - Y_k^*) \quad 2.18$$

- Where \tilde{Y}_k and Y_k^* are the mass fractions of species k as cell average and inside the fine structures, respectively.

2.3 Turbulence Modeling:

Turbulence plays a significant role in the combustion process, affecting the mixing of fuel and oxidant, flame propagation, and heat transfer. The turbulence in the system is modeled using the Reynolds-averaged Navier-Stokes (RANS) equations, which describe the time-averaged flow behavior. In this study, the realizable k-epsilon turbulence model was used to model turbulence.

It consists of two partial differential equations, one for the turbulent kinetic energy (k) and one for the rate of dissipation of turbulent kinetic energy (epsilon) [63];

- **Transport equation for k :**

$$\frac{\partial(\rho k)}{\partial t} + \frac{\partial(\rho u k)}{\partial x_i} = \frac{\partial}{\partial x_j} \left[\frac{\left(\mu + \frac{\mu t}{\sigma_k}\right) \partial k}{\partial x_j} \right] + Gk + Gb - \rho \varepsilon - Y_M + S_k \quad 2.19$$

➤ where:

- x is the position in the j -direction;
- μ is the molecular viscosity of the fluid;
- μt is the eddy viscosity;
- σk is the turbulent Prandtl number for k ;
- Gk is the turbulent kinetic energy generation term, which represents the production of turbulent kinetic energy due to mean velocity gradients;
- Gb is the generation of the turbulence kinetic energy due to buoyancy;
- Y_M represents the contribution of the fluctuating dilatation in compressible turbulence to the overall dissipation rate;
- S_k is user-defined source term.

- **Transport equation for epsilon:**

$$\frac{\partial(\rho\varepsilon)}{\partial t} + \frac{\partial(\rho u \varepsilon)}{\partial x_i} = \frac{\partial}{\partial x_j} \left[\left(\mu + \frac{\mu_t}{\sigma_\varepsilon} \right) \frac{\partial \varepsilon}{\partial x_j} \right] + \rho C_1 S \varepsilon - \rho C_2 \frac{\varepsilon^2}{k + \sqrt{v \varepsilon}} + C_{1\varepsilon} \frac{\varepsilon}{k} C_{3\varepsilon} G b + S_\varepsilon \quad 2.20$$

➤ where:

$$C_1 = \max \left[0.43, \frac{\eta}{\eta + 5} \right]$$

2.21

$$\eta = S \frac{k}{\varepsilon}$$

2.22

$$S = \sqrt{2 S_{ij} S_{ij}}$$

2.23

$$S_{ij} = \frac{1}{2} \left(\frac{\partial u_j}{\partial x_i} + \frac{\partial u_i}{\partial x_j} \right)$$

2.24

- $C_{1\varepsilon}$, $C_{2\varepsilon}$ and $C_{3\varepsilon}$ are constants;
- S_ε represents any additional source or sink term for turbulent dissipation rate;
- S is the modulus of the mean rate-of-strain-tensor.

- **The eddy viscosity μ_t is given by:**

$$\mu_t = \rho C_\mu \frac{k^2}{\varepsilon} \quad 2.25$$

➤ Where:

$$C_{\mu} = \frac{1}{A_0 + A_s \frac{kU^*}{\varepsilon}}$$

2.26

$$U^* = \sqrt{S_{ij}S_{ij} + \tilde{\Omega}_{ij}\tilde{\Omega}_{ij}}$$

2.27

- A_0 and A_s are model constants.

➤ and:

$$\tilde{\Omega}_{ij} = \Omega_{ij} - 2\varepsilon_{ijk}\omega_k \quad 2.28$$

$$\Omega_{ij} = \overline{\Omega_{ij}} - \varepsilon_{ijk}\omega_k \quad 2.29$$

- Where $\overline{\Omega_{ij}}$ is the mean rate-of-rotation tensor viewed in a rotating reference frame with the angular velocity ω_k .

Together, these equations form a closed system that can be solved numerically to obtain the values of k , ε , and other flow variables.

2.4 Numerical Methods and Software Used:

2.4.1 Computational Fluid Dynamics (CFD):

Computational Fluid Dynamics (CFD) is a powerful tool for simulating fluid flows and heat transfer. CFD uses numerical methods to solve the governing equations of fluid motion, such as the Navier-Stokes equations, and the conservation equations of mass, momentum, and energy. In this study, CFD was used to simulate combustion in a

kerosene/air flame and methane/air flame, and the effect of hydrogen addition on methane/air flame.

2.4.2 Software Used:

The ANSYS Fluent software was used for all simulations in this study, which is a widely used CFD software package that provides a comprehensive set of tools for simulating fluid flows and heat transfer. ANSYS uses finite volume method (FVM) to discretize the governing equations, and provides a variety of turbulence models, chemical reaction models, and other physical models for simulating complex fluid flows. ANSYS Fluent is capable of handling complex geometries and boundary conditions, making it a suitable choice for simulating combustion in realistic combustion systems.

2.4.3 Numerical Methods:

➤ The numerical methods used for simulating combustion in this study are:

a. Finite Volume Method (FVM):

The finite volume method is a numerical method for solving partial differential equations that arise in fluid mechanics. In FVM, the domain is divided into a finite number of control volumes, and the governing equations are integrated over each control volume. The conservation equations are then discretized using finite difference approximations, and the resulting algebraic equations are solved iteratively to obtain the solution.

b. Turbulence Modeling:

Turbulence is an important factor in combustion simulations, as it affects mixing, heat transfer, and pollutant formation. In this study, the turbulence model we used is the Reynolds-Averaged Navier-Stokes (RANS), which is a widely used turbulence model that provides a time-averaged solution of the governing equations.

c. Chemical Reaction Modeling:

Chemical reactions are a critical aspect of combustion simulations. In this study, a chemical reaction mechanism was used to model the combustion of kerosene, methane, and hydrogen, which consists of 53 chemical species and 325 chemical reactions, this mechanism was implemented using the ANSYS Fluent User Defined Function (UDF) feature

CHAPTER 3
PROBLEM SET-UP
AND SOLUTION

3.1 Introduction:

In this chapter, we will describe the set-up and solution of a computational fluid dynamics simulation of combustion in a model aircraft engine combustion chamber. The simulation was based on the 3D geometry used by Mohammad Golam Mostafa in his study titled "3D Simulation of Jet-A Combustion in A Model Aircraft Engine Combustion Chamber" [1]. The goal of our simulation is to study the combustion process in the chamber and evaluate the performance of different fuel mixtures. To achieve this, we will first describe the geometry of the combustion chamber, including its dimensions and key features. We will then discuss the meshing strategy used to discretize the geometry and the set-up of the simulation, including the boundary conditions and solver settings. Finally, we will present the results of our convergence check to ensure the accuracy and reliability of the simulation. By providing a detailed account of our problem set-up and solution procedure, this chapter aims to facilitate the replication and validation of our simulation by other researchers in the field of combustion science.

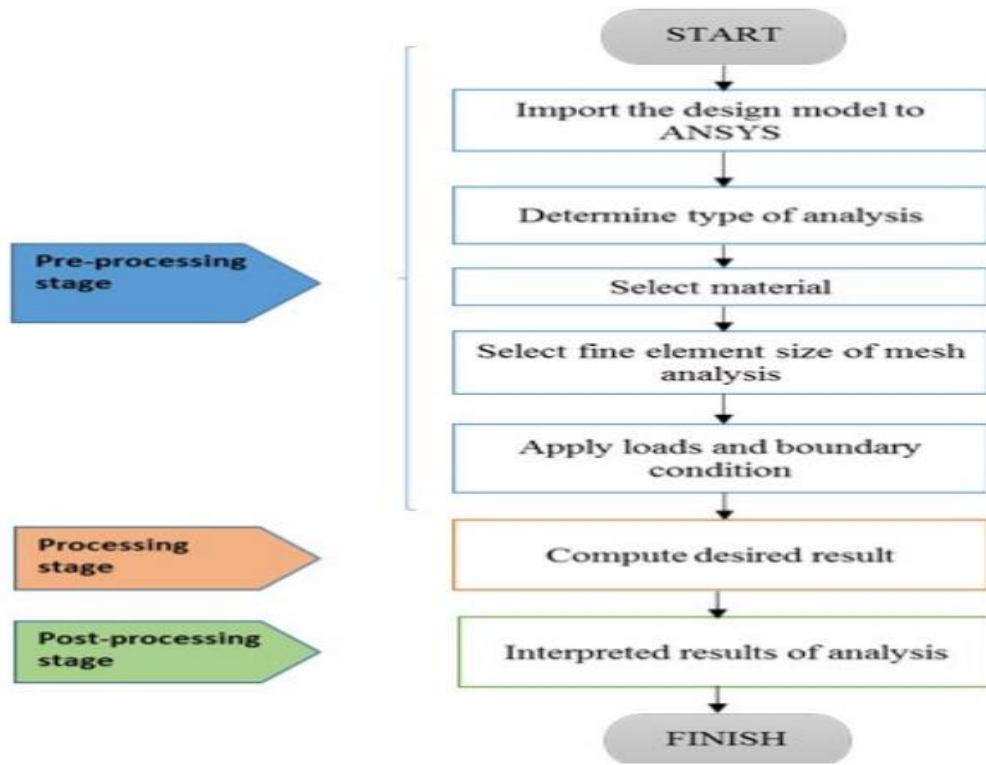


Figure 3.11 Flowchart diagram of numerical modeling using ANSYS Fluent [64]

3.2 Combustion Chamber geometry:

In this section, we will provide a detailed description of the combustion chamber geometry used in our simulation. The design of the combustion chamber includes a cylindrical shape with an annular injection system. The flow rate will be adjusted to achieve the required residence time for the gas mixture inside the chamber.

The burner-up section is a cylindrical fluid volume with an inlet and outlet diameter of 6cm. The length of this zone is 2.5cm. The injection system starts right after the burner-up section and extends from 4.0cm to 4.5cm. The outermost circle of the injection system has a radius of 3cm.

The flame holder section is a cylindrical chamber that slightly converges and diverges at the ends. The inlet and outlet diameters are both 6cm, and the maximum diameter of the chamber is 10cm. The flame holder section extends 17cm with a maximum diameter. There are 80 holes periodically arranged across the length and radial directions of the flame holder section. Each hole has a uniform diameter of 0.8cm. Along the axis, there are five sets of holes. Each set contains 16 holes periodically arranged along the circumferences of the flame holder section. The angular distance between two consecutive holes is 22.5°. The axial position of the holes is at $Z = 5.5, 8, 11, 14, 17$ cm. The first set of holes at $Z = 5.5$ cm makes a 30° angle with the Z -axis (axis of the chamber). However, the other four sets are perpendicular to the Z -axis.

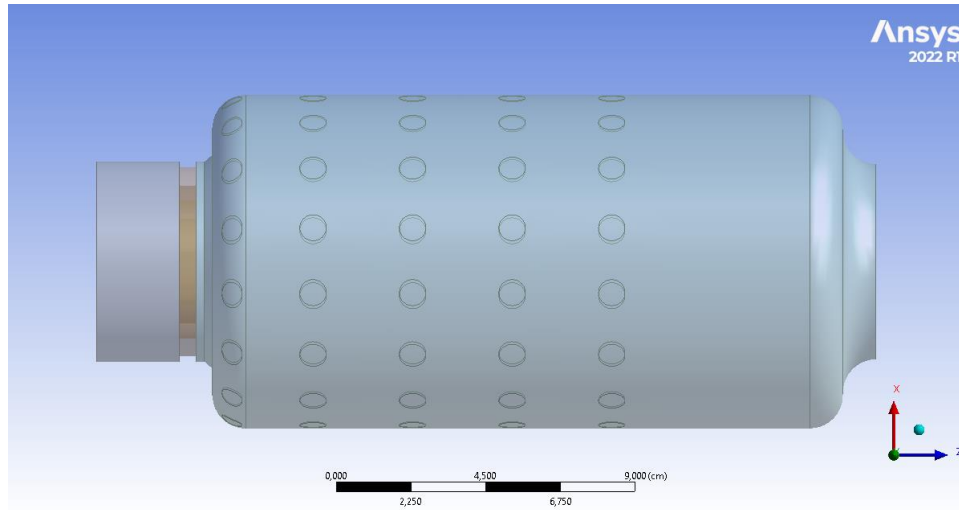


Figure 3.12 Representation of combustion chamber geometry

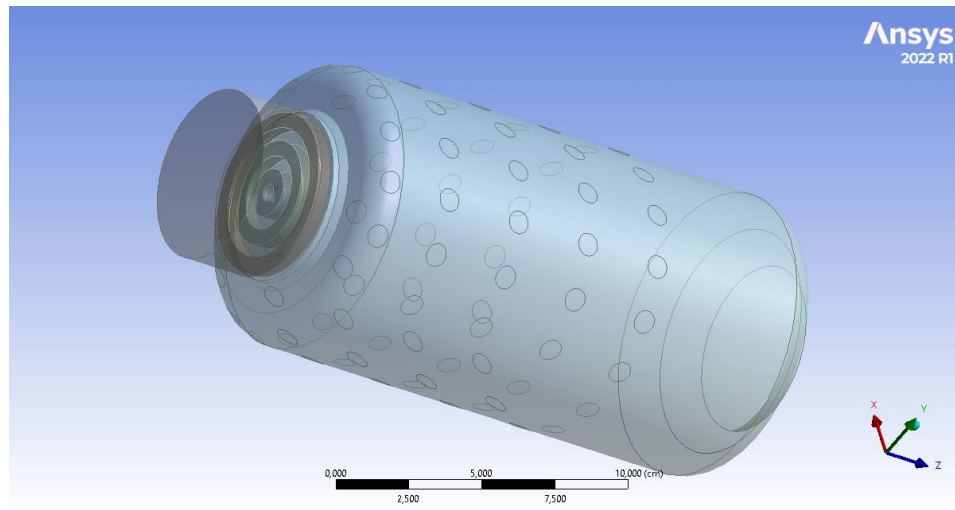


Figure 13 Representation of combustion chamber geometry (2)

Due to the rotational periodicity of our designed chamber, with a period angle of 22.5° , we can simulate only one-sixteenth (1/16th) of the chamber. This approach will considerably reduce computational time, making the simulation at least 16 times faster.

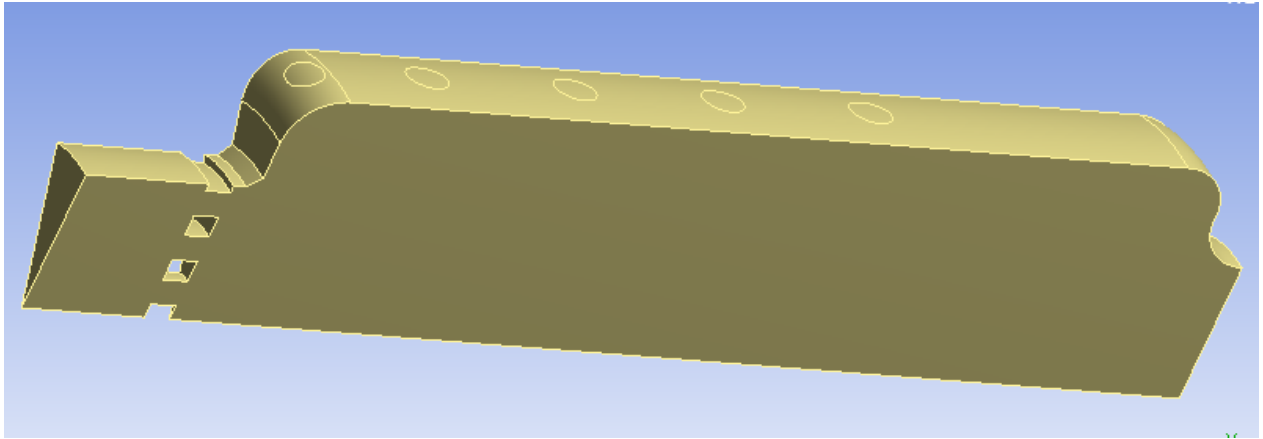


Figure 3.14 splitted geometry

- In the figure, several boundary zones with names used in the Fluent setup are displayed:

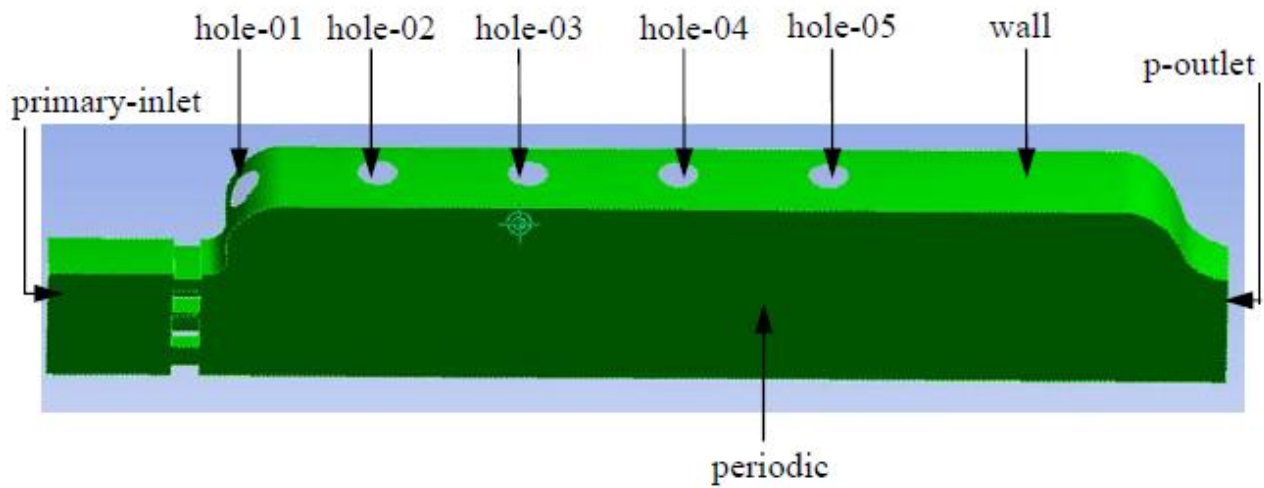


Figure 15 Boundary zones

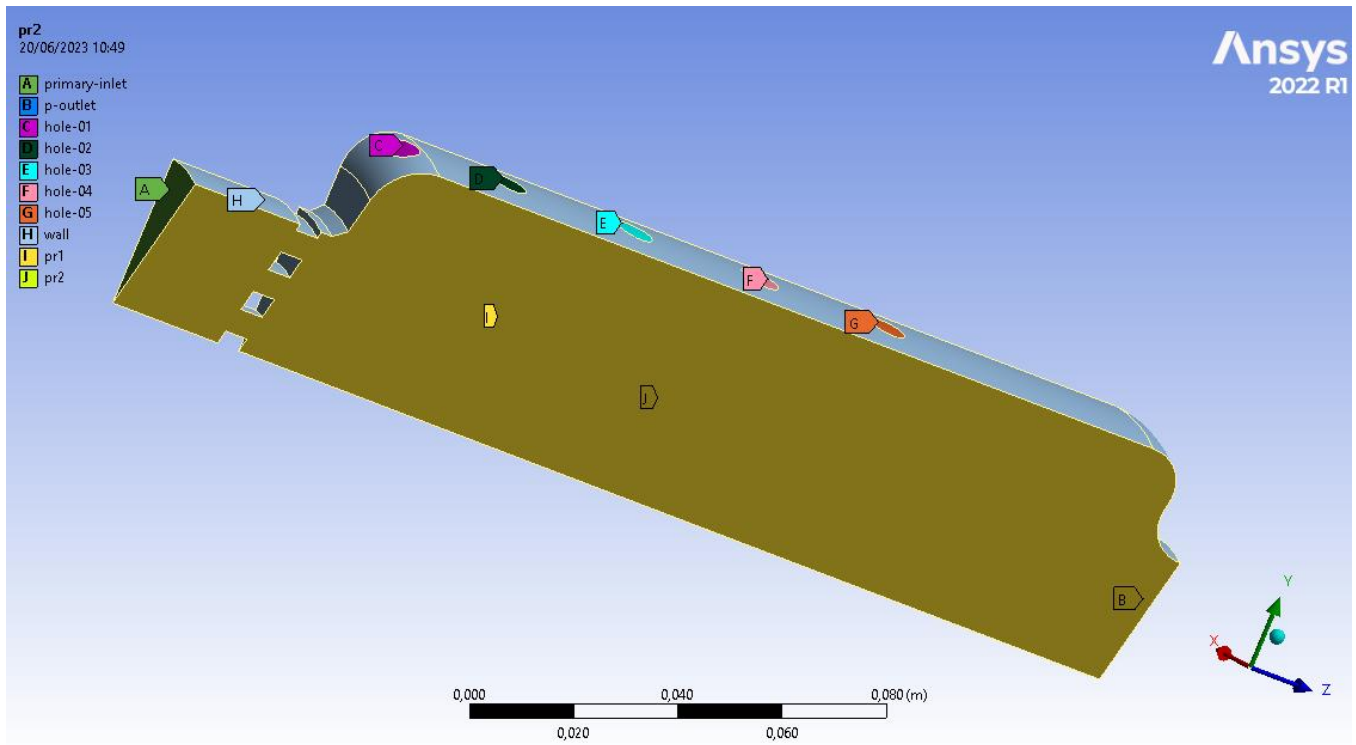


Figure 3.16 boundary zones (2)

3.3 Meshing:

The quality of the mesh has a significant impact on the accuracy and computational efficiency of the simulation. A good mesh should have enough resolution to capture the relevant physical phenomena, while at the same time maintaining a reasonable number of elements to ensure computational feasibility.

The mesh was evaluated based on parameters such as element quality, skewness, and orthogonal quality. A minimum average element mesh quality of 0.8 was deemed acceptable.

Skewness mesh metrics spectrum:



Orthogonal Quality mesh metrics spectrum:

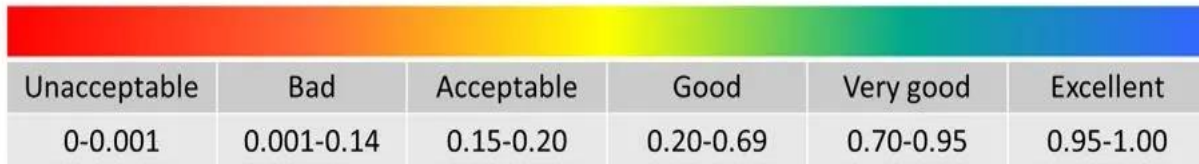


Figure 17 Skewness and Orthogonal Quality mesh metrics spectrum [65]

3.3.1 Description of Meshing Parameters and their Selection Criteria:

The mesh was generated using an advanced size function was applied to the meshing process to account for the curvature of the geometry. Center-coarse relevance was selected to ensure that meshing was focused on the most important regions of the geometry.

Medium smoothing and slow transition were applied to avoid mesh distortion and ensure that element quality was maintained. Center fine span angle and default minimum and maximum sizes were chosen to obtain a balance between mesh resolution and computational cost. Finally, a defeaturing tolerance of 1E-07 was applied to simplify the geometry and improve mesh quality.

- For full geometry, our mesh consists of 64501 nodes and 333808 elements:

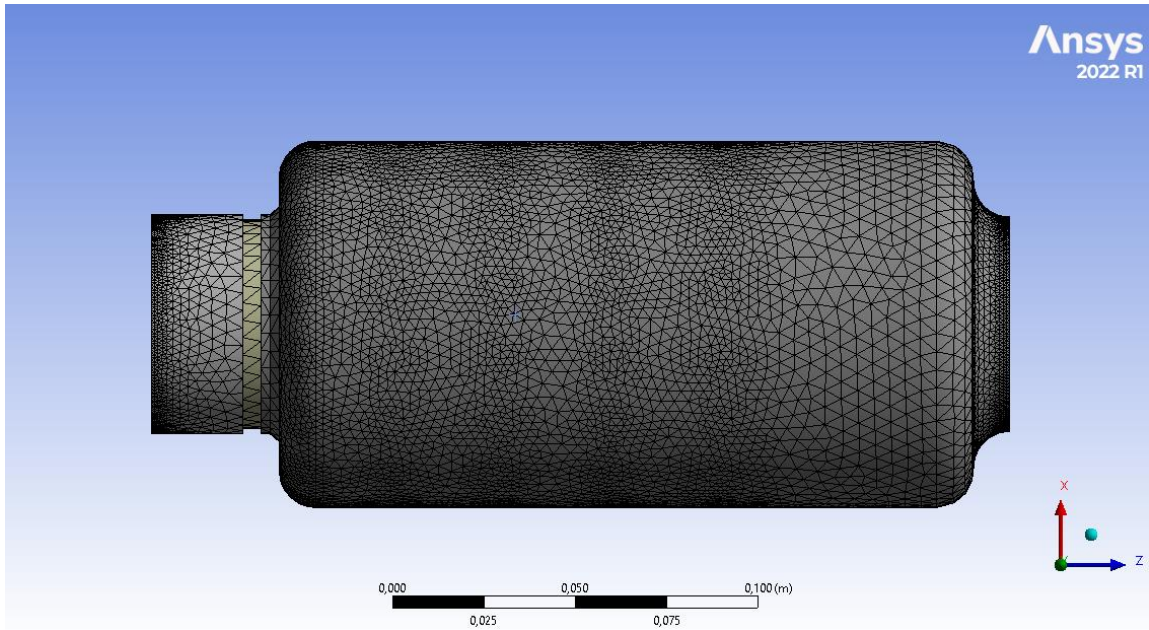


Figure 3.18 Meshed geometry

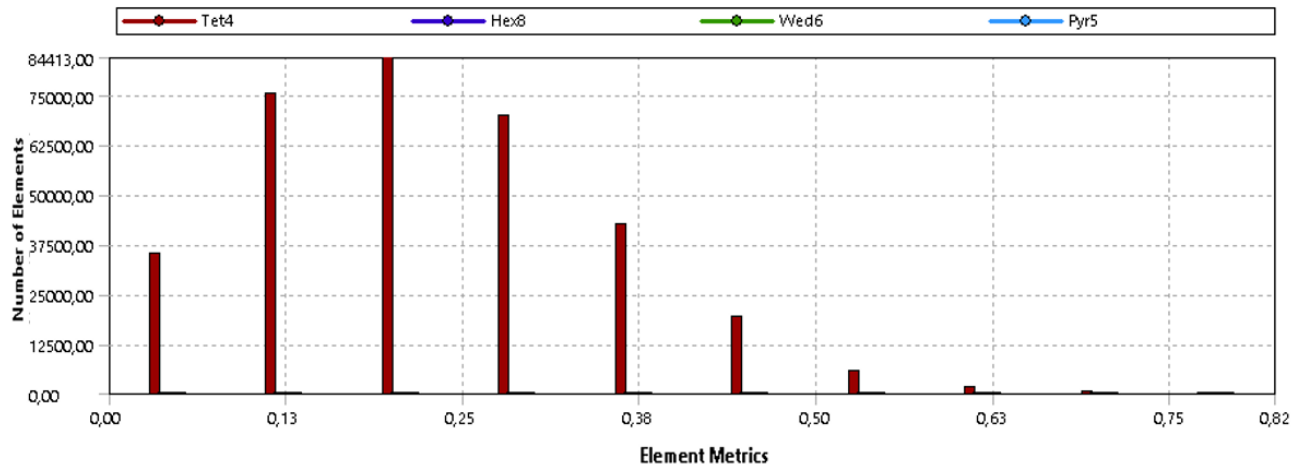


Figure 19 Skewness metrics for the generated mesh

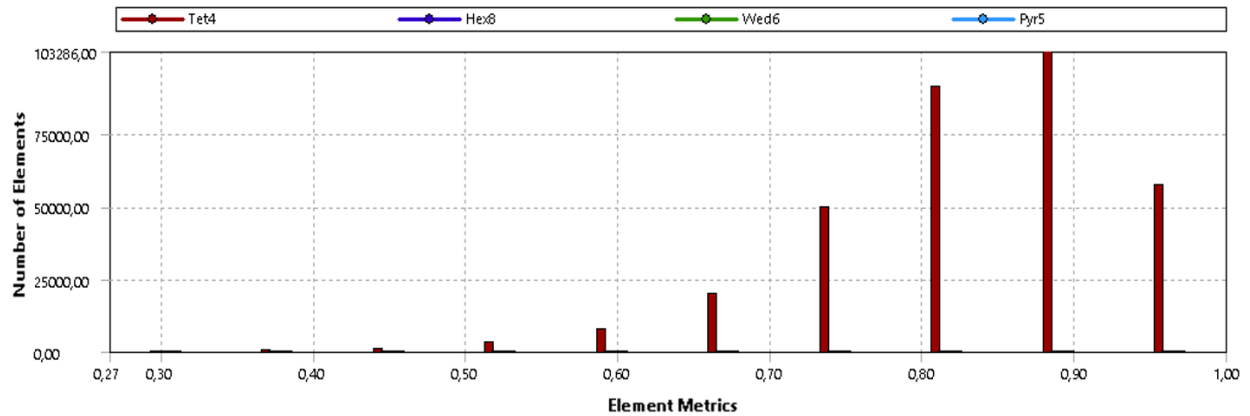


Figure 3.10 Element quality metrics for the generated mesh

3.3.2 Splited geomety:

The selected mesh configuration for the splited geometry consists of 9893 nodes and 44580 elements;

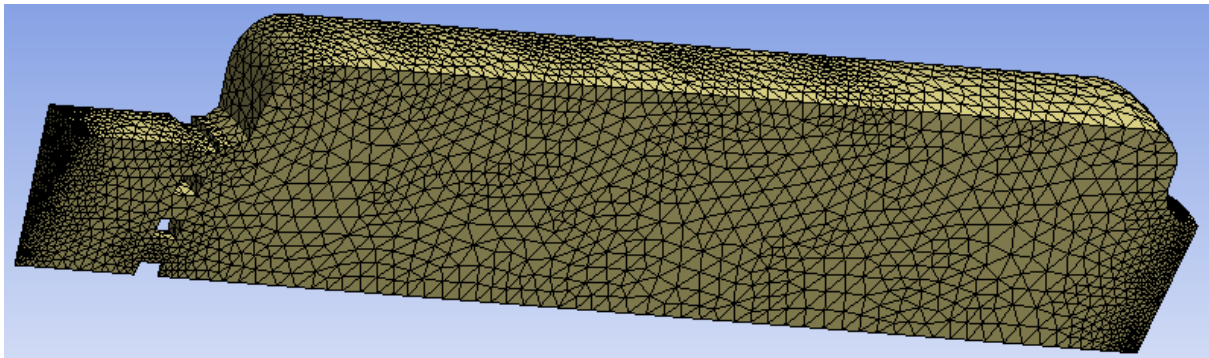


Figure 3.11 Meshed Splited geometry

We employed the "Match Control" method for meshing the geometry. This choice was based on the utilization of rotational periodicity in the simulation. By implementing this method, I ensured that the meshing of the geometry aligned with the rotational periodicity, enabling accurate representation of the system;

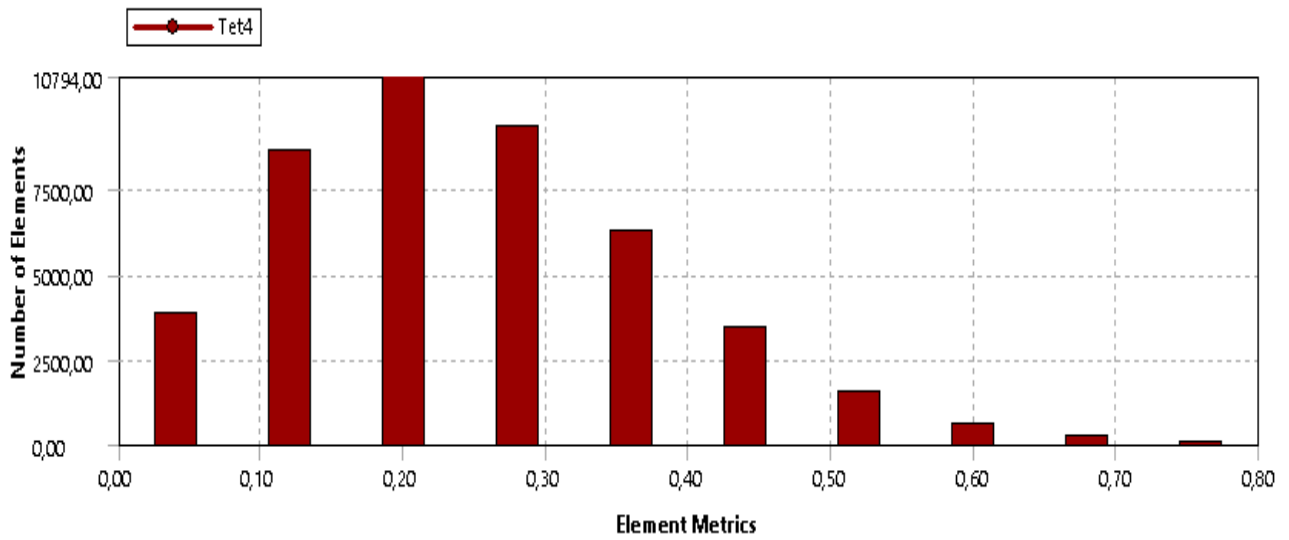


Figure 3.12 Skewness metrics for the generated mesh

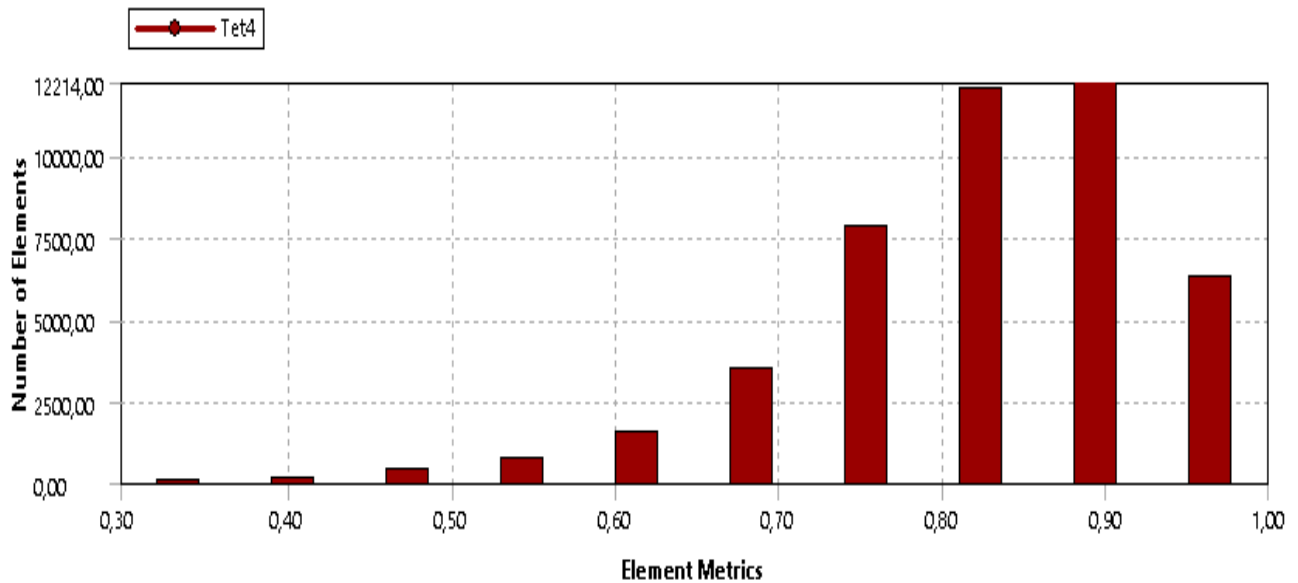


Figure 3.13 Element quality metrics for the generated mesh

3.3.3 mesh sensitivity study:

In this section, we present a detailed methodology and procedures for conducting a mesh sensitivity study for the splitted geometry to assess the impact of mesh refinement on the results of our combustion simulation. Mesh sensitivity analysis plays a crucial role in numerical simulations by evaluating the convergence and accuracy of the solution.

Understanding the influence of mesh density on the simulation results is essential for obtaining reliable and meaningful predictions of the combustion process.

Table 3.1 Different meshes

Mesh	Max face size	Calculation time	Number of elements
Mesh 01	1e-02	15 min	33049
Mesh 02	8e-03	18 min	34983
Mesh 03	4e-03	29 min	44580
Mesh 04	1e-03	5 h 10 min	729126

The chart below depicting the temperature at the outlet of the combustion chamber, specifically the Temperature Inlet Turbine (TIT). The chart illustrates the variation in outlet temperature for different mesh configurations, each characterized by a specific element number:

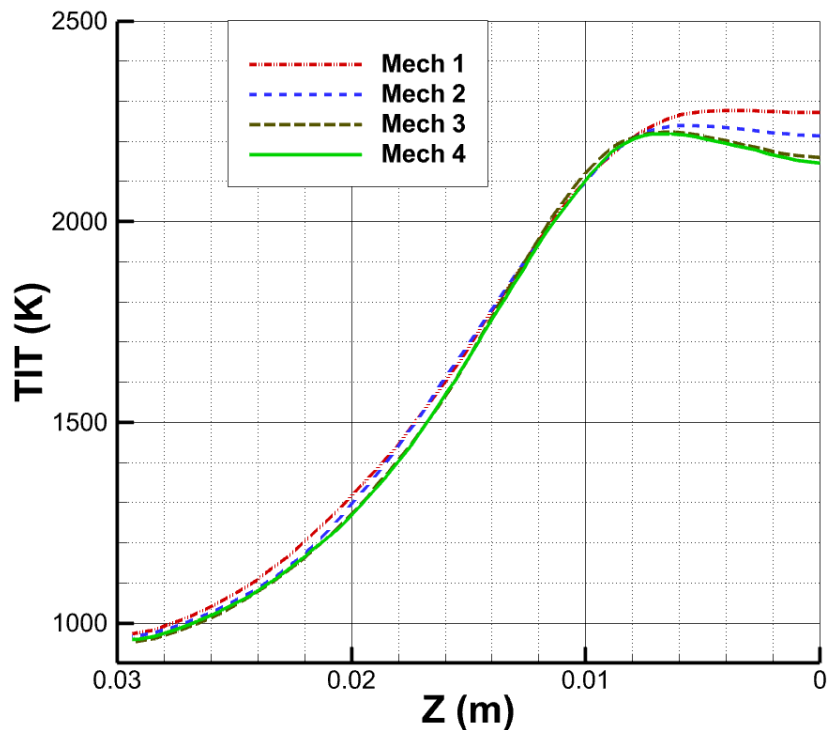


Figure 20 Temperature Variation at Combustion Chamber Outlet for Different Mesh

The selected mesh configuration for the splited geometry is the mech 03 which consists of 44580 elements., the chosen mesh configuration provides a balance between resolution and computational efficiency, allowing us to capture important thermal phenomena while keeping the simulation time manageable.

For the Full geometry , We would like to acknowledge the valuable contribution of M. Ala Eddine AZZOUZ and Mme. Loubna ALIOUAT in their research paper titled 'Simulation de la combustion turbulente dans une chambre de combustion tubulaire pour le mélange kérosène/air et méthane/air' [53] for providing reference parameters for our mesh sensitivity study. Their work serves as a benchmark for validating our mesh configuration and ensures consistency and comparability with the established literature.

3.3.4 Solver configuration:

In this section, the solver configuration and simulation parameters used in the numerical analysis are presented. These choices were made to ensure accurate and reliable results:

- Steady State and Pressure-Based Solver.
- The 'k-ε' (Realizable) turbulence model was chosen to capture the turbulence characteristics of the flow. The advanced wall function was employed to properly account for the near-wall turbulence effects.
- The species transport model with volumetric reaction was selected to accurately simulate the transport and reaction of species in the methane/air flame. This model considers the convective and diffusive transport of individual species and incorporates the volumetric reaction terms.

- The Eddy-Dissipation (ED) and Eddy-Dissipation Concept (EDC) models were chosen to capture the interaction between turbulence and chemical kinetics.
- A Reduced mechanism with 26 reactions was employed to describe the chemical kinetics of the kerosene/air, in addition to a 4-step mechanism for methane/hydrogen/air combustion system.
- The 'primary-inlet', 'hole-01', 'hole-02', 'hole-03', 'hole-04', and 'hole-05' were set as mass flow inlets. The 'pr1' and 'pr2' boundaries were defined as rotationally periodic boundaries to account for the circumferential symmetry of the flame. The 'p-outlet' boundary was set as an 'outflow'.
- The initial turbulent intensity was assumed to be 10%, providing an initial estimate of the turbulence level in the domain. The hydraulic diameter was set to 0.06m for the 'primary-inlet' and 0.008m for all the holes. These values were chosen based on the specific geometry and characteristics of the combustion system.
- The pressure-velocity coupling scheme was set to "Simple," which is a widely used and robust approach for solving the pressure-velocity coupling in steady-state simulations.
- The gradient calculation scheme was set to "Least Square Cell-Based," which provides accurate gradients across the computational domain by minimizing interpolation errors.

3.3.5 Periodic setup:

In order to simulate the periodic behavior of the combustion chamber, a periodic rotational method was implemented using Fluent. The setup process involved the following steps:

a. Accessing the Mesh:

- The mesh was accessed through the ANSYS Fluent interface.

b. Modifying Zones:

- The 'modify-zones' command was used to make adjustments to the zones.

c. Creating Periodic Zones:

- The 'make periodic' command was executed to create periodic zones.
- The software prompted for the identification of the periodic and shadow zones.
- The periodic zone was specified as '13'.
- The shadow zone was specified as '14'.

d. Selecting Rotational Periodicity:

- When prompted for the type of periodicity, the option 'yes' was selected to indicate rotational periodicity.

e. Confirming Creation of Periodic Zones:

- The software asked whether to create periodic zones.
- The option 'yes' was chosen to create the periodic zones.

f. Zone Deletion and Merging:

- The software indicated that zone 14, which represented the shadow zone, was deleted. Additionally, the software merged the remaining zones to ensure the faces became periodic boundaries.

```
Setting Post Processing and Surfaces information ... Done.

adapt/          file/          solve/
adjoint/        mesh/         surface/
close-fluent    parallel/     views/
define/         plot/
display/        report/

> mesh

/mesh> modify-zones

/mesh/modify-zones> make-periodic
Periodic zone [()] 13
Shadow zone [()] 14
Rotational periodic? (if no, translational) [yes] yes
Create periodic zones? [yes] yes

zone 14 deleted

created periodic zones.
/mesh/modify-zones>
```

Figure 21 Periodic setup

CHAPTER 4
RESULTS AND
DISCUSSION

4.1 Introduction:

In this chapter, the outcomes of the numerical simulations conducted using the ANSYS Fluent solver in a 3D turbojet combustion chamber will be presented and thoroughly discussed. The primary objective is to analyze the data obtained from the simulations and interpret their implications in relation to the research objectives. The chapter will be divided into three main sections: the results of kerosene/air flame simulations, the results of methane/air flame simulations, and the effects of hydrogen addition on combustion.

4.2 Kerosene/Air Flame Simulation Results:

This section presents the results obtained from the simulation of kerosene/air flames in the 3D turbojet combustion chamber. The power settings used in the simulations are based on the reference study by Mohammad Golam Mostafa [60]. The power settings considered in our study are categorized into four regimes: A (7% power), B (30% power), C (85% power), and D (100% power). The objective is to analyze the flame structure, temperature profiles, and species concentrations in order to gain insights into the combustion characteristics of kerosene/air mixtures and compare it with methane/hydrogen/air mixtures.

4.2.1 Temperature contour:

In this section, we present the temperature contours. By analyzing the temperature contours at these different power settings, we aim to understand the thermal behavior and characteristics of the kerosene/air flames within the combustion chamber. These results provide valuable insights into the influence of power settings on the temperature distribution, aiding in the optimization of combustion processes in jet engines.

The temperature contours below obtained from the kerosene/air flame simulations at different power settings reveal distinct variations in flame temperature.

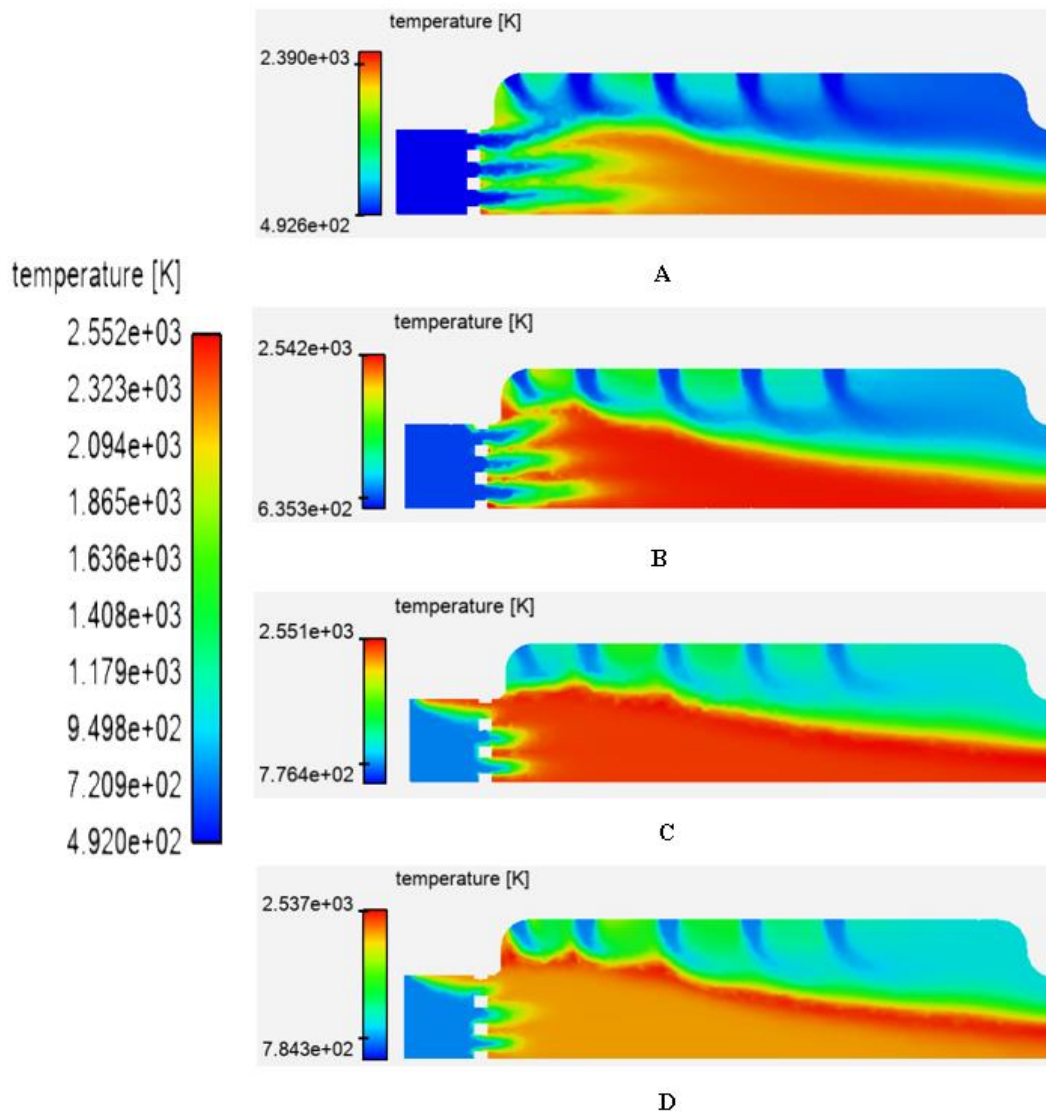


Figure 4.1 Longitudinal temperature contour for kerosene combustion at different regimes. A: 7% power, B: 30% power, C: 85% power and D: 100% power settings.

For 100% power setting. It was noted that despite the higher power input, the maximum temperature obtained was lower than that of the 85% power setting.

The temperature contour analysis of the 100% power setting revealed interesting temperature variations within the flame. Higher temperatures were observed at the edges of the flame, primarily due to the interaction with the air entering the combustion chamber

through holes. This increased air entrainment facilitated enhanced combustion and subsequently higher temperatures in these regions. However, in the middle of the flame, a different behavior was observed. Here, the temperature was comparatively lower, suggesting a deficiency in air supply and inadequate mixing.

For the flame thickness, the 100% power regime exhibits a noticeably broader flame structure compared to the other regimes. This suggests that the higher power input leads to a wider and more extensive combustion region. The increased flame thickness in the 100% power regime may be attributed to factors such as enhanced fuel-air mixing and higher heat release rates, resulting in a larger volume of the combustion zone. This observation highlights the influence of power settings on the spatial extent and overall dimensions of the flame.

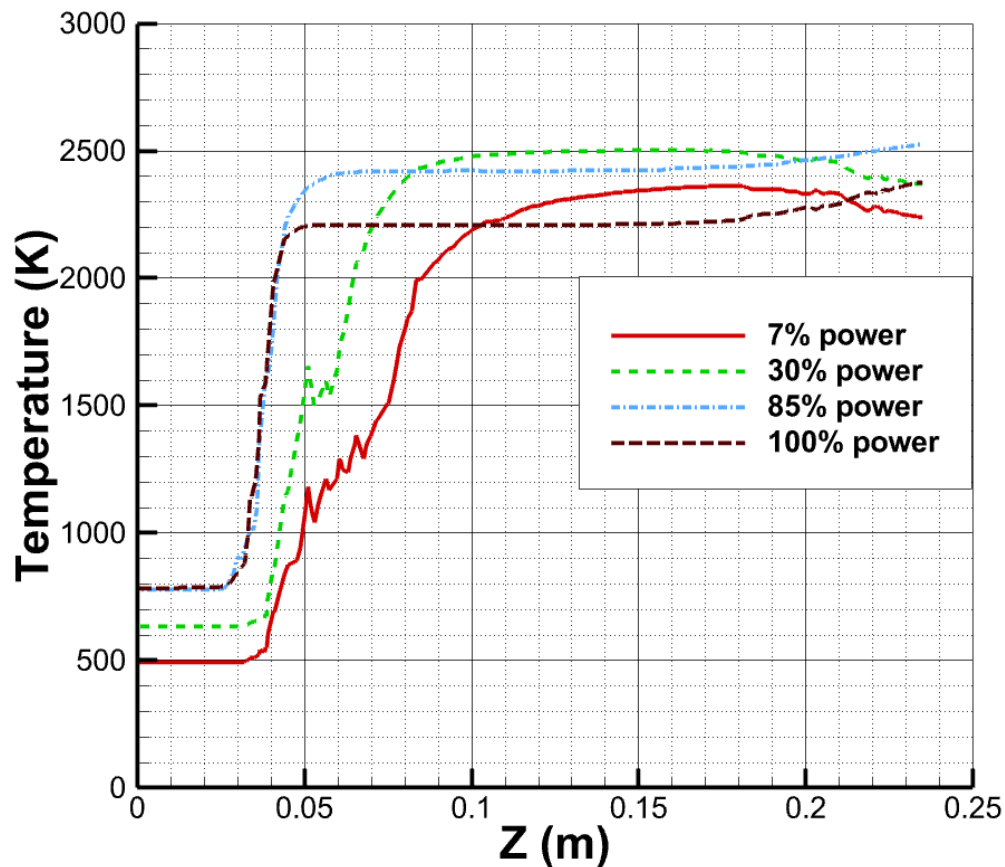


Figure 4.2 Longitudinal temperature variation chart for kerosene combustion at different regimes. A: 7% power, B: 30% power, C: 85% power and D: 100% power settings.

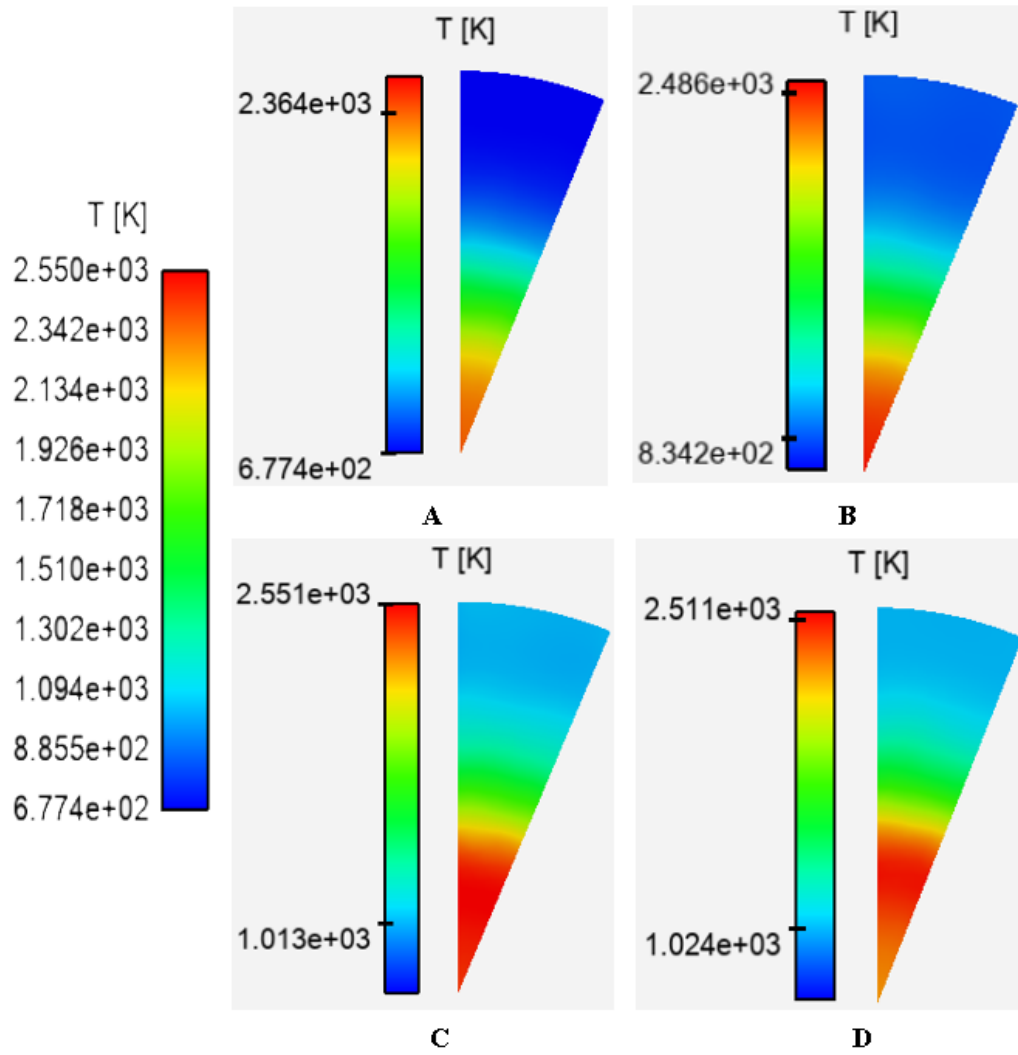


Figure 4.3 TIT contour for kerosene combustion at different regimes. A: 7% power, B: 30% power, C: 85% power and D: 100% power settings.

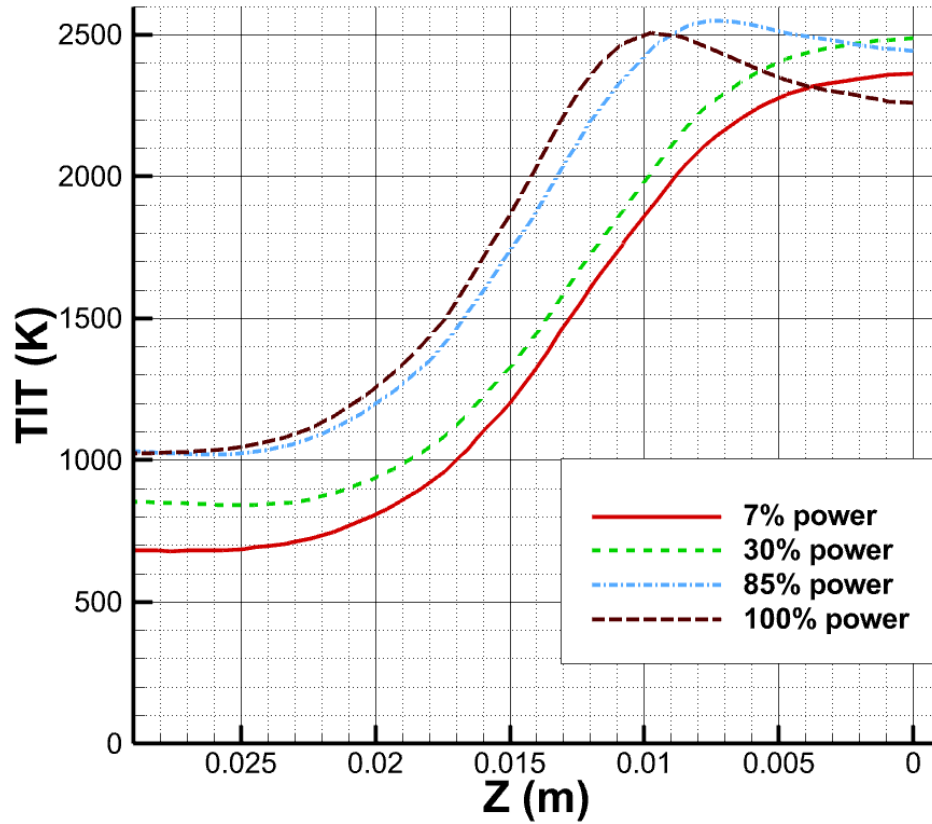


Figure 4.4 TIT variation chart for kerosene combustion at different regimes. A: 7% power, B: 30% power, C: 85% power and D: 100% power settings.

4.2.2 Velocity contour:

In this section, we present the velocity contours obtained from simulations conducted at different power settings: 7%, 30%, 85%, and 100%.

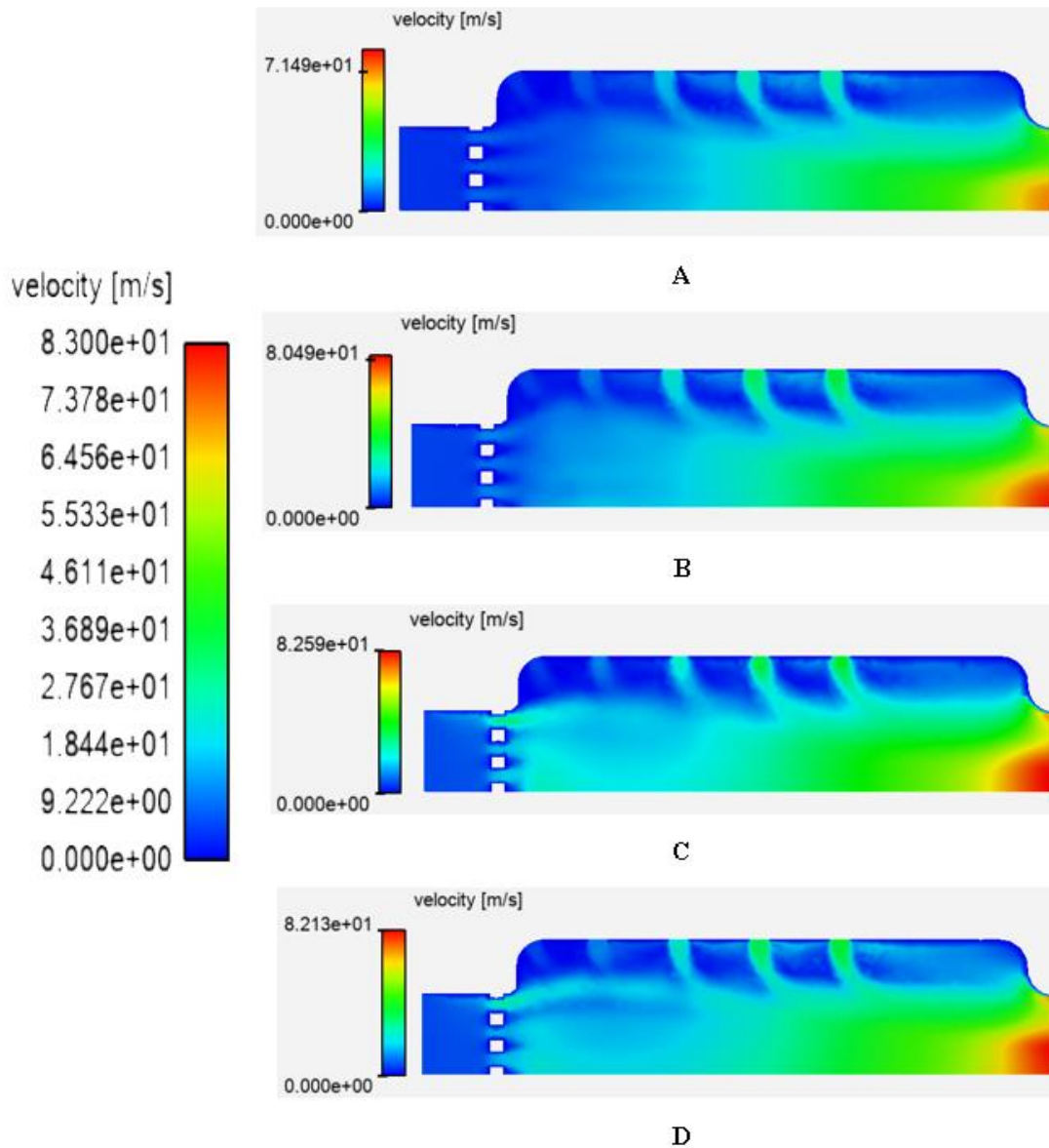


Figure 4.5 Longitudinal velocity contour for kerosene combustion at different regimes. A: 7% power, B: 30% power, C: 85% power and D: 100% power settings.

The velocity of the combustion products is a critical parameter that reflects the flow dynamics within the combustion chamber. In this study, the velocity was found to increase with increasing power settings, indicating a higher rate of energy release and combustion

intensity. Specifically, the velocities recorded for the 7%, 30%, and 85% power settings demonstrated a noticeable increase, with values of 71.49 m/s, 80.49 m/s, and 82.59 m/s, respectively. These results indicate that as the power setting is elevated, the combustion process becomes more energetic and efficient, leading to an accelerated flow of combustion products. However, it is interesting to note that the velocity at the 100% power setting closely approximated that of the 85% power setting, with a value of 82.13 m/s. This suggests that reaching the maximum power output may result in diminished returns in terms of further increasing the velocity.

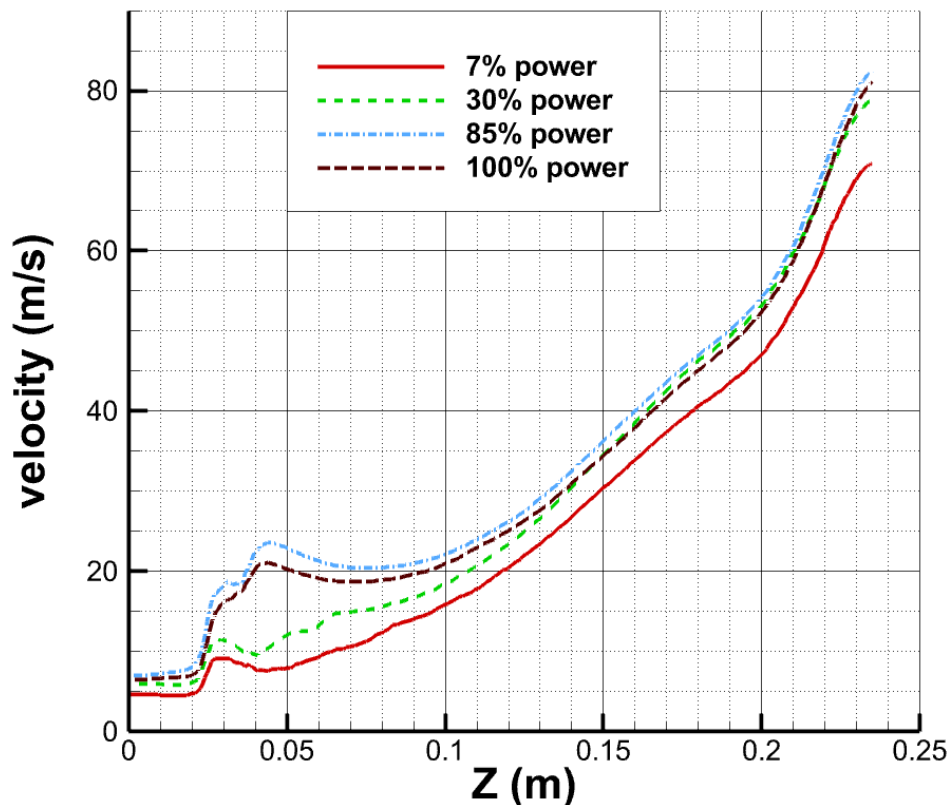


Figure 4.6 Longitudinal velocity variation chart for kerosene combustion at different regimes. A: 7% power, B: 30% power, C: 85% power and D: 100% power settings.

4.2.3 Species variation:

In this section, we present the emission contours of NO (nitrogen oxide), CO₂ (carbon dioxide), and CO (carbon monoxide) obtained from the simulations conducted at different power settings: 7%, 30%, 85%, and 100%. These emissions are significant

contributors to air pollution and greenhouse gas emissions, and their spatial distribution within the combustion chamber plays a vital role in understanding the combustion efficiency and environmental performance of the system.

4.2.3.1 NO Mass Fraction Contours:

In this section, we present the No masse fraction contours obtained from simulations conducted at different power settings: 7%, 30%, 85%, and 100%.

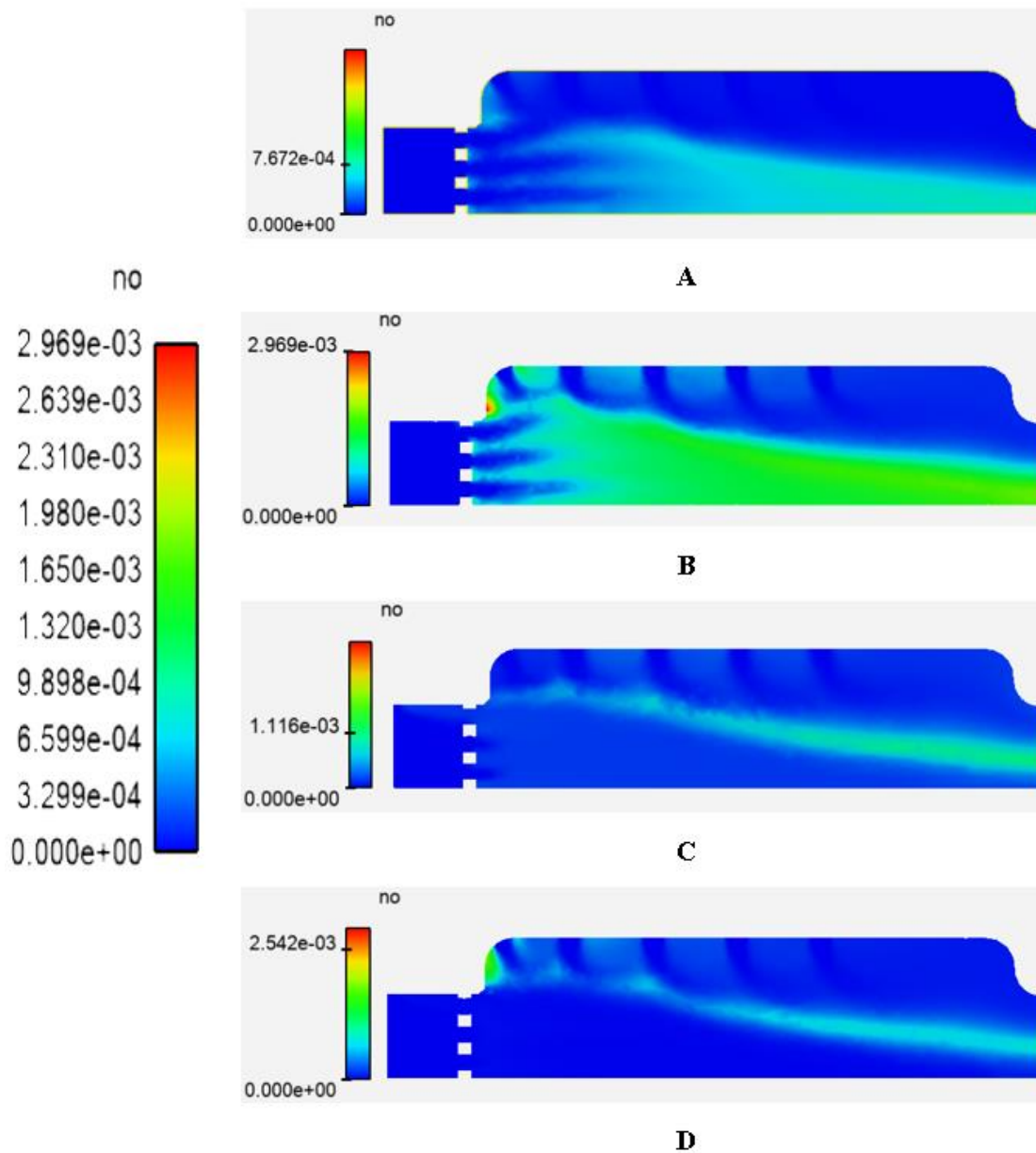


Figure 4.7 Longitudinal NO masse fraction contour for kerosene combustion at different regimes. A: 7% power, B: 30% power, C: 85% power and D: 100% power settings.

The distribution of NO (nitrogen oxide) mass fraction exhibits distinct patterns across the different power settings. For the 7% and 30% power regimes, high NO values are primarily concentrated around the high-temperature zone, indicating favorable conditions for NO formation. The 30% power setting stands out with comparatively higher NO emission rates. In contrast, the 85% and 100% power regimes show a shift in the distribution of high NO values towards the edges of the flame.

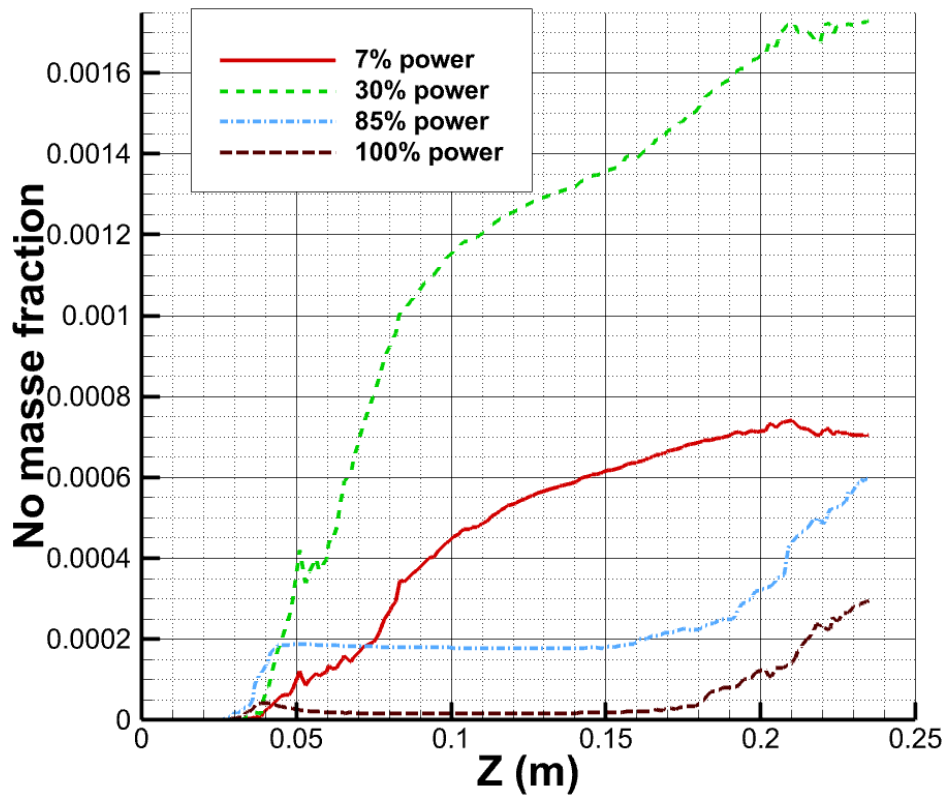


Figure 4.8 Longitudinal NO mass fraction variation chart for kerosene combustion at different regimes. A: 7% power, B: 30% power, C: 85% power and D: 100% power settings.

4.2.3.2 CO₂ Mass Fraction Contours:

This section presents the CO₂ mass fraction contours obtained from simulations conducted at various power settings, including 7%, 30%, 85%, and 100%.

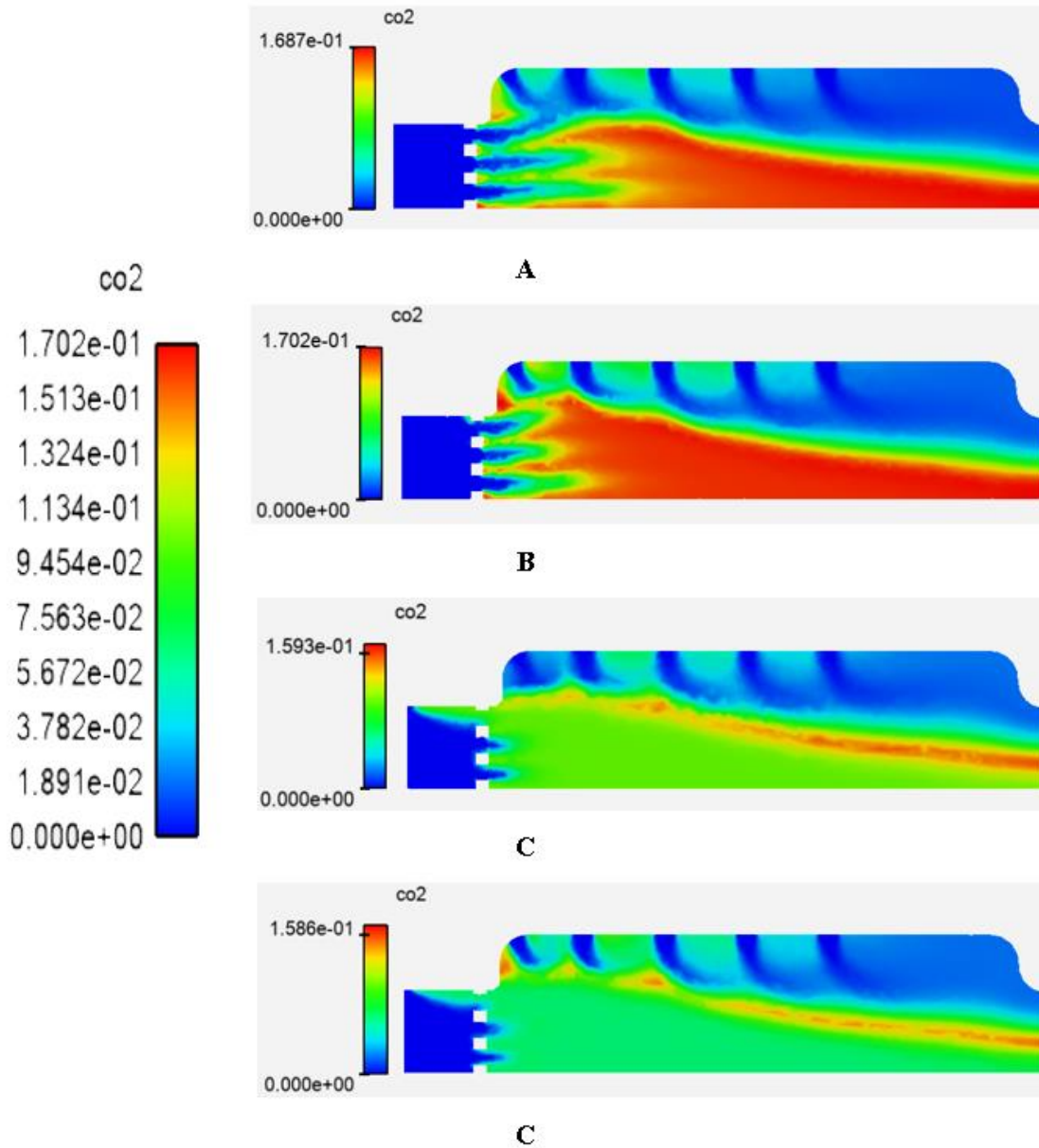


Figure 4.9 Longitudinal Co₂ masse fraction contour for kerosene combustion at different regimes. A: 7% power, B: 30% power, C: 85% power and D: 100% power settings.

The CO₂ mass fraction distribution within the combustion chamber was investigated for different power settings, including 7%, 30%, 85%, and 100%. The analysis revealed that in the 7% and 30% power regimes, the high values of CO₂ were

predominantly observed in the vicinity of the high-temperature zone within the flame. Interestingly, the 30% power setting exhibited a particularly high CO₂ emission rate compared to the other power regimes. Similarly, the 7% power setting showed a similar trend but with slightly lower CO₂ values. In contrast, for the 85% and 100% power settings, the high values of CO₂ were primarily concentrated towards the edges of the flame.

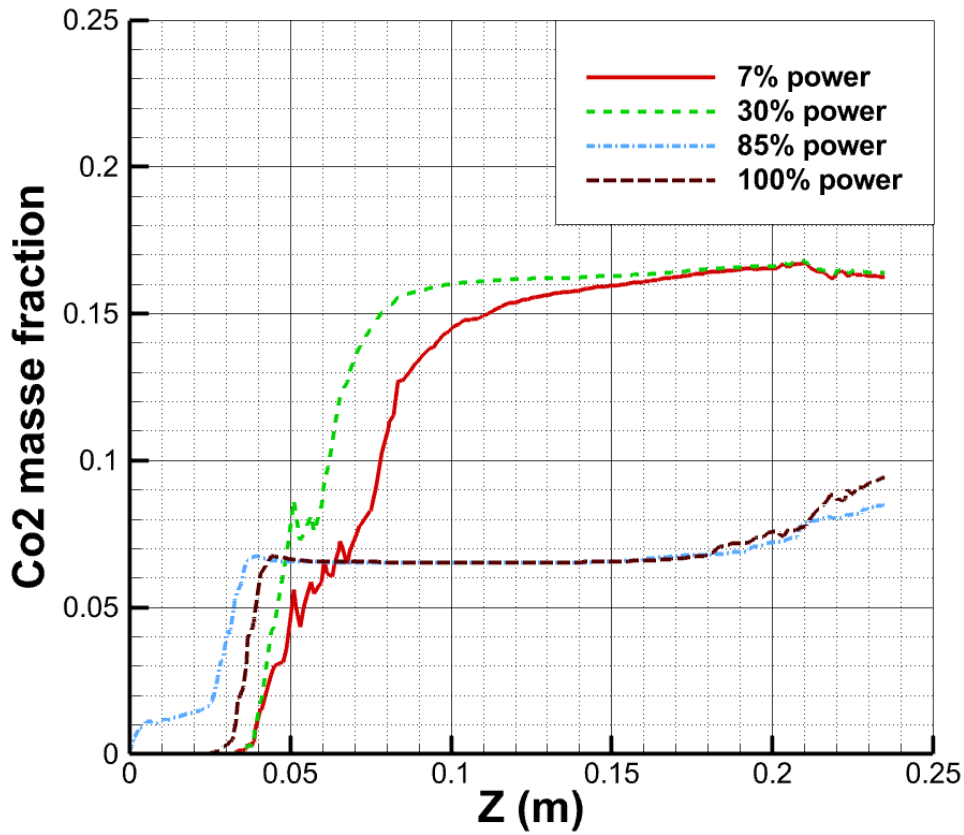


Figure 4.10 Longitudinal Co₂ masse fraction variation chart for kerosene combustion at different regimes. A: 7% power, B: 30% power, C: 85% power and D: 100% power settings.

4.2.3.3 CO Mass Fraction Contours:

This section presents the CO mass fraction contours obtained from simulations conducted at various power settings, including 7%, 30%, 85%, and 100%.

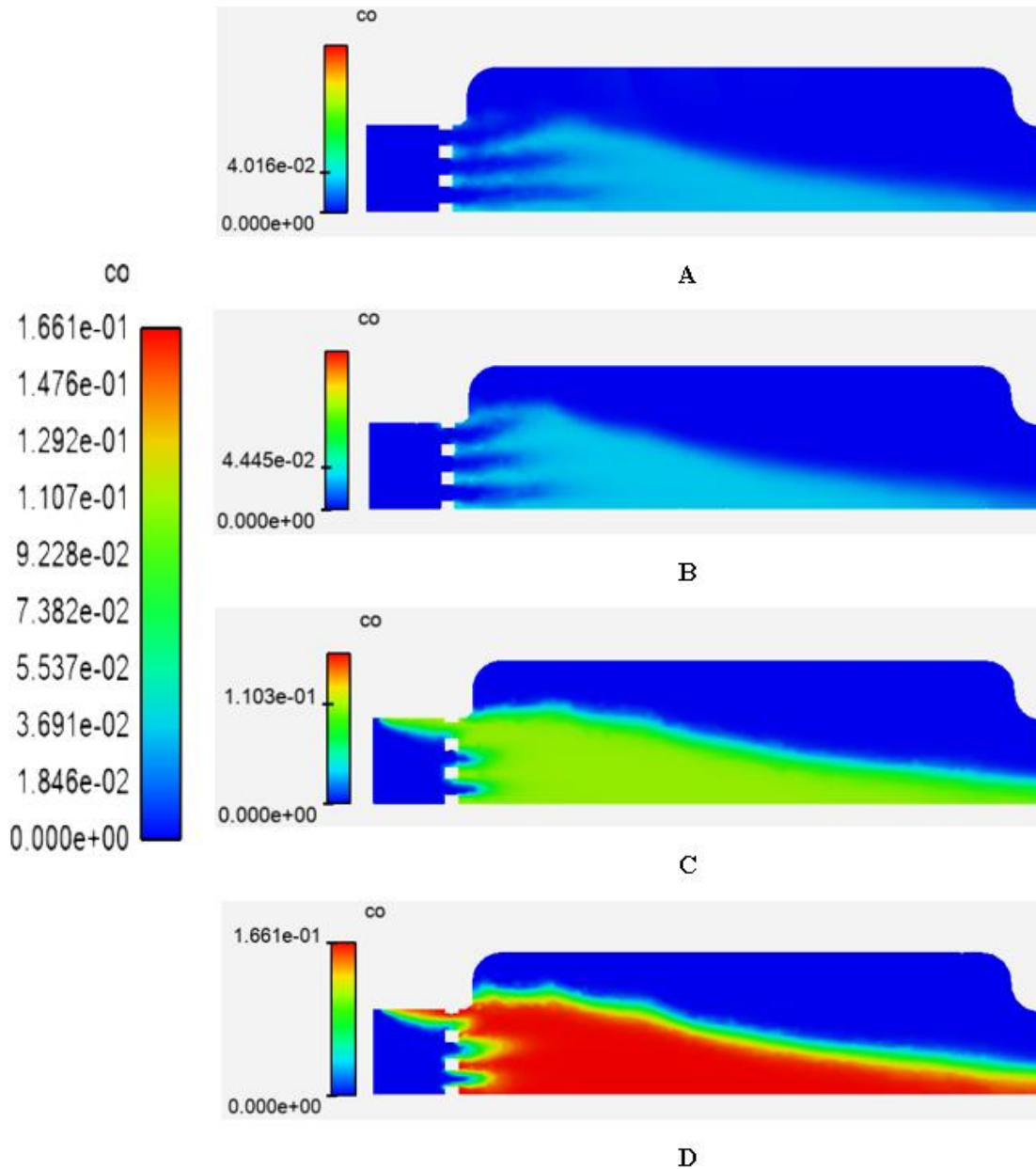


Figure 4.11 Longitudinal Co masse fraction contour for kerosene combustion at different regimes. A: 7% power, B: 30% power, C: 85% power and D: 100% power settings.

The results demonstrated a clear trend of increasing CO mass fraction with increasing power settings. Notably, the 100% power regime exhibited the highest CO values among the investigated power settings. This indicates that higher power settings contribute to increased CO production within the combustion chamber.

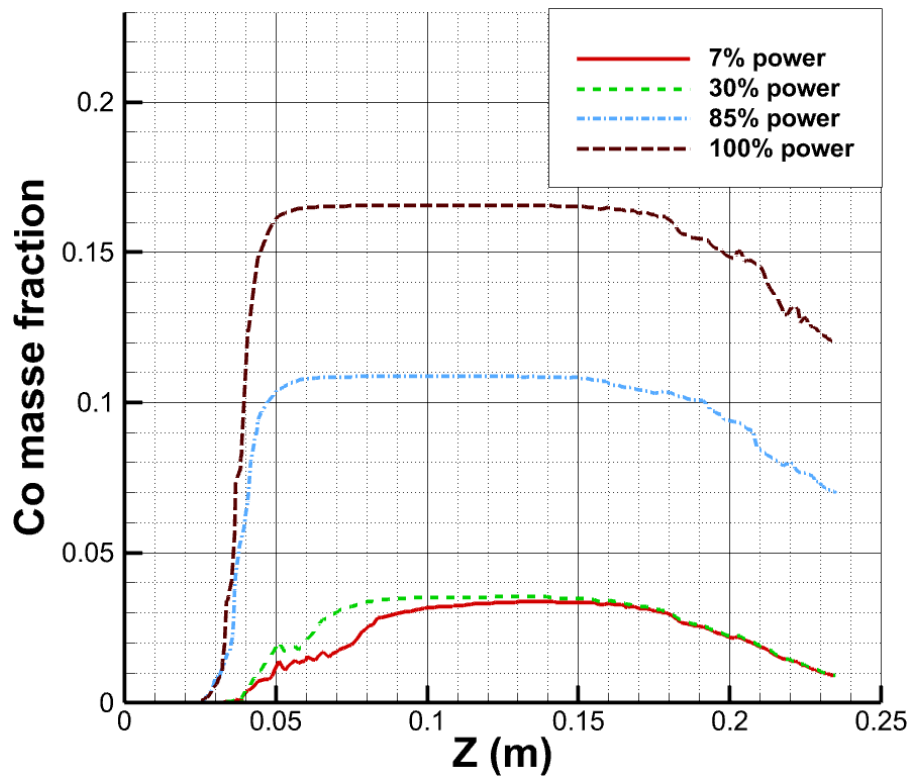


Figure 4.12 Longitudinal Co masse fraction variation chart for kerosene combustion at different regimes. A: 7% power, B: 30% power, C: 85% power and D: 100% power settings.

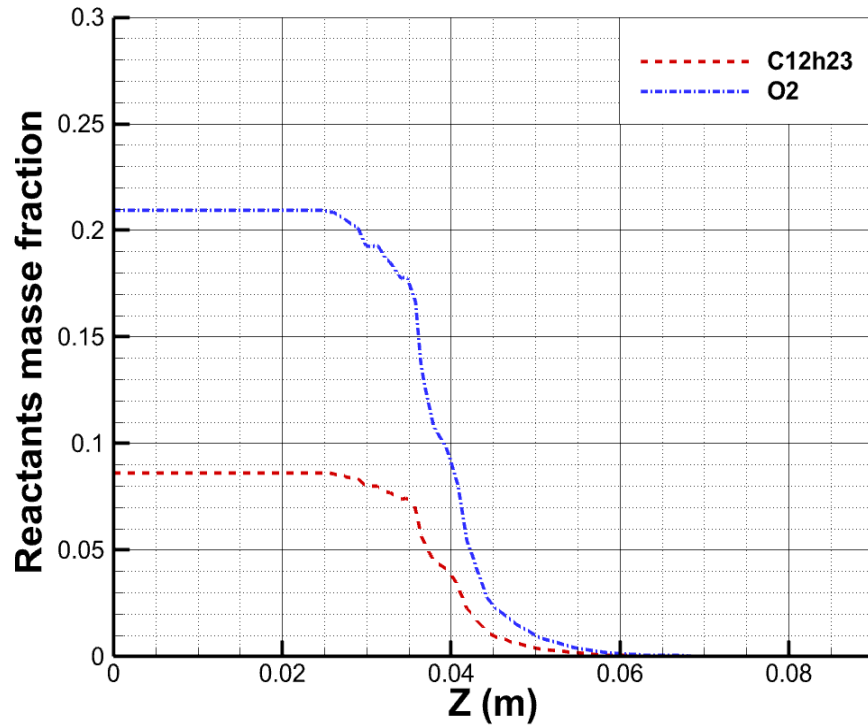


Figure 4.13 Masse fraction variation for reactants at 85% power, $POP= 1850144$ Pa, $T= 776.55$ k for kerosene/air flame

4.3 Methane/Air Flame Simulation Results:

4.3.1 Effect of Preheat Temperature on Combustion Performance and Characteristics:

In this section, we delve into an investigation of the effect of preheat temperature on the performance and characteristics of the combustion process. Preheat temperature plays a crucial role in influencing the ignition, flame propagation, and overall combustion behavior. Understanding how changes in preheat temperature impact these factors is vital for optimizing combustion systems, enhancing energy efficiency, and reducing emissions.

4.3.1.1 Temperature contour:

The preheat temperature of the primary inlet is varied to investigate its impact on the maximum temperature reached within the combustion chamber. Four different preheat temperatures are considered: 300 K, 350 K, 400 K, and 450 K. The simulation results are summarized in the following table:

Table 4.1 The Preheat temperatures effects on maximum temperatures for methane/air combustion

Preheat Temperature (K)	Maximum Temperature (K)
300	2194
350	2223
400	2250
450	2282

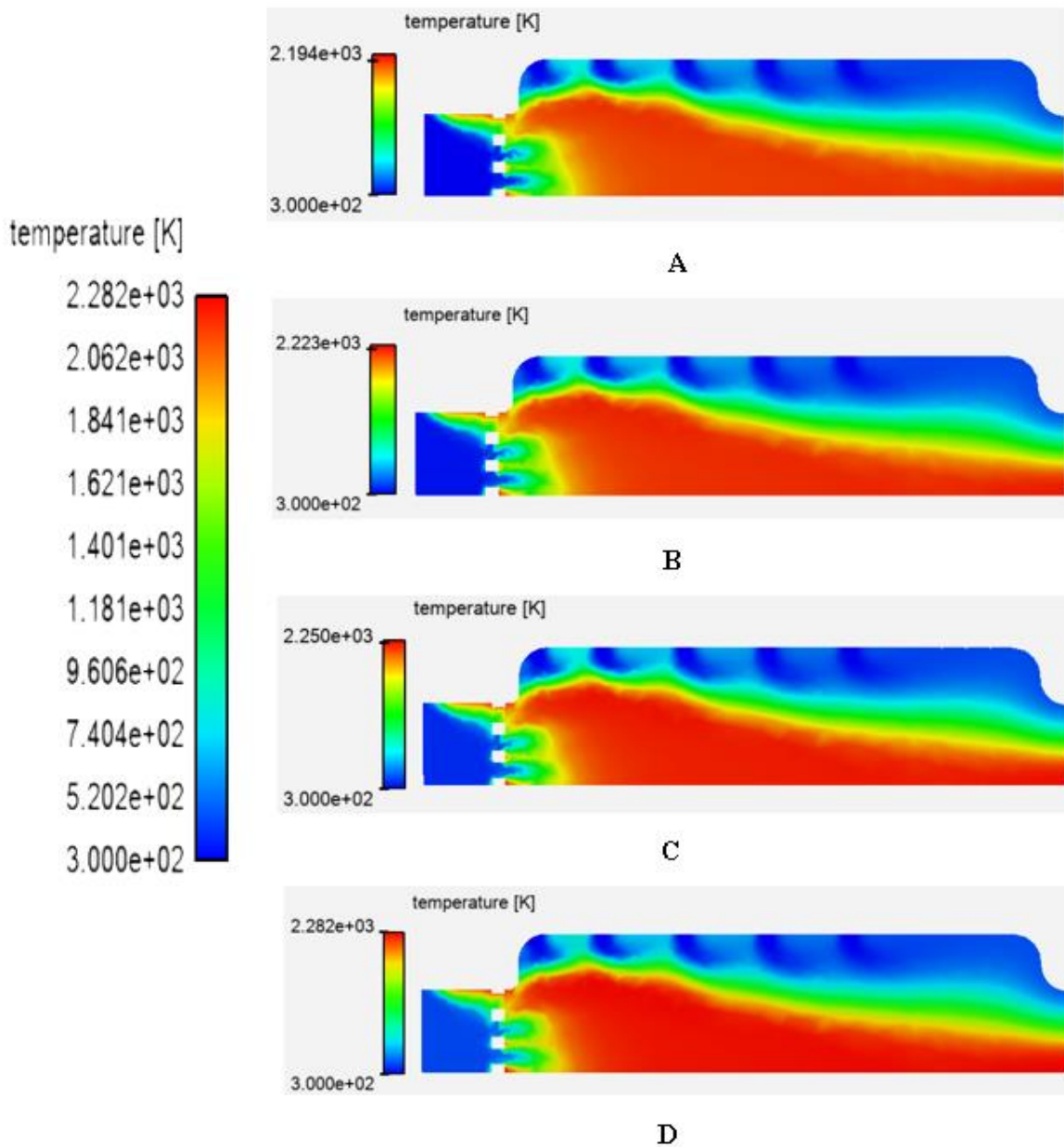


Figure 4.14 Longitudinal temperature contour for methane combustion at 85% rpm with different initial Temperature (A) $T = 300$ k, (B) $T = 350$ k, (C) $T = 400$ k, (D) $T = 450$ k

Based on the simulation results, it can be observed that the maximum temperature within the combustion chamber increases as the preheat temperature is elevated. The data obtained from the simulations indicate a direct correlation between the preheat temperature and the maximum temperature achieved during the combustion process.

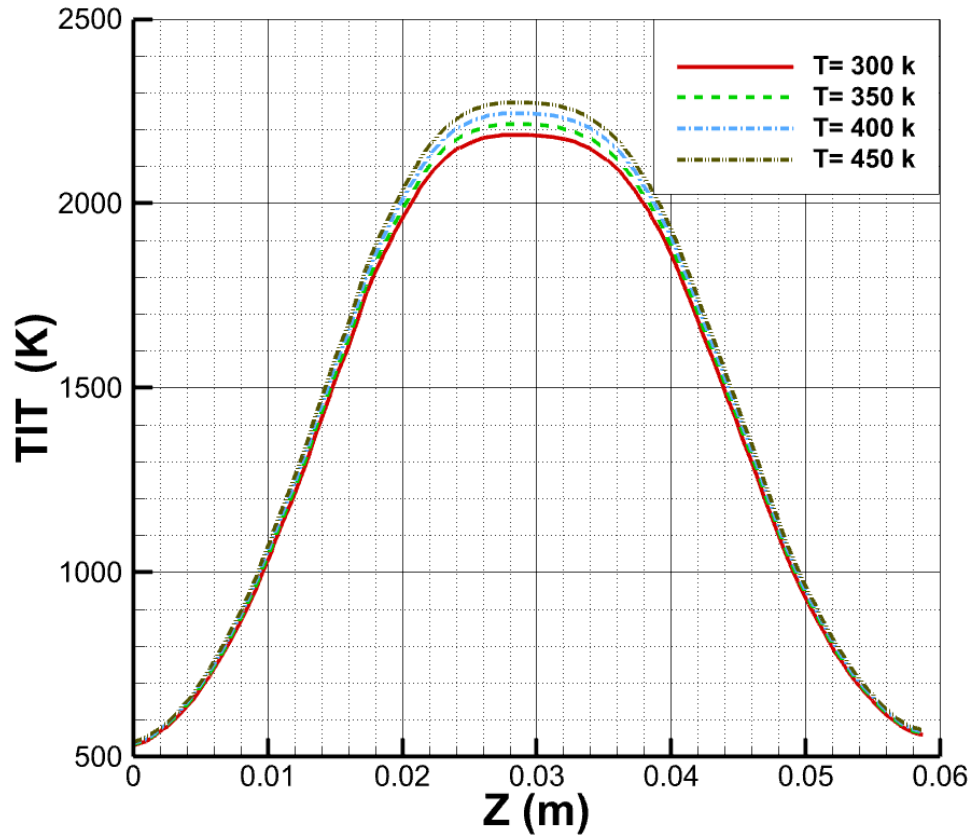


Figure 4.15 variation of TIT (temperature inlet turbine) for methane combustion at 85% rpm with different initial Temperature (A) $T= 300$ k, (B) $T= 350$ k, (C) $T= 400$ k, (D) $T= 450$ k

4.3.1.2 Velocity contour:

We will now present the variations in velocity resulting from changes in the preheat temperature. The corresponding data is summarized in the table below:

Table 4.2 variations in velocity resulting from changes in the preheat temperature of methane/air flames

Preheat Temperature (K)	Velocity [m/s]
300	71.56
350	72.4
400	73.25
450	74.12

The obtained results for the variation of velocity with different preheat temperatures, namely 300 K, 350 K, 400 K, and 450 K, are as follows: 71.56 m/s, 72.4 m/s, 73.25 m/s, and 74.12 m/s, respectively. These values indicate only a small difference between the velocities at different preheat temperatures.

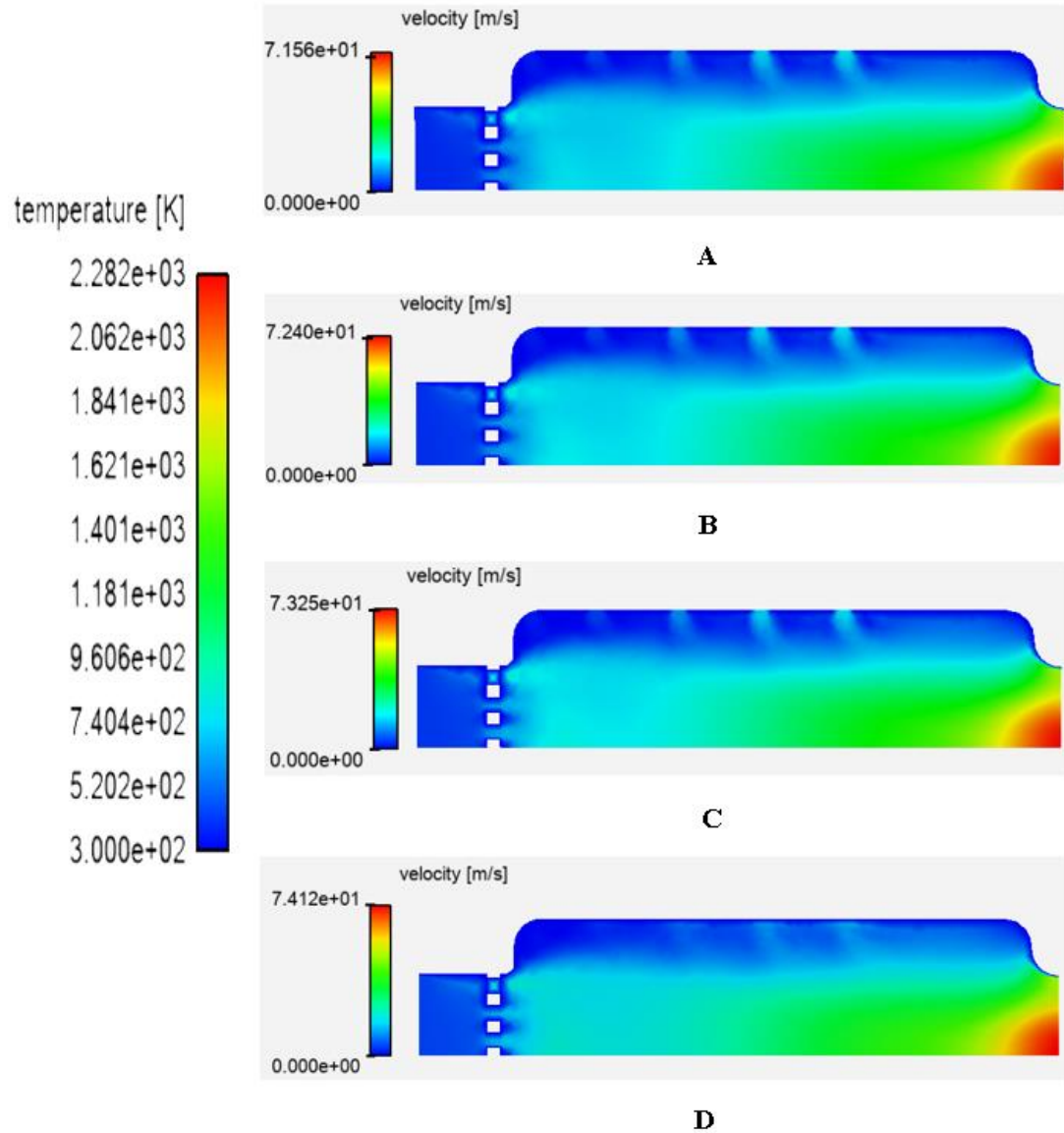


Figure 4.16 Longitudinal velocity contour for methane combustion at 85% rpm with different initial Temperature (A) $T= 300$ k, (B) $T= 350$ k, (C) $T= 400$ k, (D) $T= 450$ k

4.3.2 Effect of operating pressure on Combustion Performance and Characteristics:

In this section, we investigate the effect of operating pressure on the combustion process and its associated parameters. The operating pressure plays a significant role in

determining the performance, efficiency, and emission characteristics of combustion systems.

Higher operating pressures can lead to shorter ignition delays and faster flame speeds due to the increased reactivity of the reactants. However, the impact on flame stability can be more complex and may require further investigation [66], also higher pressures can lead to increased combustion efficiency and reduced pollutant emissions. However, the specific impact on emissions will depend on other factors such as air-to-fuel ratio, residence time, and mixing characteristics [67].

4.3.2.1 Temperature Contours:

This section presents the results obtained from the simulation of methane/air flames. The Methane/Air Flame Simulation Results revealed significant insights into the effect of operating pressure on the maximum temperature achieved within the combustion chamber. The table below displays the maximum temperature values obtained for different operating pressure: 1 atm, 3 atm, and 5 atm.

Table 4.3 the effect of operating pressure on the maximum temperature for methane/air flames

operating pressure [atm]	Temperature [K]
1	2194
3	2250
5	2283

At an operating pressure of 1 atm, the maximum temperature recorded was 2194 K. As the operating pressure increased to 3 atm, the maximum temperature rose slightly to 2250 K. Finally, at an operating pressure of 5 atm, the maximum temperature further increased to 2283 K.

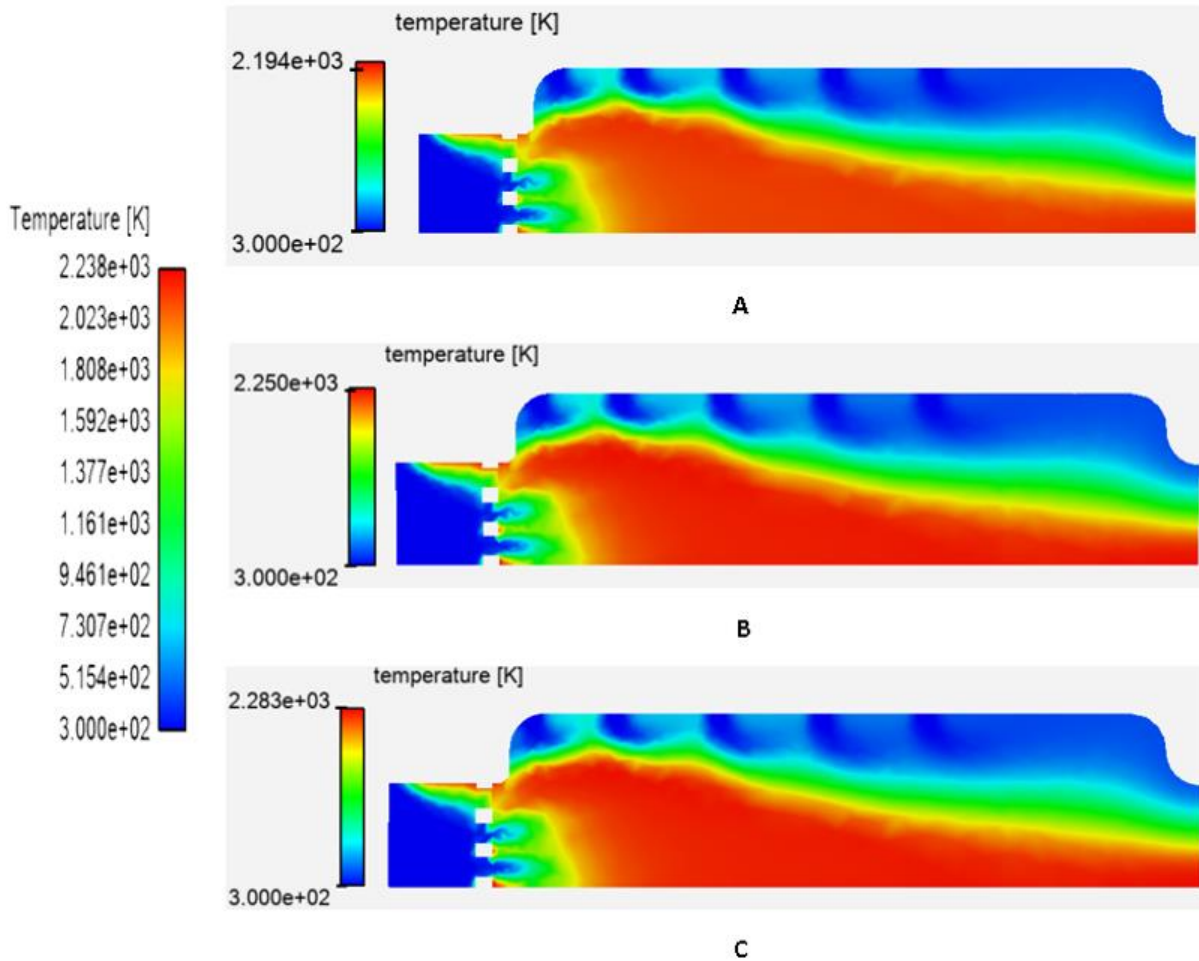


Figure 4.17 Longitudinal temperature contour for methane combustion at 85% rpm with different initial operating pressure (A) $P=1$ atm, (B) $P=3$ atm, (C) $P=5$ atm

These results demonstrate a clear correlation between operating pressure and maximum temperature in the methane/air flame. As the operating pressure increases, the maximum temperature also rises, indicating a more intense combustion process. The higher pressure allows for greater fuel-air mixing and facilitates more efficient combustion, resulting in elevated temperatures.

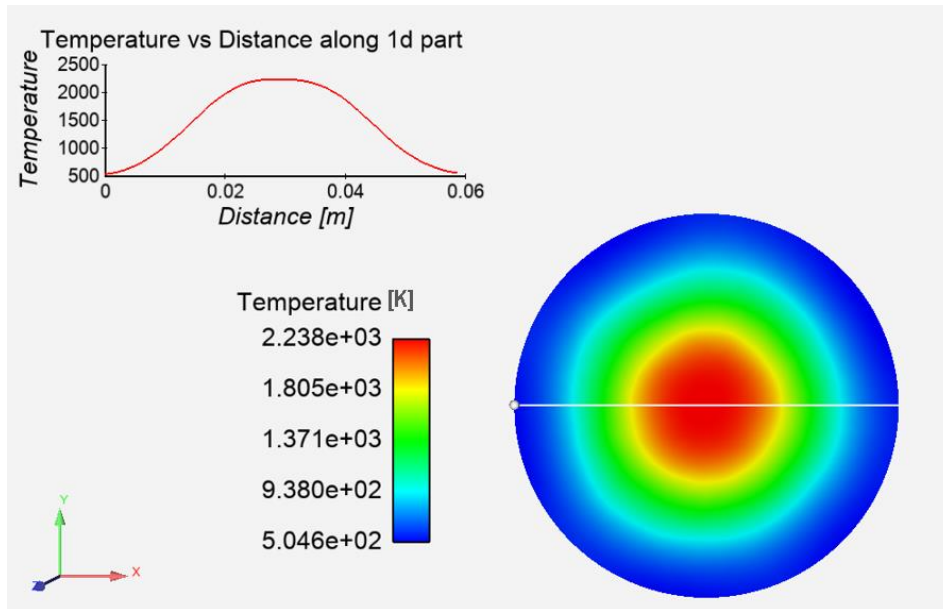


Figure 4.18 Transversal contour of Temperature inlet turbine (TIT) variation at $P= 3$ atm for methane/air flame

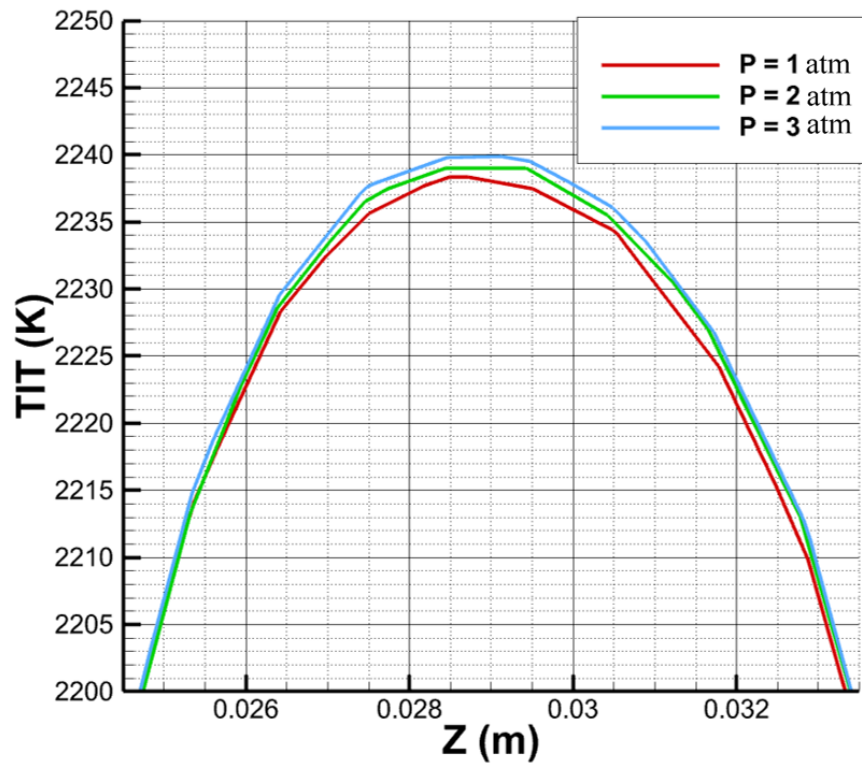


Figure 4.19 TIT variation chart for methane combustion at 85% rpm with different initial operating pressure (A) $P= 1$ atm, (B) $P= 3$ atm, (C) $P= 5$ atm

4.3.2.2 Velocity Contours:

The table below displays the maximum velocity values obtained for methane/air flames at different operating pressures of 1 atm, 3 atm, and 5 atm. The results indicate the impact of operating pressure on the combustion process and subsequent flow dynamics.

Table 4.4 the maximum velocity values obtained for methane/air flames at different operating pressures

operating pressure [atm]	Velocity [m/s]
1	72.37
3	24.14
5	14.48

At an operating pressure of 1 atm, the maximum velocity observed is 72.37 m/s. As the pressure increases to 3 atm, the maximum velocity decreases to 24.14 m/s, and further decreases to 14.48 m/s at 5 atm.

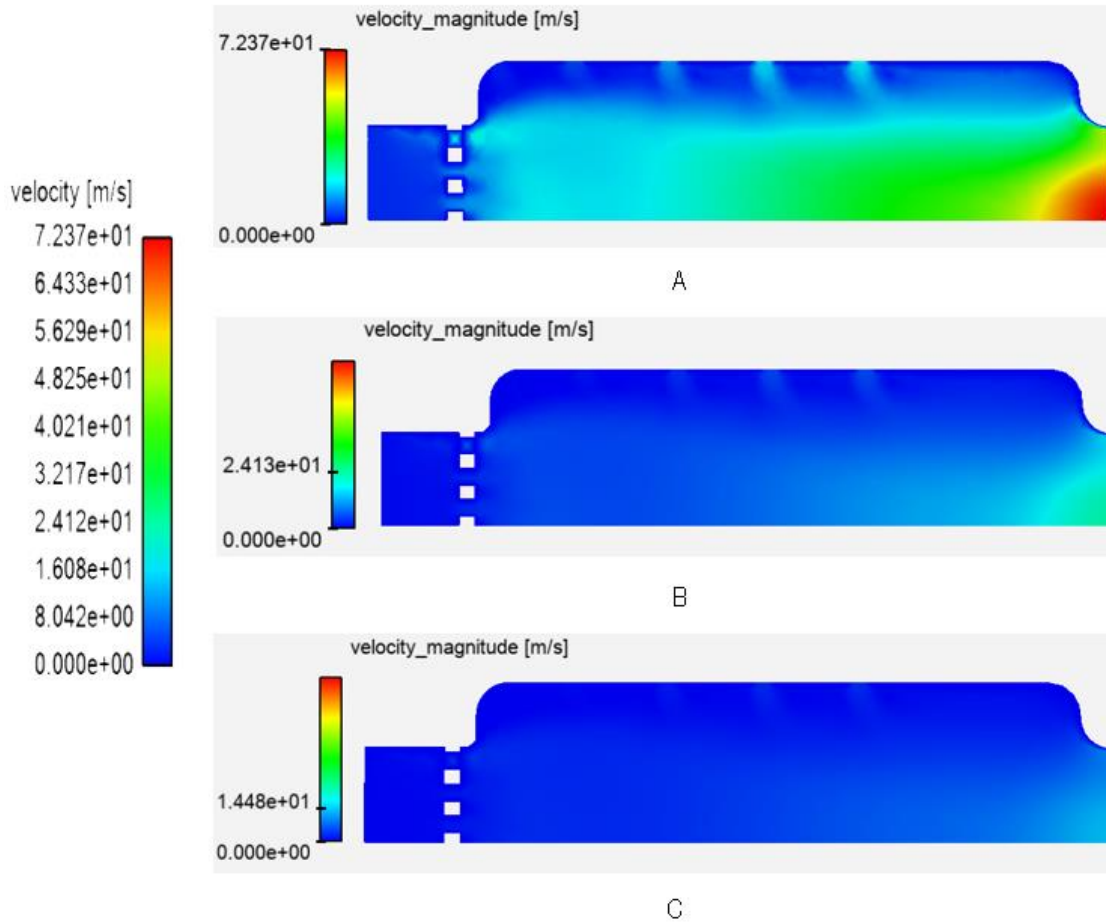


Figure 4.20 Longitudinal velocity contour for methane combustion at 85% rpm with different initial operating pressure (A) $P = 1 \text{ atm}$, (B) $P = 3 \text{ atm}$, (C) $P = 5 \text{ atm}$

Decrease in the maximum velocity of the combustion products is due to the fact that higher pressure causes increased gas density, resulting in a greater resistance to flow. As a consequence, the combustion products have to work against a higher-pressure gradient, reducing their velocity.

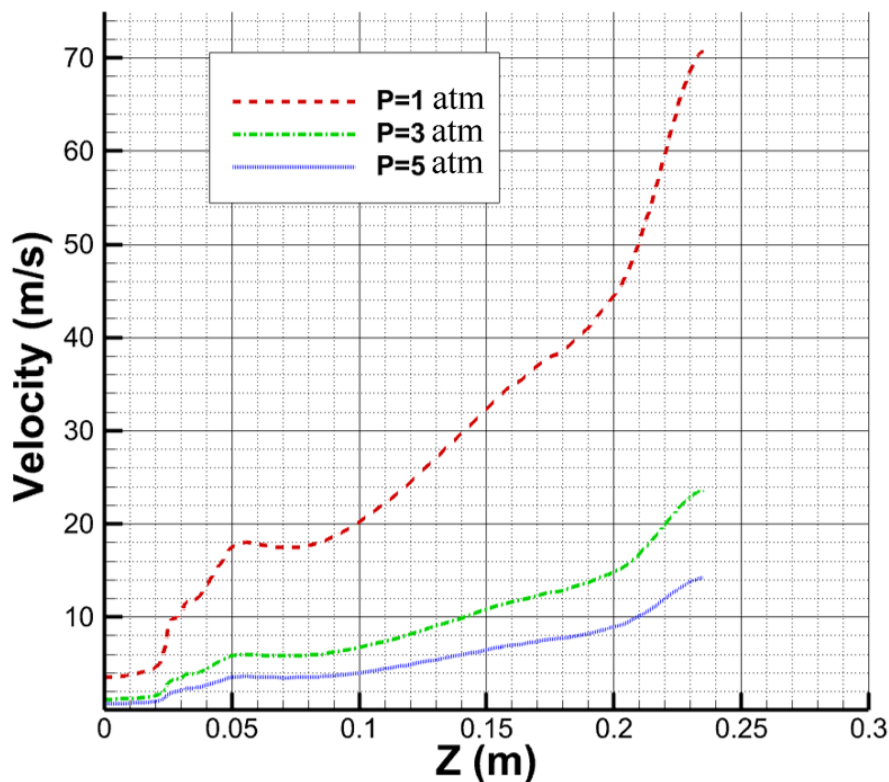


Figure 4.21 Velocity Variation chart at Different Operating Pressures for methane/air flame

4.3.2.3 Species variation:

The results obtained from the general reaction simulation for 1 atm pressure show variations in the mass fractions of different species along the combustion chamber. Initially, close to the inlet, the mass fractions of CH₄ (methane), O₂ (oxygen), CO₂ (carbon dioxide), and H₂O (water) are relatively constant.

As the combustion progresses, the mass fractions of CH₄ and O₂ start to decrease, while the mass fractions of CO₂ and H₂O increase. This behavior can be attributed to the consumption of CH₄ and O₂ during the combustion process, leading to the formation of CO₂ and H₂O as products.

As the flame moves further along the combustion chamber, the mass fraction of O₂ decreases significantly as it is consumed in the combustion process. However,

interestingly, the mass fraction of O₂ starts to increase again in certain regions of the chamber. This can be explained by the presence of holes in the chamber walls, allowing fresh air to enter the combustion chamber.

The fresh air entering through these holes leads to an increase in the mass fraction of O₂ as it mixes with the combustion products. Consequently, the increase in O₂ availability promotes further combustion reactions, resulting in a decrease in the mass fraction of CH₄.

The observed variations in the species mass fractions highlight the complex nature of the combustion process and the interactions between different species. The consumption of fuel (CH₄) and oxidizer (O₂) and the formation of combustion products (CO₂ and H₂O) are influenced by factors such as reaction kinetics, mixing, and transport processes within the combustion chamber.

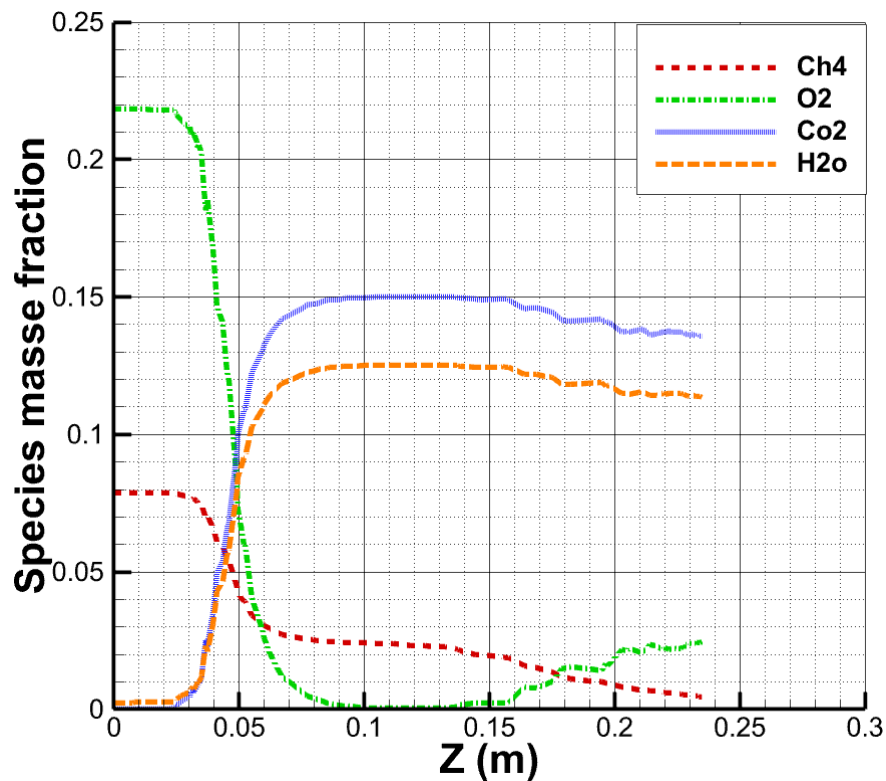


Figure 4.22 Mass fraction variation for different Species at POP= 1 atm, T= 300 k for methane/air flame

4.3.2.4 Turbulence intensity:

The longitudinal contour of turbulence intensity provides valuable insights into the flow characteristics and turbulence distribution within the combustion chamber. By analyzing the contour, several observations can be made regarding the turbulence intensity patterns in different sections of the geometry.

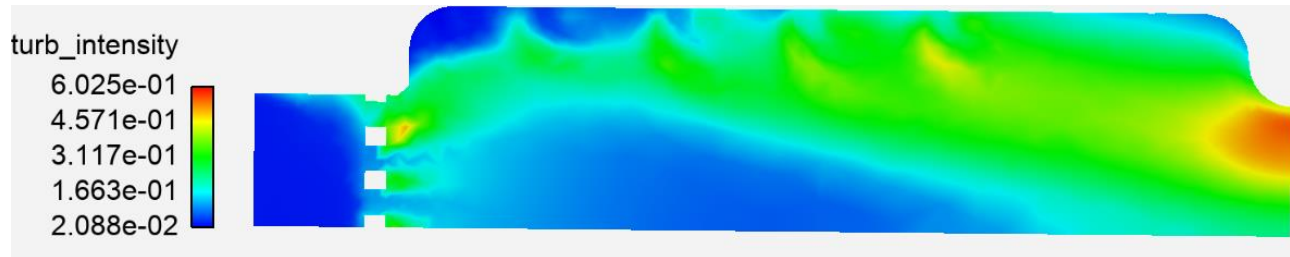


Figure 4.23 The Longitudinal contour of turbulence intensity at 1 atm Operating Pressure for methane/air flame

In the burner-up section, a small increase in turbulence intensity is observed close to the wall. This can be attributed to the frictional effects between the fluid and the wall surface. As the flow progresses towards the injection system, the turbulence intensity experiences a noticeable increase.

Moving into the flame holder section, which is a cylindrical chamber with converging and diverging ends, the turbulence intensity exhibits distinct features. Around the flame holder section, the turbulence intensity is observed to be higher, especially in the vicinity of the injection holes. This indicates that the injection system plays a significant role in enhancing turbulence levels due to the high-velocity jets entering the chamber. The periodic arrangement of 80 holes across the length and radial directions of the flame holder section further contributes to an increase in turbulence intensity. These holes promote additional mixing and flow disturbances, resulting in higher turbulence levels. Close to the outlet of the flame holder section, where the geometry diverges, the turbulence intensity further increases. This can be attributed to the acceleration and expansion of the flow, which intensify the turbulence levels in the vicinity.

4.4 Effects of Hydrogen Addition on Combustion:

In this section, we explore the influence of hydrogen addition on the combustion characteristics of methane/air flames using 4 step chemical mechanism [2] Our objective is to evaluate the effects of hydrogen on crucial aspects such as flame structure, temperature profiles, and species concentrations. The ultimate goal is to enhance the combustion efficiency of methane/air mixtures by leveraging the potential of hydrogen as an additive.

4.4.1 Temperature Contours:

In this section, we present the temperature contours obtained from conducting simulations to investigate the impact of different hydrogen percentages (0%, 5%, 15%, 25%, and 35%) on the combustion characteristics of methane/air flames at an operating pressure of 3 atm.

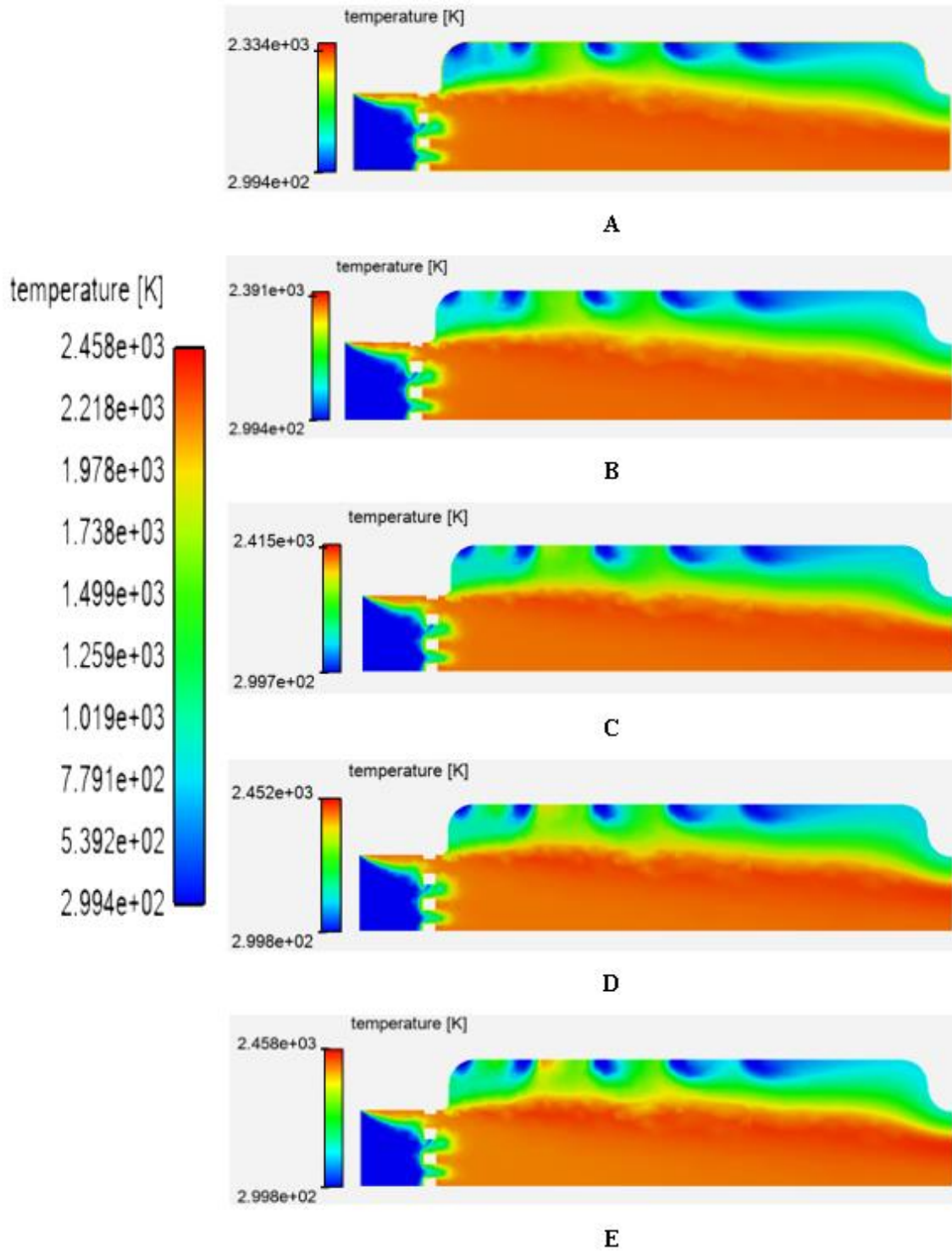


Figure 4.24 Longitudinal temperature contour for methane/hydrogen combustion at 85% rpm with 3 atm operating pressure (A) 0% H₂, (B) 5% H₂, (C) 25% H₂

Based on the analysis of the temperature contours, it is evident that the temperature increases with an increasing hydrogen percentage in the methane/air flames. This observation indicates that the addition of hydrogen has a direct impact on the combustion process, leading to higher temperatures.

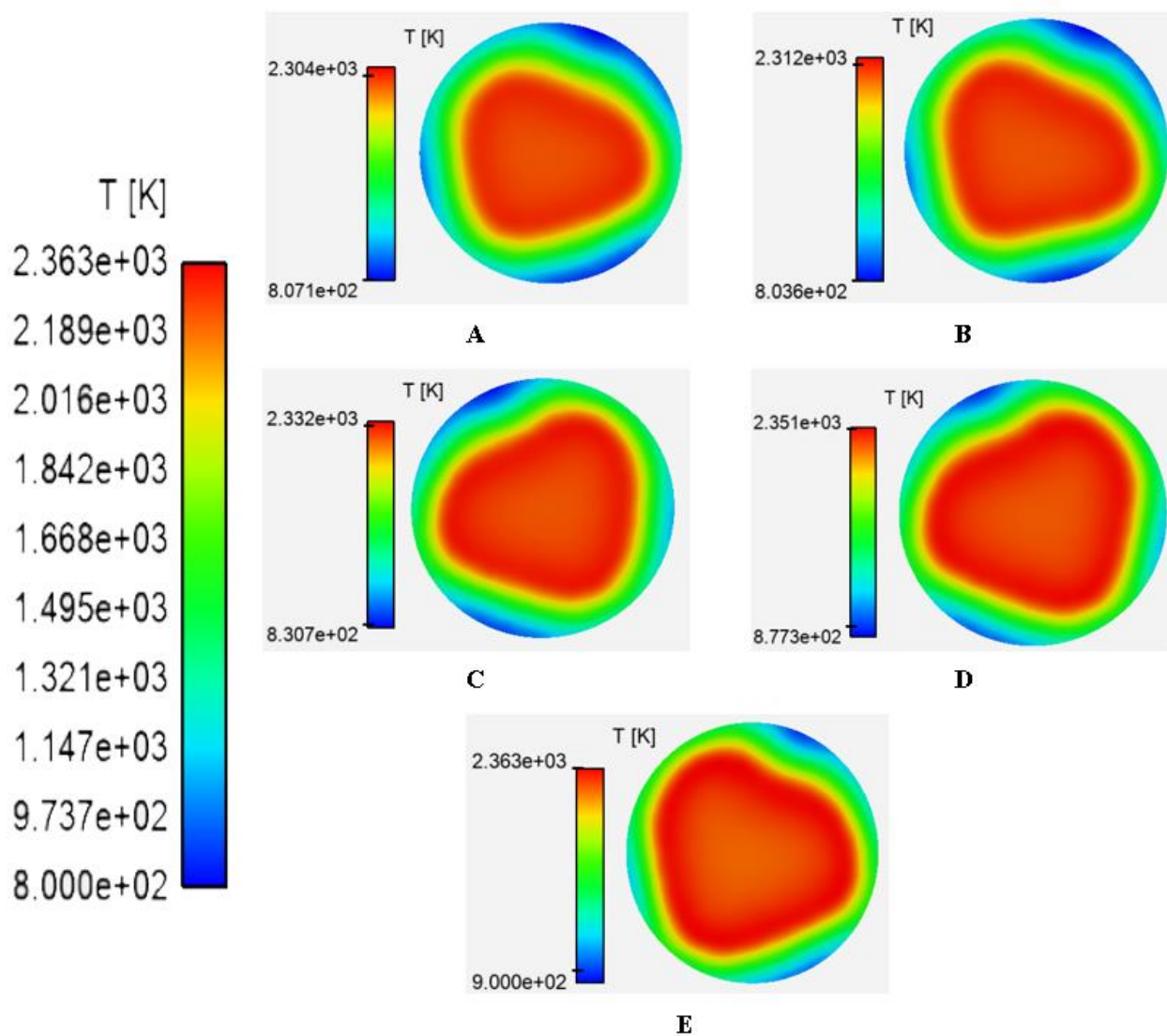


Figure 4.25 TIT contour for methane/hydrogen combustion at 85% rpm with 3 atm operating pressure (A) 0% H₂, (B) 5% H₂, (C) 25% H₂

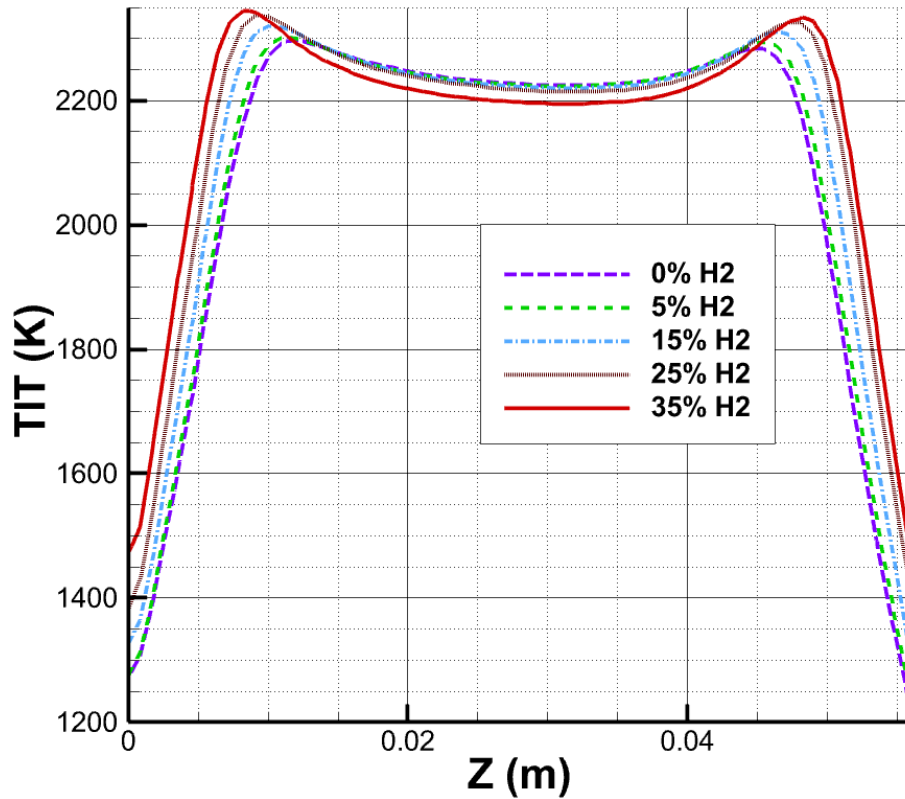


Figure 4.26 TIT variation chart for methane/hydrogen combustion at 85% rpm with 3 atm operating pressure (A) 0% H₂, (B) 5% H₂, (C) 25% H₂

As shown in Figure 26, we observed a decrease in the temperature of the inner layer of the flame, which is supported by the previous results obtained by previous studies [57].

4.4.2 Velocity contour:

In this section, we examine the velocity contours obtained from simulations aimed at exploring the influence of various hydrogen percentages (0%, 5%, 15%, 25%, and 35%) on the combustion characteristics of methane/air flames.

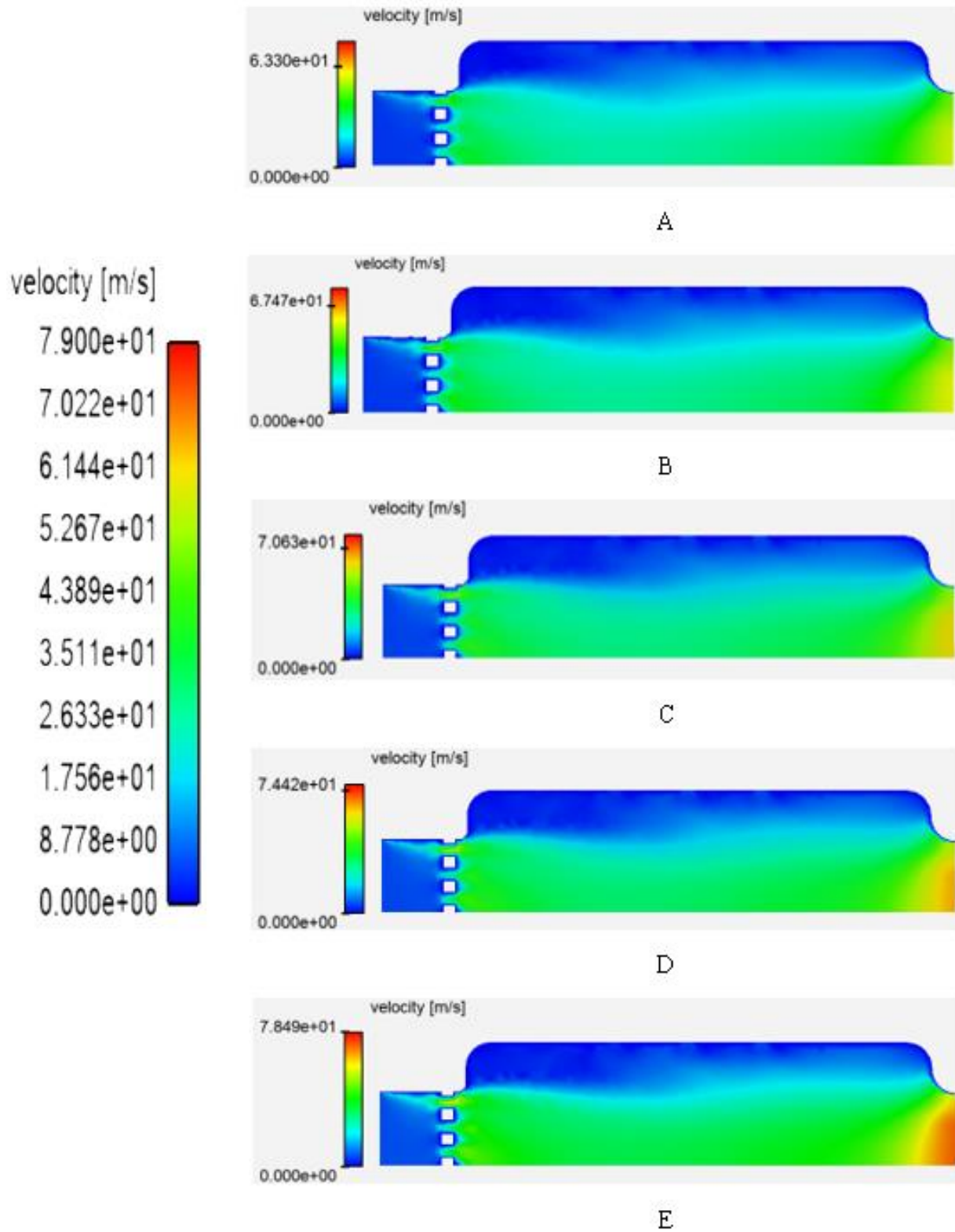


Figure 4.27 Longitudinal Velocity contour for methane/hydrogen combustion at 85% rpm with 3 atm initial operating pressure (A) 0% H₂, (B) 5% H₂, (C) 25% H₂

From the analysis of the velocity contours, it is evident that the velocity increases with the increasing percentage of hydrogen in the methane/air flames. As the hydrogen content is augmented, the flow dynamics within the combustion chamber undergo noticeable changes. The enhanced velocity distribution signifies improved air-fuel mixing and more vigorous combustion processes.

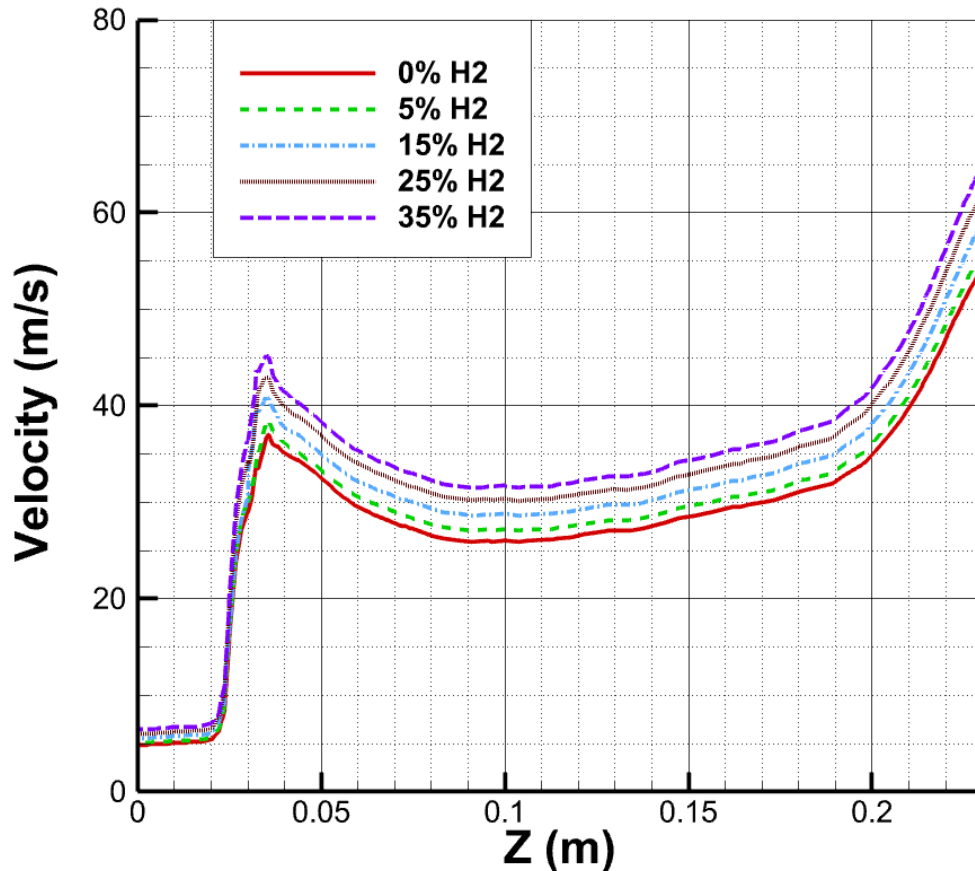


Figure 4.28 Longitudinal Velocity variation chart for methane/hydrogen combustion at 85% rpm with 3 atm initial operating pressure (A) 0% H₂, (B) 5% H₂, (C) 25% H₂

4.4.3 CO₂ Masse Fraction contours:

In this section, we analyze the CO₂ mass fraction contours obtained from simulations conducted to investigate the impact of different hydrogen percentages (0%, 5%, 15%, 25%, and 35%).

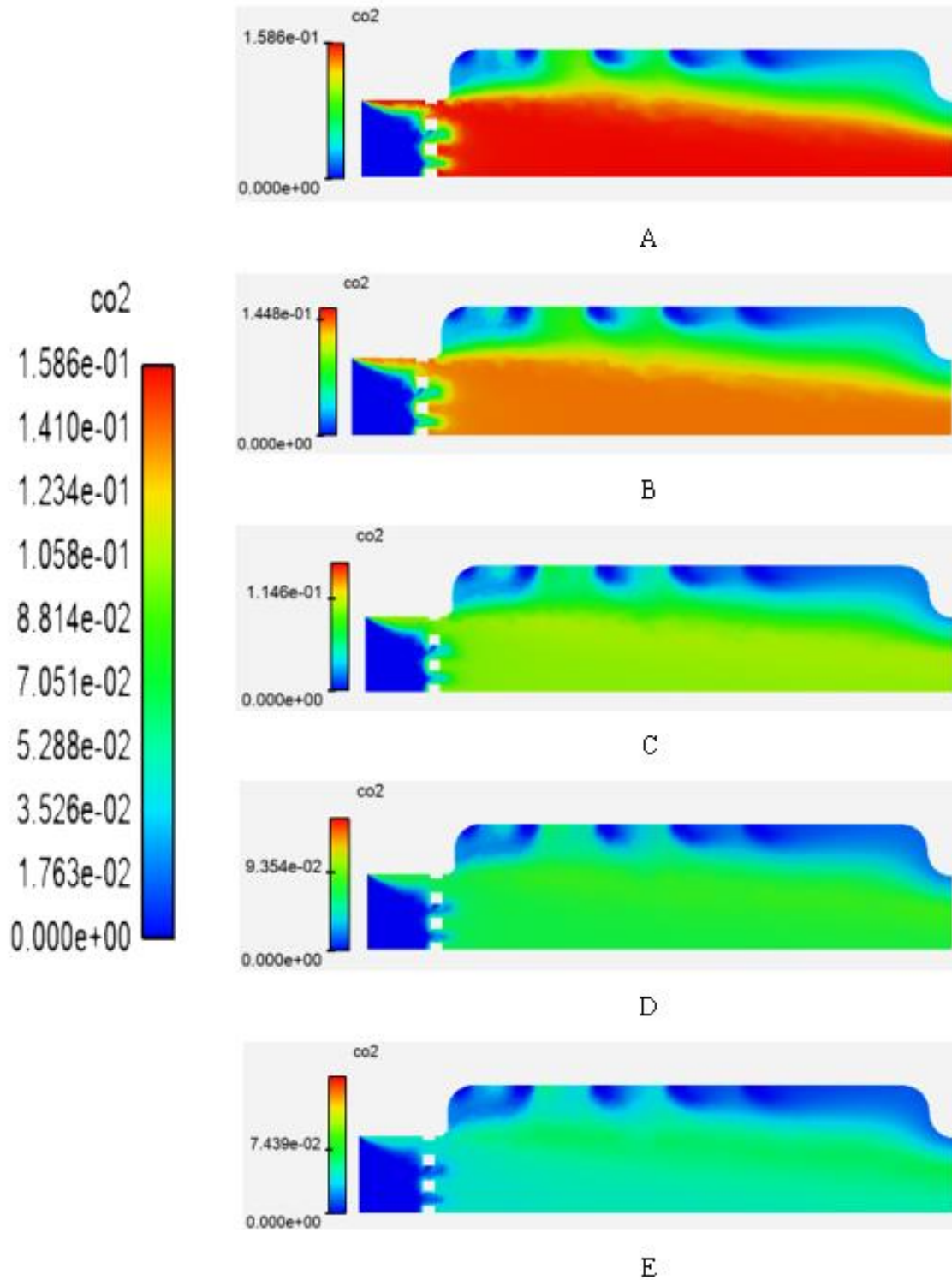


Figure 22.29 Longitudinal co_2 mass fraction contour for methane/hydrogen combustion at 85% rpm with 3 atm initial operating pressure (A) 0% H₂, (B) 5% H₂, (C) 25% H₂

These contours consistently show a significant reduction in CO₂ concentration as the percentage of hydrogen increases in methane/air flames. This decline can be attributed to the heightened reactivity of hydrogen, resulting in more complete combustion and a shift towards the formation of water vapor (H₂O) instead of CO₂. The inclusion of hydrogen in the fuel mixture enhances the combustion process, leading to better fuel utilization and decreased CO₂ emissions. These findings emphasize the potential of hydrogen addition in mitigating CO₂ emissions and promoting cleaner combustion in methane/air flame systems.

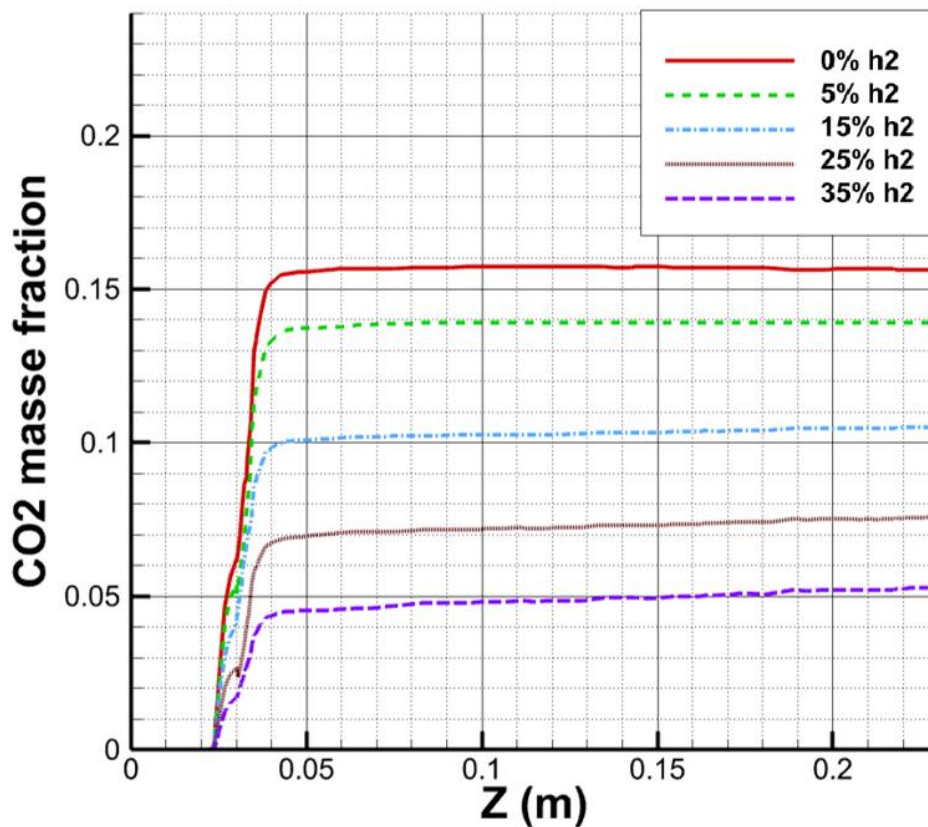


Figure 4.30 Co₂ masse fraction variation chart for methane/hydrogen combustion at 85% rpm with 3 atm initial operating pressure (A) 0% H₂, (B) 5% H₂, (C) 25% H₂

4.5 Comparison and validation of results:

In the present study, we aim to validate and compare the simulation results of kerosene/air flame with the reference article by Mohammad Golam Mostafa [6]. This validation process serves to assess the accuracy and reliability of our computational model and further enhance the credibility of our findings. We will specifically focus on comparing the temperature distribution, velocity profiles, and species mass fractions obtained from our simulations with the corresponding data reported in the reference article. This rigorous comparison will enable us to evaluate the agreement between our results and the established findings in the literature [60].

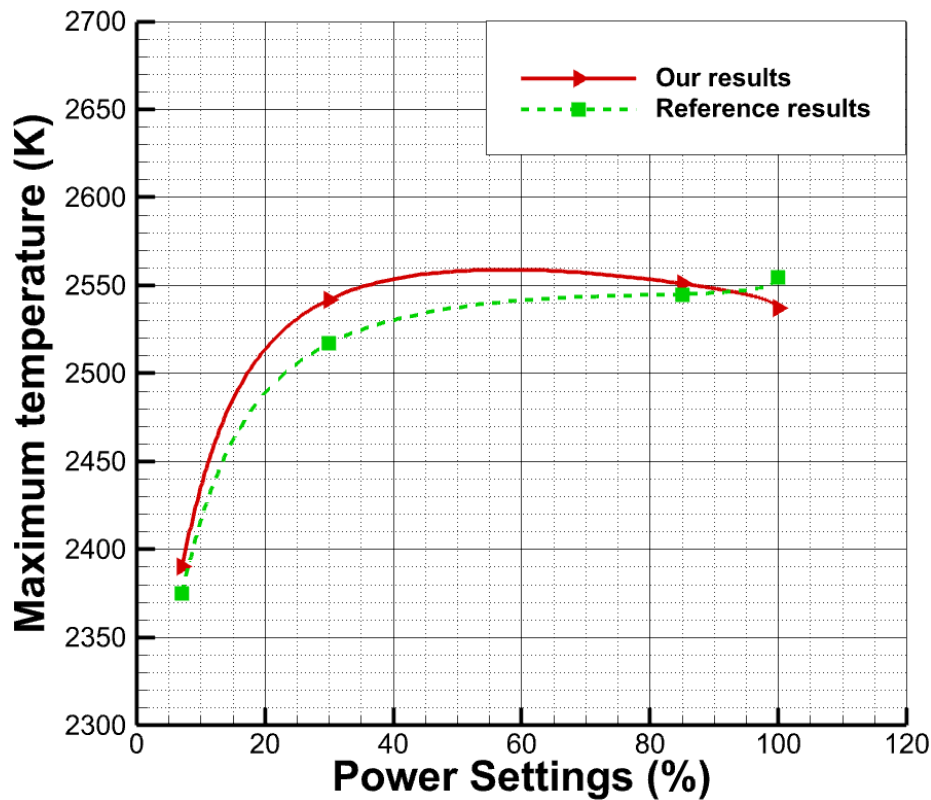


Figure 4.31 Maximum temperature variation at different power settings

The maximum temperature values obtained from the simulations for different power settings (7%, 30%, 85%, and 100%) were compared with the corresponding results from the reference study. The maximum error percentage for the maximum temperature is

approximately 0.9934%. This is a close agreement between the two sets of data, indicating that the simulations accurately captured the temperature distribution within the combustion system.

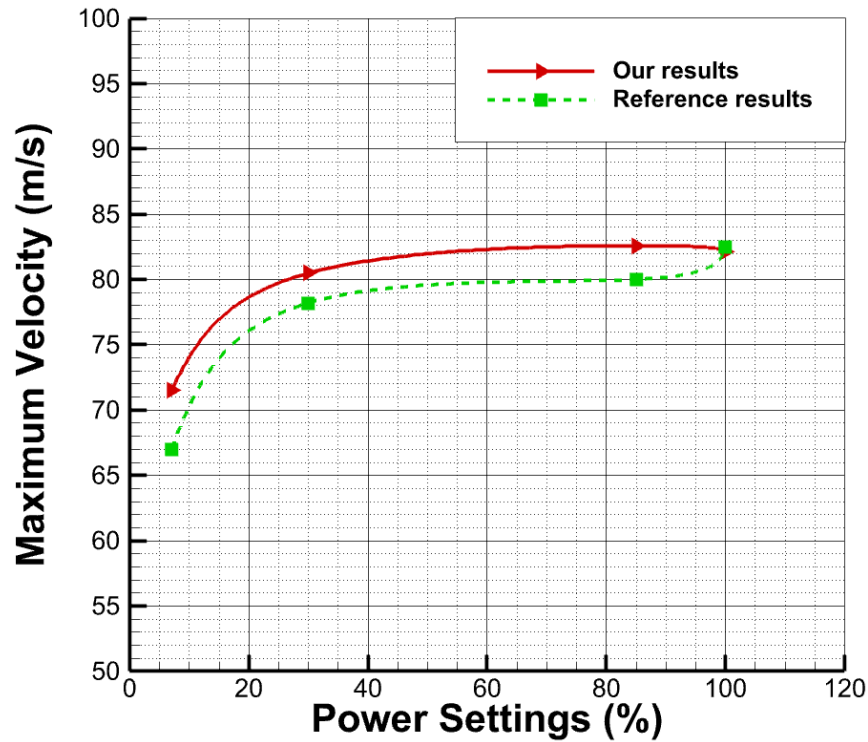


Figure 4.32 Maximum velocity variation at different power settings

The comparison between the maximum velocities obtained from our simulation results and the reference simulation provides valuable insights into the accuracy and agreement of our findings with maximum error percentage 6.64%. For most power settings, our simulation yields slightly higher velocities compared to the reference results. This observation suggests that our simulation captures the combustion dynamics adequately, resulting in enhanced fluid flow and increased velocity. However, it is noteworthy that for the 100% power setting, our simulation shows a slightly lower velocity than the reference data.

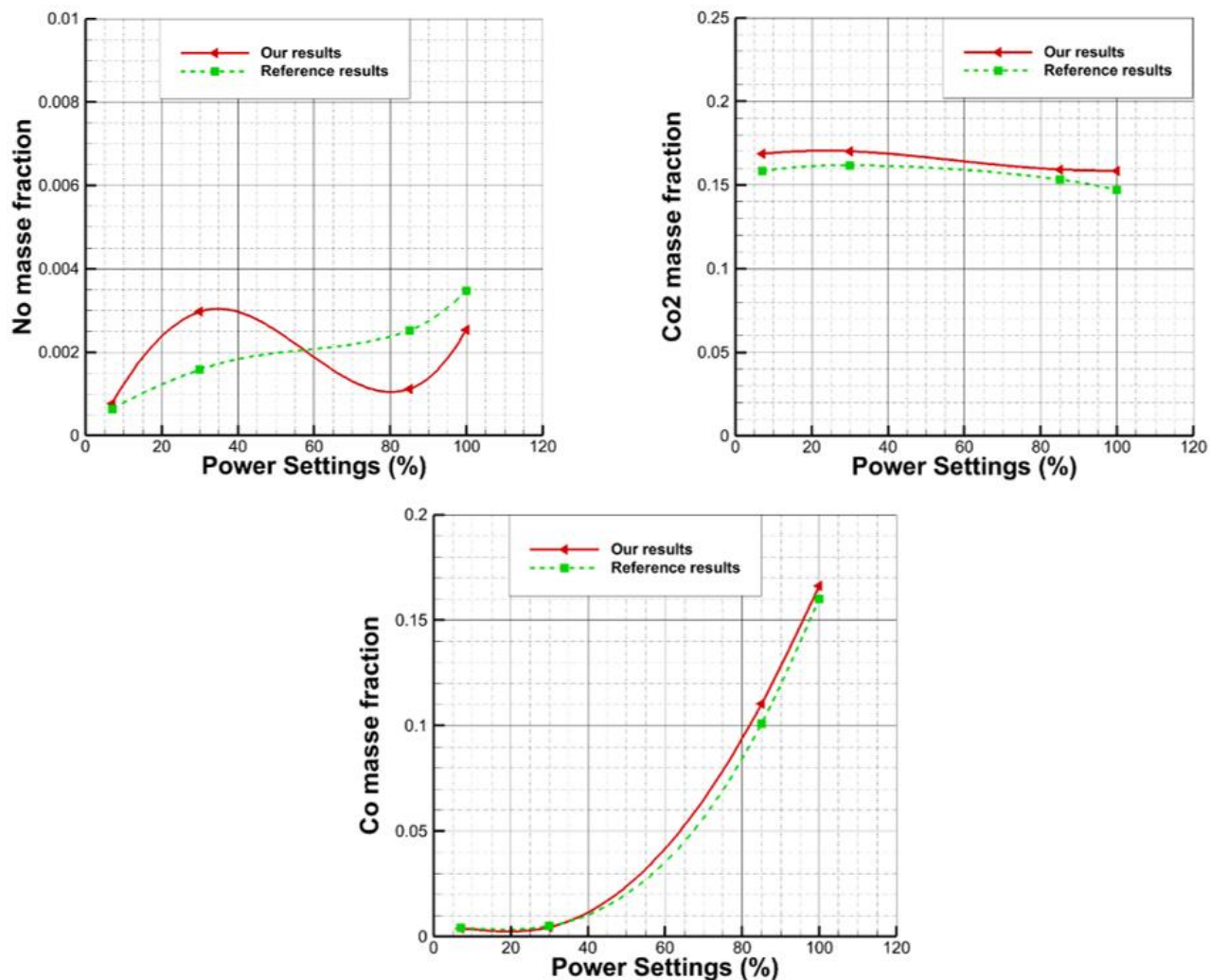


Figure 4.33 Maximum Species masse fraction variation at different power settings

The comparison between our simulation results and the reference simulation for the maximum mass fractions of NO, CO, and CO₂ demonstrates a high level of agreement, confirming the reliability and accuracy of our model in accurately representing the combustion characteristics. Across all power settings, our simulation closely aligns with the reference data, showcasing consistent trends and magnitudes of the species mass fractions. This strong agreement signifies that our simulation effectively captures the intricate chemical reactions and processes involved in pollutant formation within the combustion system.

In conclusion, the comparison and validation of our simulation results with the reference data have provided valuable insights into the accuracy and reliability of our model. The agreement observed in terms of maximum temperature, velocity, and species mass fractions between our simulation and the reference simulation indicates the robustness of our approach in capturing the combustion characteristics. This validation process instills confidence in the predictive capabilities of our model and highlights its ability to accurately simulate and analyze kerosene/air and methane/air flame systems. The findings further support the potential of hydrogen addition in promoting cleaner combustion and mitigating CO₂ emissions.

CONCLUSION

CONCLUSION

In conclusion, this research aimed to investigate the potential of replacing kerosene/air combustion with methane/air combustion, supplemented by the addition of hydrogen to enhance efficiency. The study was conducted in several stages, beginning with the simulation of kerosene/air flames using a reduced chemical mechanism and comparing the results with the reference study by Mohammad Golam Mostafa. The agreement between our simulation and the reference data validated the accuracy of our model, our simulation yielded maximum temperatures of 2390 K, 2542 K, 2551 K, and 2537 K for the respective power settings of 7%, 30%, 85%, and 100%. In the reference study, the corresponding maximum temperatures were reported as 2375 K, 2517 K, 2545 K, and 2554.5 K. The comparison revealed a remarkable consistency, with a maximum error percentage for the maximum temperature of only 0.9934%.

Moving forward, the focus shifted to simulating methane/air flames using a general equation incorporating the eddy dissipations model. Two specific studies were conducted to explore the effects of operating pressure and preheat temperature on methane/air combustion.

The preheat temperature studies conducted for methane/air flames at 1 atm operating pressure provided valuable insights into the combustion behavior. The simulations were performed with initial temperatures of 300 K, 350 K, 400 K, and 450 K, resulting in maximum temperatures of 2194 K, 2223 K, 2250 K, and 2282 K, respectively. Comparing these results with the kerosene/air simulations, a noticeable reduction of approximately 10-15% in the maximum temperature values was observed. This observation aligns with the findings presented in the reference article "A study on the effects of air preheat on the combustion and heat transfer characteristics of Bunsen flames" by Zhang, et al. (2017) "[68], which supports the validity of our work.

Furthermore, the operating pressure studies revealed interesting findings regarding the maximum velocity. For an operating pressure of 5 atm and an initial temperature of 300

CONCLUSION

K, the simulation yielded a maximum velocity of 14.48 m/s. Comparing this result with the reference article by Rolf Reitz [49], who obtained a laminar velocity of 12 m/s under the same boundary conditions, further validates the accuracy of our simulation.

Finally, the investigation extended to methane/hydrogen/air flames using a 4-step mechanism, with variations in the percentage of hydrogen in the mixture. The aim was to assess the influence of hydrogen addition on combustion performance, efficiency, and pollutant emissions. The simulation results yielded valuable insights into the impact of hydrogen supplementation on temperature profiles, velocity distribution, and species mass fractions.

The findings revealed that increasing the hydrogen percentage in the mixture led to an increase in flame velocity, indicating enhanced combustion kinetics. Moreover, the introduction of hydrogen resulted in higher flame temperatures, attributed to hydrogen's higher reactivity and its contribution to the overall combustion process. Additionally, it was observed that the flame thickness increased with higher hydrogen percentages.

Specifically, the maximum temperature varied from 2334 K for 0% H₂ to 2458 K for 35% H₂, while the velocity ranged from 63.3 m/s to 78.49 m/s. These results can be supported by the reference article by Andrea Unich [50].

Furthermore, comparing these results with the kerosene/air simulations at 7% power settings (where $T=2390$ K and $V=71.49$ m/s), it is evident that the methane/hydrogen/air flames exhibit higher maximum temperatures and velocities. This comparison highlights the potential of hydrogen addition in promoting cleaner combustion, improving combustion performance, and reducing CO₂ emissions in methane/hydrogen/air flame systems.

OUTLOOK

In the future, several areas of research can be explored to further enhance our understanding of combustion processes and the potential benefits of hydrogen supplementation. Some suggestions for future research include:

Optimization of Hydrogen Addition: Conduct optimization studies to determine the optimal hydrogen percentage for achieving the desired combustion performance and emission reduction. This can involve exploring a wider range of hydrogen percentages and their effects on flame characteristics, efficiency, and pollutant formation.

Impact of Hydrogen Fuel Composition: Investigate the influence of different hydrogen fuel compositions on combustion performance and emissions. This can include variations in the purity of hydrogen, impurities in the hydrogen source, or the addition of other alternative fuels alongside hydrogen.

Environmental Impact Assessment: Conduct comprehensive environmental impact assessments to evaluate the overall environmental benefits and drawbacks of transitioning from kerosene/air combustion to methane/air or methane/hydrogen/air combustion. Assessments can include life cycle analysis, carbon footprint calculations, and comparisons of pollutant emissions.

Integration of Renewable Hydrogen: Explore the integration of renewable hydrogen sources, such as electrolysis using renewable electricity, into the combustion system. Investigate the impact of using renewable hydrogen on combustion performance, emissions, and overall sustainability.

Combustion Chamber Design Optimization: Investigate the impact of different combustion regimes on turbine design and performance. Optimize turbine design parameters, such as blade geometry and cooling techniques, to maximize the efficiency and durability of the turbine in methane/air or methane/hydrogen/air combustion systems.

APPENDIX

APPENDIX A: BOUNDARY CONDITIONS

1. Kerosene/air:

Table A.1 Flow variables for 7% engine power setting, operating pressure 357171 Pa and inlet temperature 492.6 K

Boundary	Flow Rate, kg/s	O₂ mass fraction	H₂O (v) mass fraction	C₁₂H₂₃ mass fraction
primary-inlet	0.00217	0.2135	0.0025	0.0691
hole-01	0.00039	0.2294	0.0027	--
hole-02	0.00097	0.2294	0.0027	--
hole-03	0.00203	0.2294	0.0027	--
hole-04	0.00300	0.2294	0.0027	--
hole-05	0.00329	0.2294	0.0027	--

Table A.2 Flow variables for 30% engine power setting, operating pressure 852447 Pa and inlet temperature 635.36 K.

Boundary	Flow Rate, kg/s	O₂ mass fraction	H₂O (v) mass fraction	C₁₂H₂₃ mass fraction
primary-inlet	0.00518	0.2137	0.0017	0.0691
hole-01	0.00096	0.2296	0.0019	--
hole-02	0.00241	0.2296	0.0019	--
hole-03	0.00505	0.2296	0.0019	--
hole-04	0.00746	0.2296	0.0019	--
hole-05	0.00818	0.2296	0.0019	--

Table A.3 Flow variables for 85% engine power setting, operating pressure 1850144 Pa and inlet temperature 776.55 K.

Boundary	Flow Rate, kg/s	O₂ mass fraction	H₂O (v) mass fraction	C₁₂H₂₃ mass fraction
primary-inlet	0.01092	0.2096	0.0024	0.0863
hole-01	0.00179	0.2294	0.0027	--
hole-02	0.00449	0.2294	0.0027	--
hole-03	0.00942	0.2294	0.0027	--
hole-04	0.01391	0.2294	0.0027	--
hole-05	0.01525	0.2294	0.0027	--

Table A.4 Flow variables for 100% engine power setting, operating pressure 1943008 Pa and inlet temperature 784.39K.

Boundary	Flow Rate, kg/s	O₂ mass fraction	H₂O (v) mass fraction	C₁₂H₂₃ mass fraction
primary-inlet	0.01075	0.2059	0.0017	0.1030
hole-01	0.00182	0.2296	0.0027	--
hole-02	0.00454	0.2296	0.0027	--
hole-03	0.00954	0.2296	0.0027	--
hole-04	0.01409	0.2296	0.0027	--
hole-05	0.01545	0.2296	0.0027	--

2. Methane/air flame:

a- Preheat temperature effect study:

Table A.5 Flow variables for Preheat temperature effect study, the operating pressure 101325 Pa and four different preheat temperatures are considered: 300 K, 350 K, 400 K, and 450 K.

Boundary	Flow Rate, kg/s	O₂ mass fraction	H₂O (v) mass fraction	CH₄ mass fraction
primary-inlet	0.01092	0.2096	0.0024	0.0789
hole-01	0.00179	0.2294	0.0027	--
hole-02	0.00449	0.2294	0.0027	--
hole-03	0.00942	0.2294	0.0027	--
hole-04	0.01391	0.2294	0.0027	--
hole-05	0.01525	0.2294	0.0027	--

b- Operating pressure effect study:

Table A.6 Flow variables for operating pressure effect study, the inlet temperature 300 K and three different operating pressure are considered: 1 atm, 3 atm, 5 atm.

Boundary	Flow Rate, kg/s	O ₂ mass fraction	H ₂ O (v) mass fraction	CH ₄ mass fraction
primary-inlet	0.01092	0.2096	0.0024	0.0789
hole-01	0.00179	0.2294	0.0027	--
hole-02	0.00449	0.2294	0.0027	--
hole-03	0.00942	0.2294	0.0027	--
hole-04	0.01391	0.2294	0.0027	--
hole-05	0.01525	0.2294	0.0027	--

3. Methane/air/hydrogen study:

Table A.7 Flow variables for methane/air/hydrogen study, the inlet temperature 300 K and the operating pressure is 3 atm.

Boundary	Flow Rate, kg/s	O ₂ mass fraction	H ₂ O (v) mass fraction
primary-inlet	0.01092	0.2096	0.0024
hole-01	0.00179	0.2294	0.0027
hole-02	0.00449	0.2294	0.0027
hole-03	0.00942	0.2294	0.0027
hole-04	0.01391	0.2294	0.0027
hole-05	0.01525	0.2294	0.0027

Table A.8 CH₄, H₂ masse fractions variation for different hydrogen percentages.

H ₂ percentage	CH ₄ masse fraction	H ₂ masse fraction
0%	0.0789	0
5%	0.074955	0.003945
15%	0.067065	0.011835
25%	0.059175	0.019725
35%	0,051285	0.027615

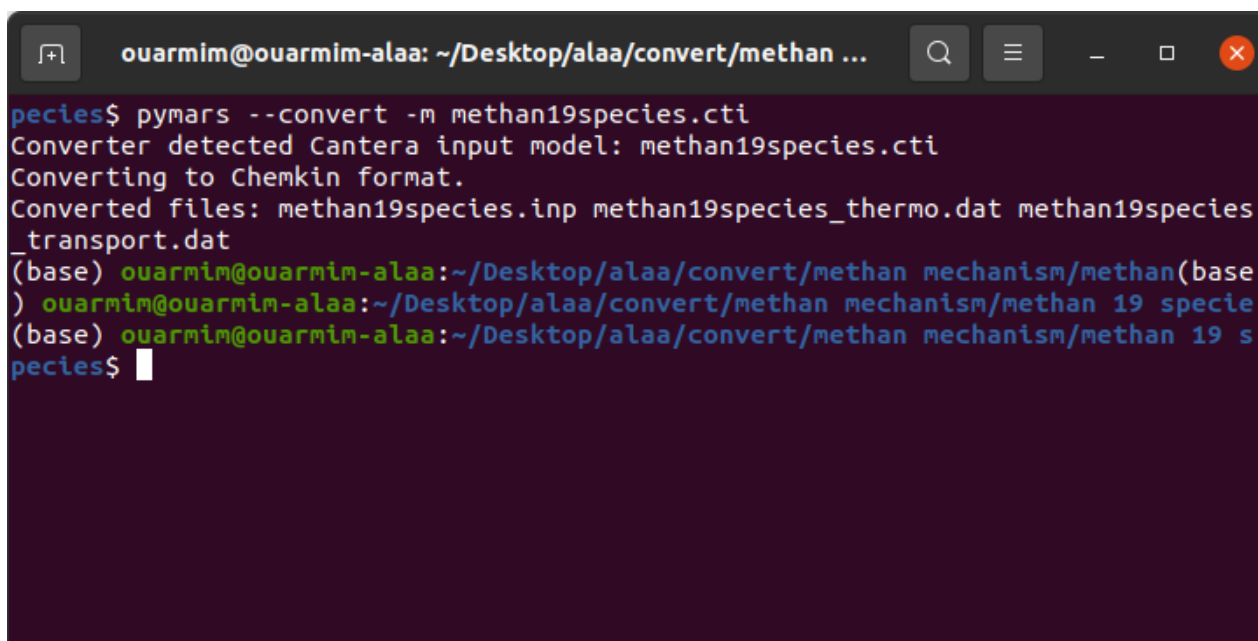
APPENDIX B: CHEMKIN PROCEDURES

Cantera (.CTI) To Chemkin (.DAT) File Conversion Procedure:

In the context of converting Cantera files into Chemkin format, which is something that we had to do in a stage of our thesis preparation, it is needed to follow the next steps:

- Add Pymars by following the instructions in the following web page: (<https://niemeyer-research-group.github.io/pyMARS/>).
- Input the next command: (pymars --convert -m model.cti).

This procedure will convert the CTI file into Chemkin format, the Linux Ubuntu OS was used for this conversion.



```
ouarmim@ouarmim-alaa: ~/Desktop/alaah/convert/methan ...
species$ pymars --convert -m methan19species.cti
Converter detected Cantera input model: methan19species.cti
Converting to Chemkin format.
Converted files: methan19species.inp methan19species_thermo.dat methan19species_transport.dat
(base) ouarmim@ouarmim-alaa:~/Desktop/alaah/convert/methan mechanism/methan
) ouarmim@ouarmim-alaa:~/Desktop/alaah/convert/methan mechanism/methan 19 specie
(base) ouarmim@ouarmim-alaa:~/Desktop/alaah/convert/methan mechanism/methan 19 s
pecies$
```

Figure A.1 Conversion process

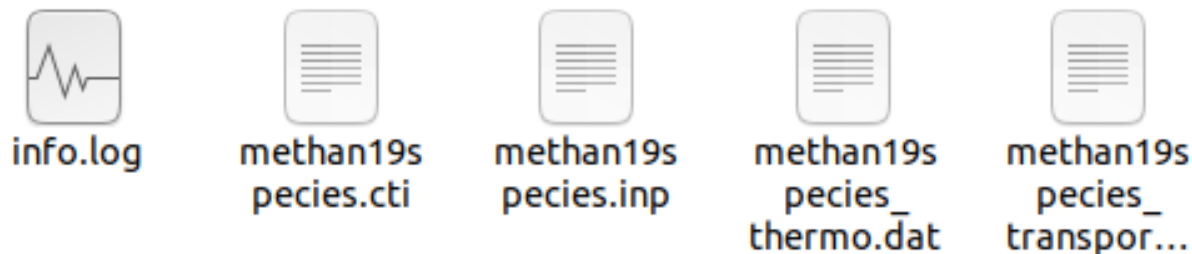


Figure A.2 Converted Chemkin files

Reducing Chemkin Mechanism:

One of the most popular ways to reduce Chemkin mechanisms is to use Chemkin Pro Software, which is a chemical kinetics simulator that models idealized reacting flows and provides insights into results before production testings, the software includes a wide range of tools for analyzing reaction kinetics, thermodynamic properties, and transport phenomena, and can be used to model complex chemical systems with thousands of species and reactions.

In order to reduce a chosen Chemkin mechanism (GRI-3 model for example), the following main steps are followed:

- 1) After installing Chemkin Pro to your device, open the software “ANSYS Chemkin” then create a new project;

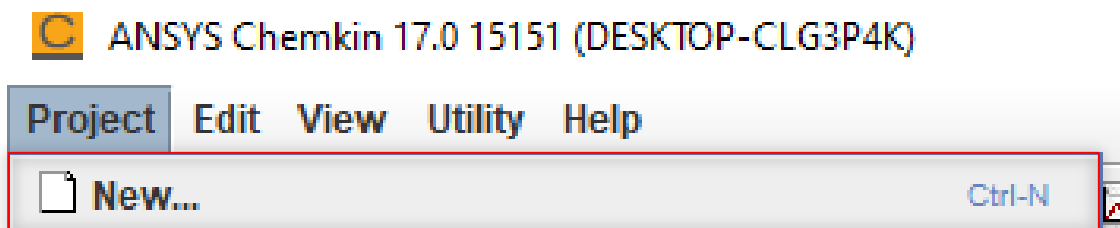


Figure A.3 Creating New Project

- 2) In ‘Diagram View’ choose ‘Models’ to create the system that simulate our project, then click ‘Update Project’.

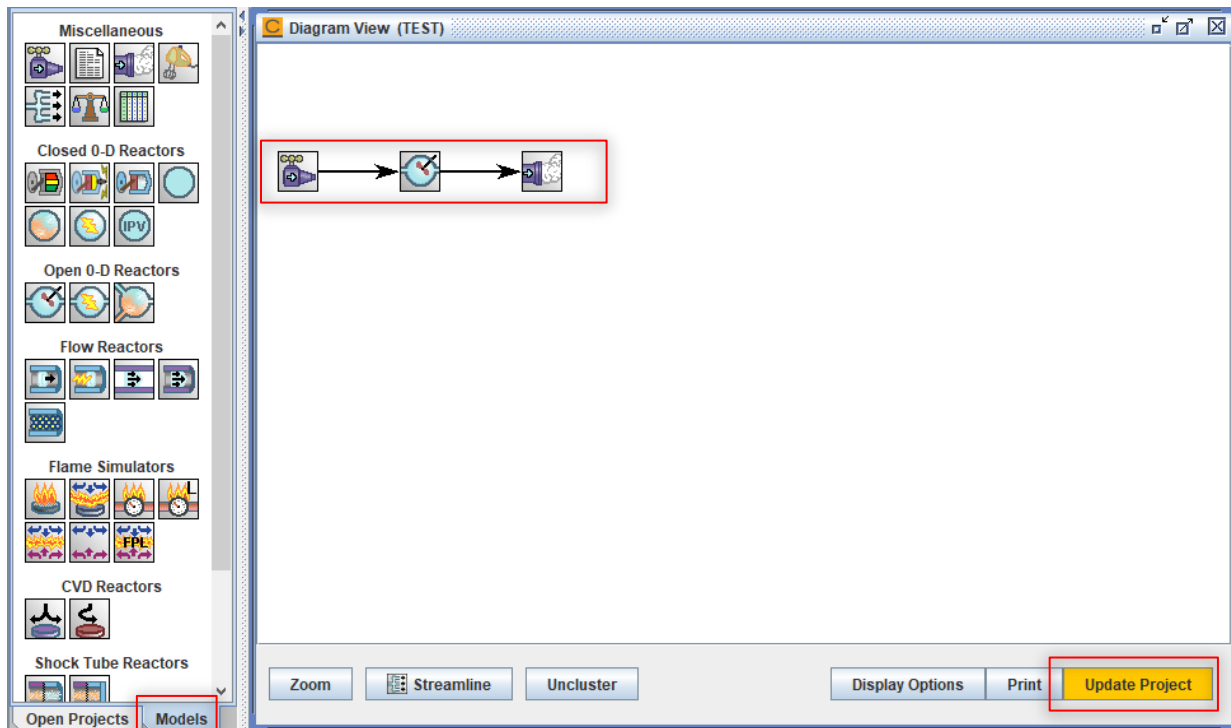


Figure A.4 Diagram view and set-up

- 3) We have chosen Inlet-Reactor-Outlet system for simulating the combustion chamber (some of the next steps may change if the system is different), in Pre-Processing we choose 'New Chemistry Set', then we input the master mechanism files then we save the '.ckprj' file in the desired location, then we click on 'Run Pre-Processor'.

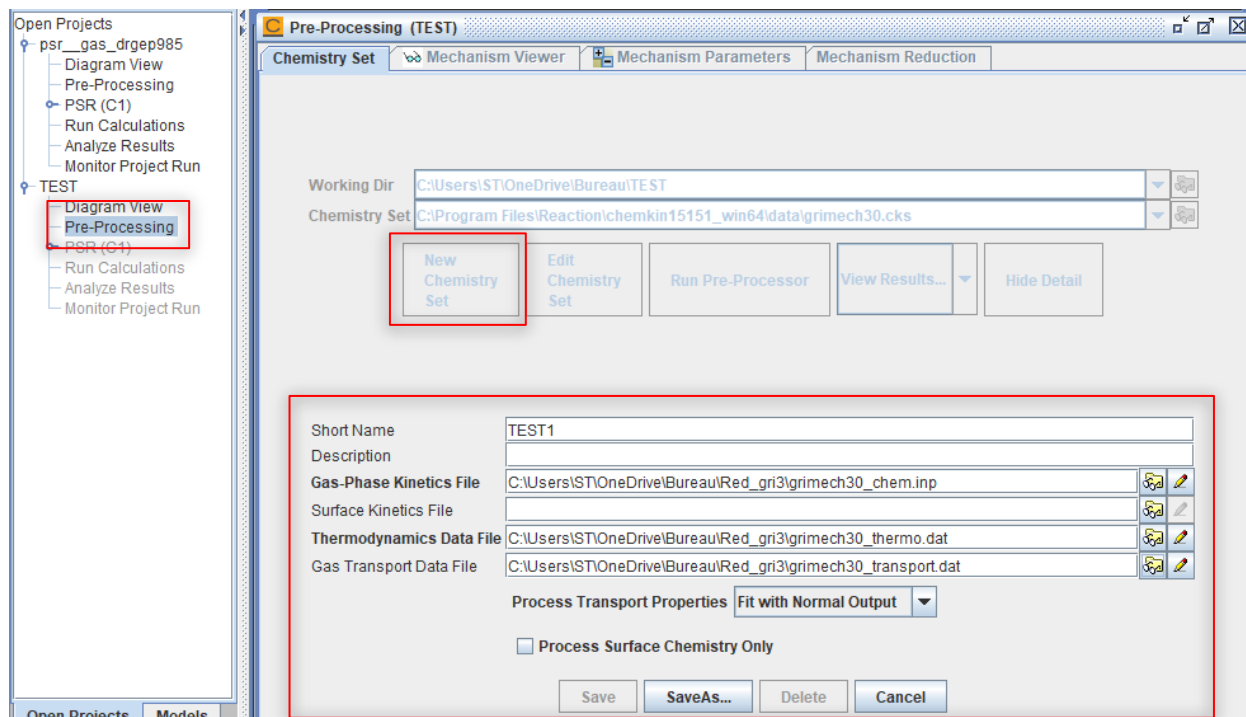


Figure A.5 Pre-Processing data entry

- 4) After choosing C1_PSR In PSR (C1), we enter the preferred data and parameters in the Reactor Physical Properties in addition to Species-specific Properties;

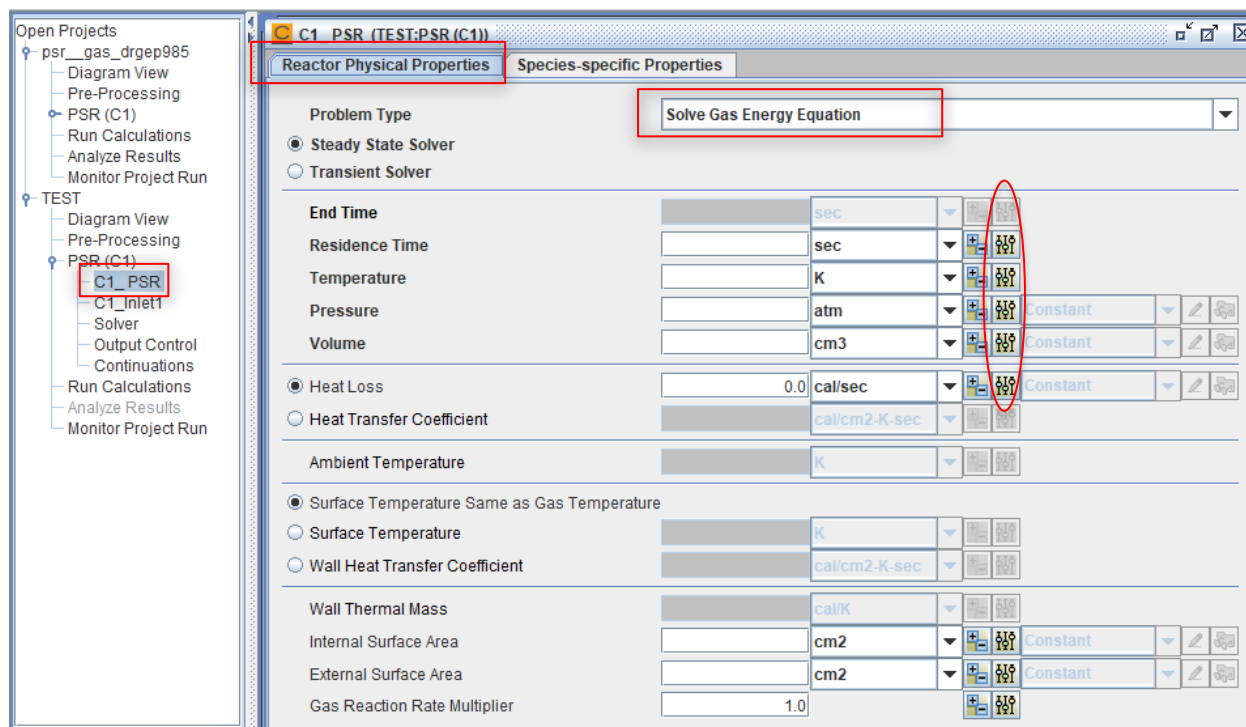


Figure A.6 PSR configuration

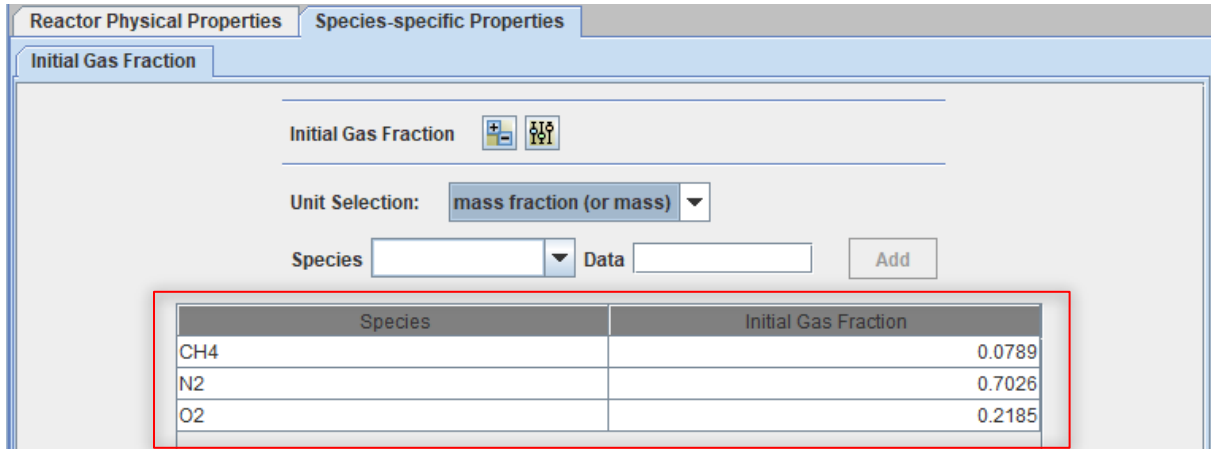


Figure A.7 Species data entry

- We can set-up a parameter study in the ellipse surrounded zone shown in figure 31.

5) After that we click on the ‘ANSYS Reaction Workbench’ icon then we choose “Start Mechanism Reduction” to start the reduction process;

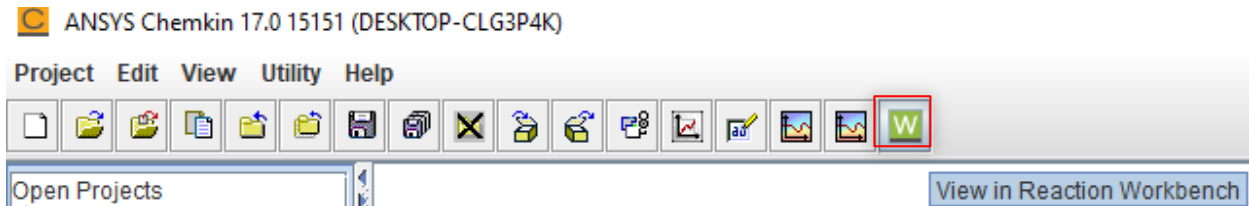


Figure A.8 Ansys Reaction Workbench selection

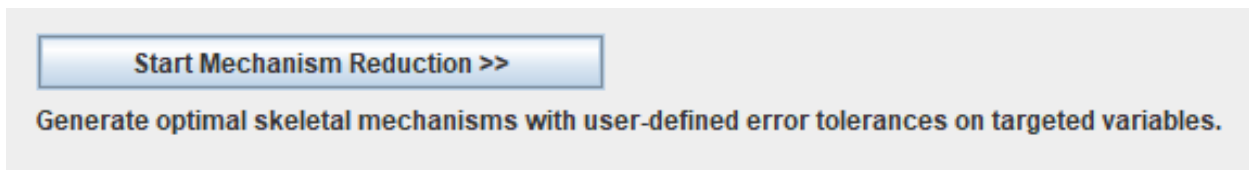


Figure A.9 Choosing Start Mechanism Reduction

6) In ‘Operation Setup’ enter Chemkin project (.ckprj) then choose ‘Next’.

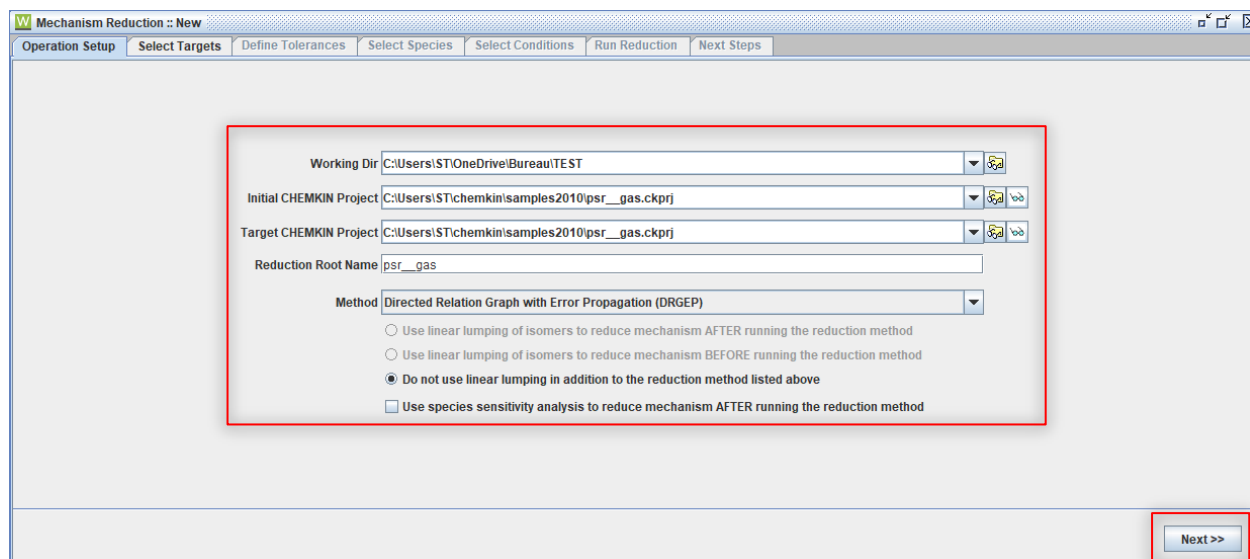


Figure A.10 Chemkin project entry

- 7) In 'Select Targets' select the target parameters which are evaluated for each produced mechanism, and used to compare the reduced mechanism to the master mechanism, then click 'Next'.
- 8) Defining tolerances allows us to control how much the reduced mechanism can differ from the master mechanism, absolute tolerances defines how much the target parameters determined from the reduced mechanism may differ from the same parameters determined from the master mechanism, relative tolerance controls how large the percent difference between target parameters in the reduced mechanism and the master mechanism can be.
 - If endpoint is selected, the comparison of target parameter values between the master mechanism and the skeletal mechanism will only be performed on the last value of the time/spatial profile if maximum is selected, the comparison will only be performed on the maximum value of the time/spatial profile By default, the comparison is performed on the entire time/spatial profile of target parameter In case of continuations being used in the model, the last value is the value from the last continuation while the maximum is the maximum in each continuation.

APPENDIX

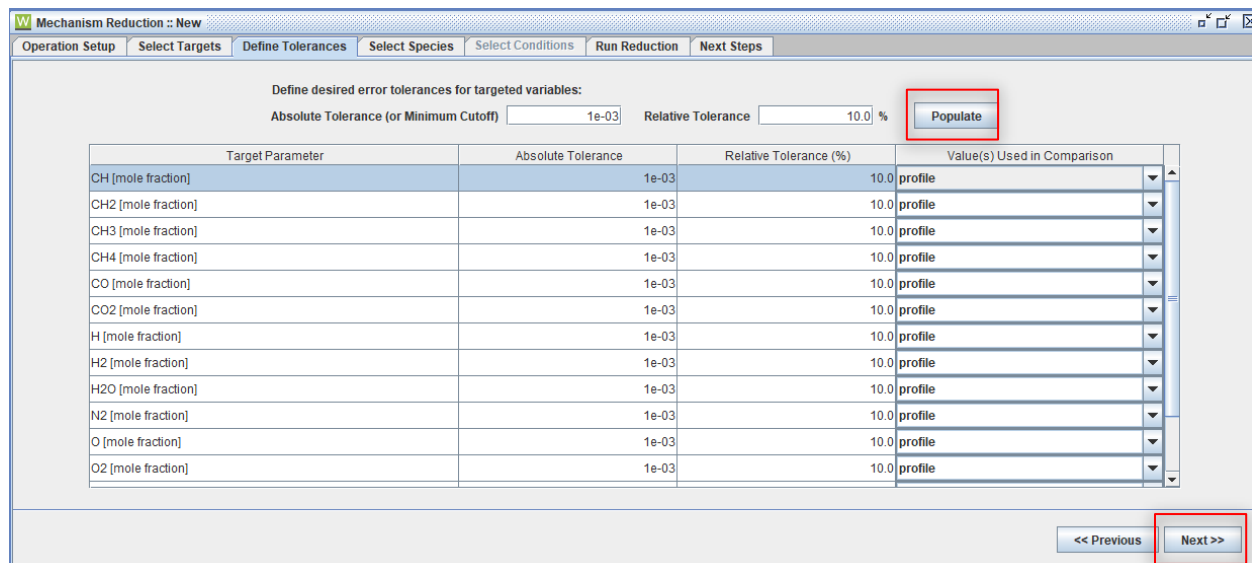


Figure A.11 Defining tolerances

- 9) Next in ‘Select Species’ we will define the species which will be conserved in the reduced mechanism;

- 10) If a parameter study is set-up, we can choose under which condition the mechanism is reduced, multiple parameters may be selected;

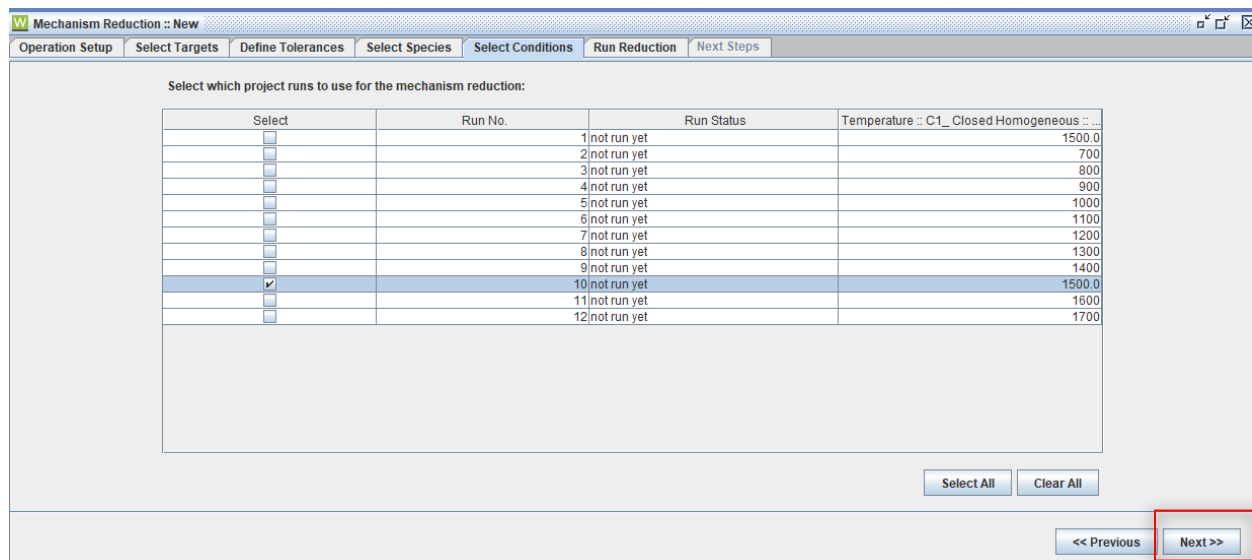


Figure A.12 Selecting conditions

11) Then we run the reduction calculation, if everything is done properly the results will be shown shortly and the software will decide the best reduced mechanism generated automatically;

Mechanism Reduction :: C:\Users\ST\OneDrive\Bureau\TEST3\TEST3_RED.ckmrt

Operation Setup | Select Targets | Define Tolerances | Select Species | Select Conditions | Run Reduction | Next Steps

Status of the mechanism reduction: (number of species in master mechanism 53)

Trial No.	Mech. Size	Target Tol.	View Results	View Project	Plot Comparison	Post-Process	
1 (drgep001)	47	2.7%	View Results	View Project	Plot Comparison	Post-Process	
2 (drgep005)	47	2.7%	View Results	View Project	Plot Comparison	Post-Process	
3 (drgep025)	42	20.4%	View Results	View Project	Plot Comparison	Post-Process	
4 (drgep045)	40	1.7%	View Results	View Project	Plot Comparison	Post-Process	
5 (drgep001)	40	1.7%	View Results	View Project	Plot Comparison	Post-Process	
6 (drgep005)	40	1.7%	View Results	View Project	Plot Comparison	Post-Process	
7 (drgep025)	39	1.7%	View Results	View Project	Plot Comparison	Post-Process	
8 (drgep045)	39	1.7%	View Results	View Project	Plot Comparison	Post-Process	
9 (drgep065)	38	1.7%	View Results	View Project	Plot Comparison	Post-Process	
✓	10 (drgep085)	37	1.7%	View Results	View Project	Plot Comparison	Post-Process
	11 (drgep105)	35	150.6%	View Results	View Project	Plot Comparison	Post-Process

Figure A.13 Running reduction

- We can also further reduce the reduced mechanism by choosing ‘Options’ then ‘Setup Next Operation’ in the ‘Run Reduction’ section;
- This is an example of a reduced GRI-3 mechanism that contains 36 elements and 201 reactions:

```

! GRI-Mech Version 3.0 7/30/99  CHEMKIN-II format
! See README30 file at anonymous FTP site unix.sri.com, directory gri;
! WorldWideWeb home page http://www.me.berkeley.edu/gri_mech/ or
! through http://www.gri.org , under 'Basic Research',
! for additional information, contacts, and disclaimer
!THERMO
! Insert GRI-Mech thermodynamics here or use in default file
!END
ELEMENTS
O H C N AR
END
SPECIES
H2 H O O2 OH
H2O HO2 H2O2 CH CH2
CH2(S) CH3 CH4 CO CO2
HCO CH2O CH2OH CH3O C2H4
C2H5 C2H6 HCCO CH2CO N
NH NNH NO NO2 N2O
HNO HCN H2CN HCNO NCO
N2 CH2CHO
END

THERMO ALL

```

Figure A.14 Resulted reduced mechanism

APPENDIX C: RESIDUALS

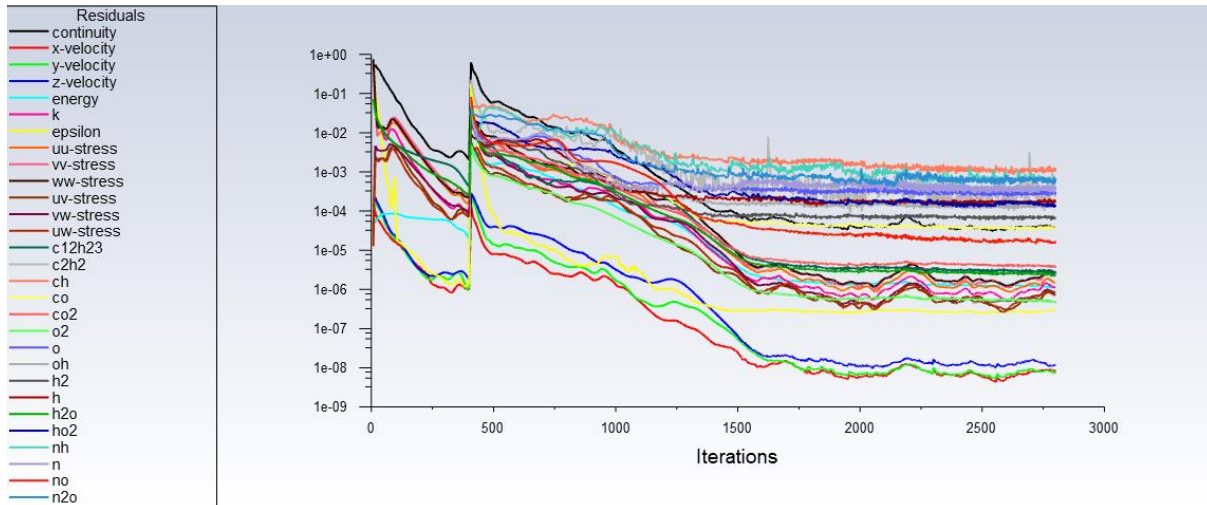


Figure B.1 Residuals-100% power settings

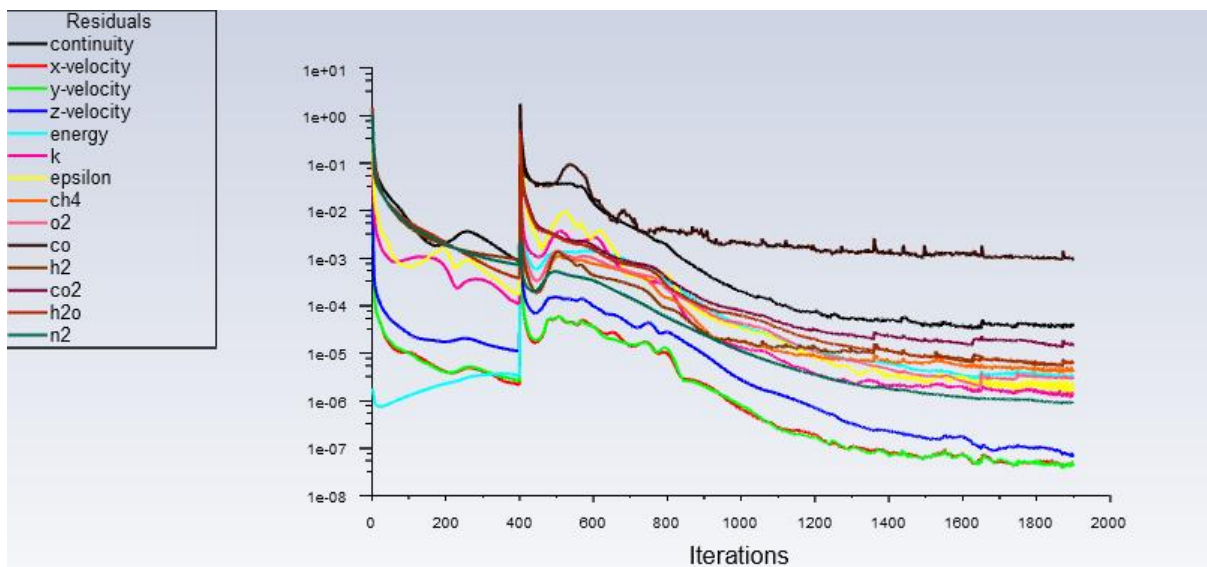


Figure B.2 Residuals – 5 % H2

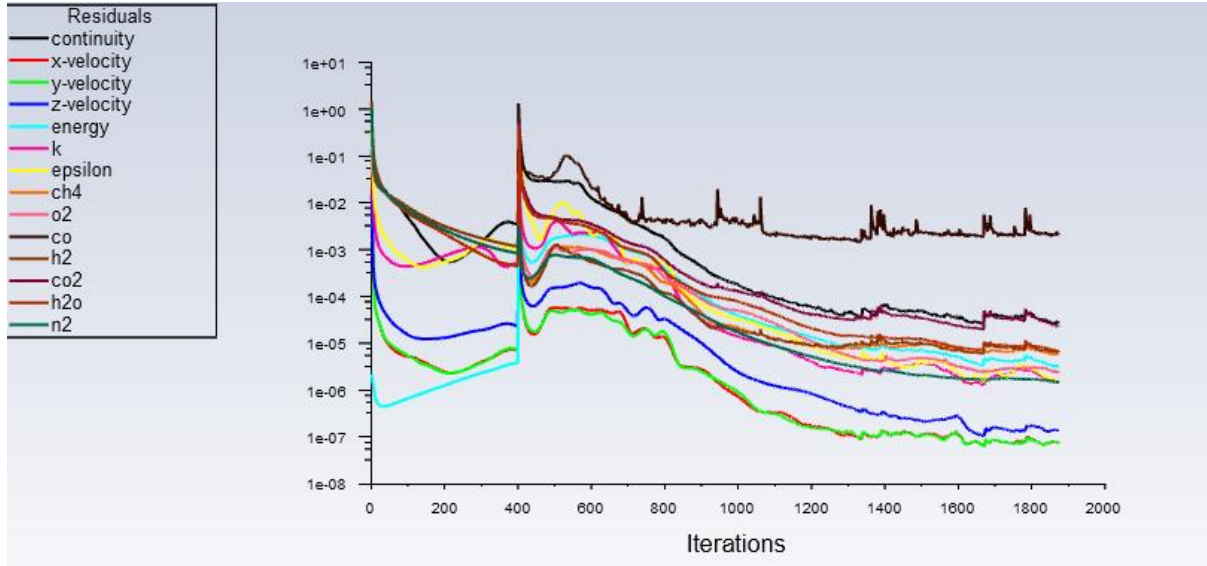


Figure B.3 Residuals – 35 % H2

APPENDIX D: ADDITIONAL CONTOUR PLOTS (C12H23)

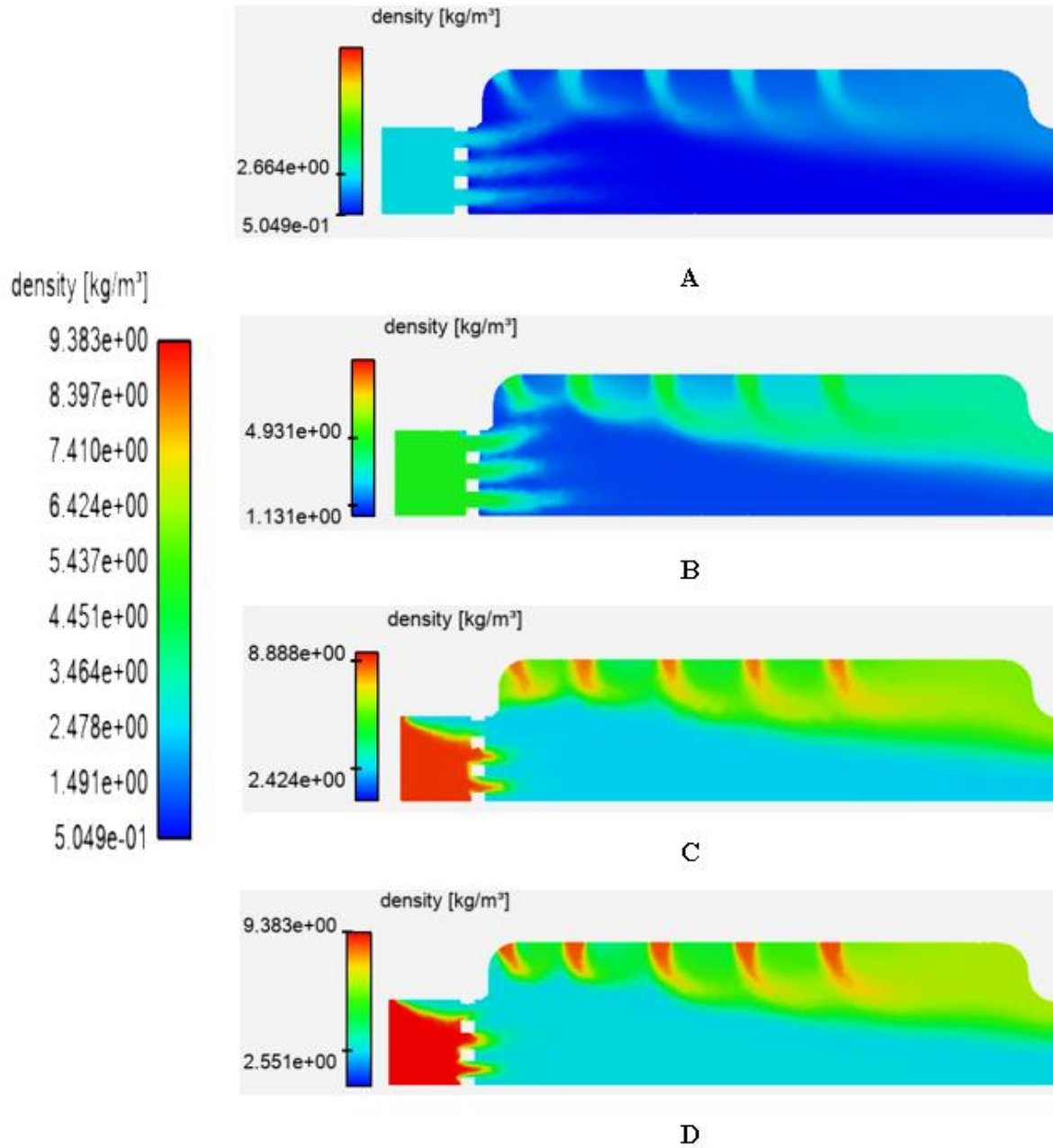


Figure C.1 Longitudinal density contour for kerosene combustion at different regimes. A: 7% power, B: 30% power, C: 85% power and D: 100% power settings.

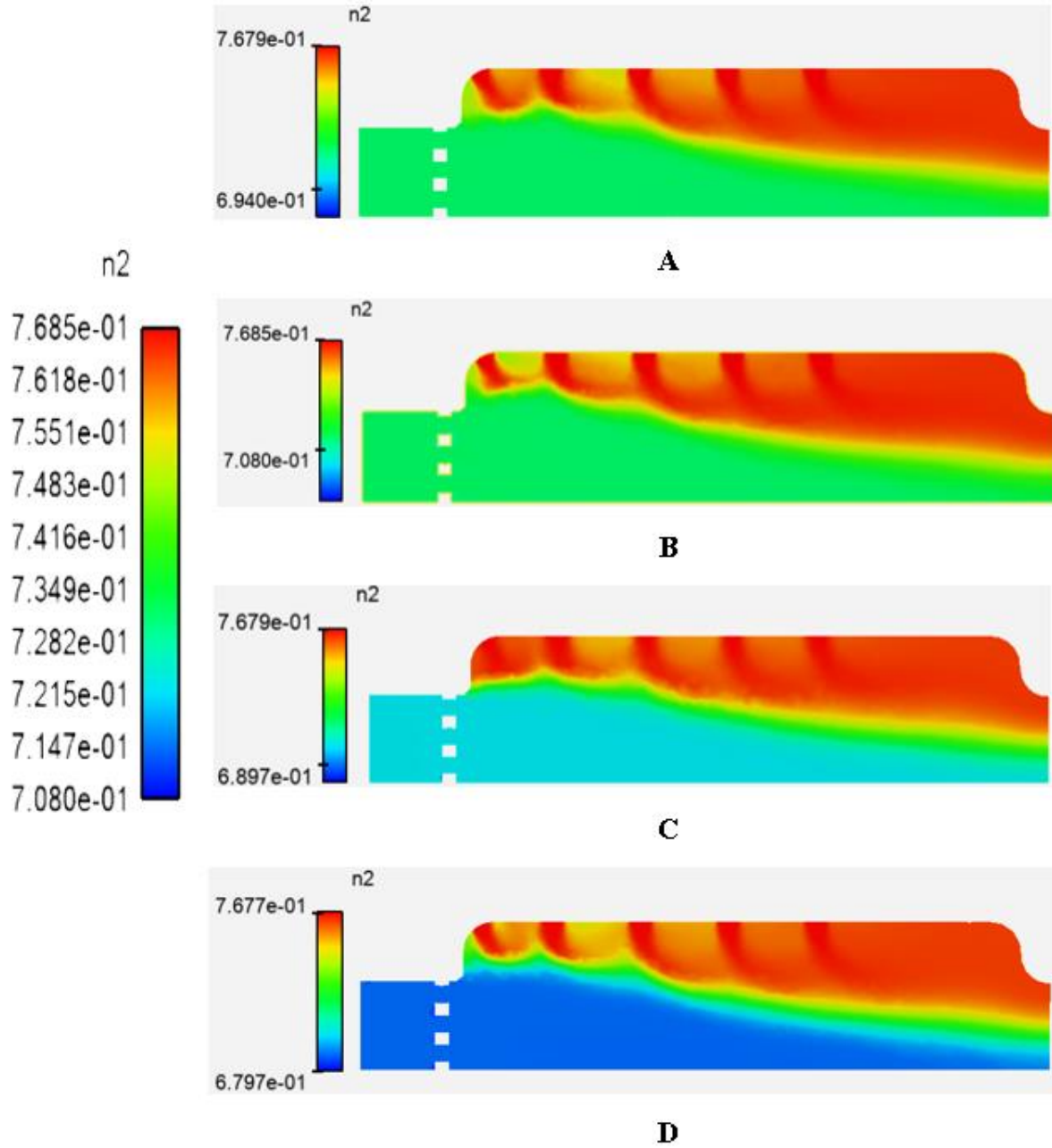


Figure C.2 Longitudinal N₂ masse fraction contour for kerosene combustion at different regimes. A: 7% power, B: 30% power, C: 85% power and D: 100% power settings.

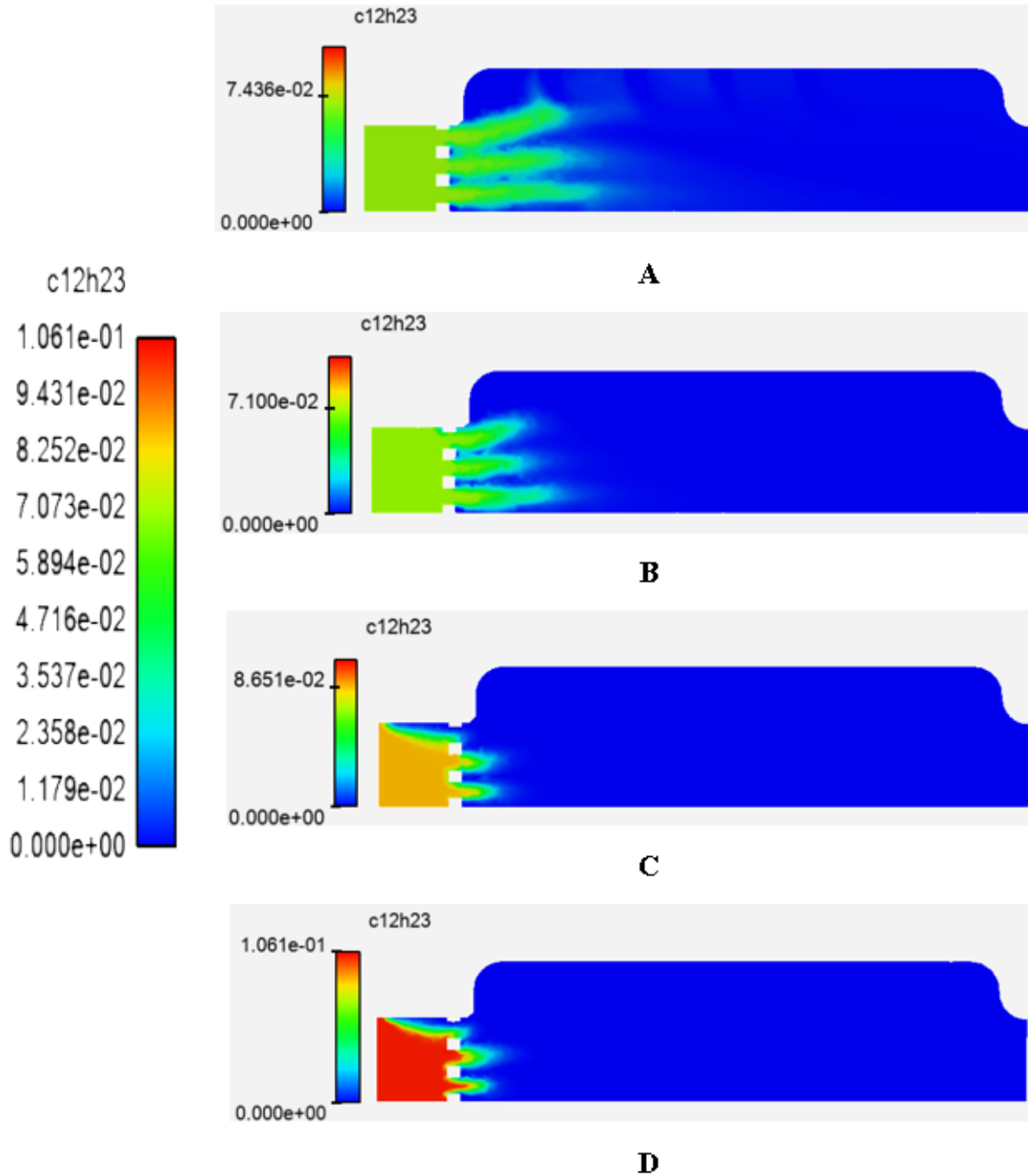


Figure C.3 Longitudinal $C_{12}H_{23}$ mass fraction contour for kerosene combustion at different regimes. A: 7% power, B: 30% power, C: 85% power and D: 100% power settings.

APPENDIX E: SOLVER CONFIGURATION

1) Chemkin mechanism import:

Import CHEMKIN Format Mechanism

Material Name
chemkin-import

Gas-Phase

Kinetics Input File
F:/ouarsou2023/mechanism/chem.che Browse...

Thermodynamic Database
 All contained in Kinetics Input File
ROGRA~1\ANSYSI~1\v221\fluent\fluent22.1.0\isat\data\thermo.db Browse...

Transport Property Data
 Import database

Import Surface Mechanism

Import Close Help

Figure D.1 Chemkin import step 1

Species Model

Model
 Off
 Species Transport
 Non-Premixed Combustion
 Premixed Combustion
 Partially Premixed Combustion
 Composition PDF Transport

Reactions
 Volumetric
 Wall Surface
 Particle Surface
 Electrochemical

Chemistry Solver
CHEMKIN-CFD Solver
Integration Parameters...

Options
 Inlet Diffusion
 Diffusion Energy Source
 Full Multicomponent Diffusion
 Thermal Diffusion

Mixture Properties
Mixture Material: chemkin-import Edit...
Import CHEMKIN Mechanism...
Number of Volumetric Species: 18

Turbulence-Chemistry Interaction
 Finite-Rate/No TCI
 Finite-Rate/Eddy-Dissipation
 Eddy-Dissipation
 Eddy-Dissipation Concept
Coal Calculator...

Options
EDC Model
 Constant Coefficients
 Partially Stirred Reactor
Flow Iterations per Chemistry Update: 1
Aggressiveness Factor: 0.5
Temperature Threshold [K]: 200
Volume Fraction Constant: 2.1377
Time Scale Constant: 0.4083
User Defined EDC Scales: none

Select Boundary Species
Select Reported Residuals

Thermodynamic Database File Name
I-1\v221\fluent\fluent22.1.0\isat\data\thermo.db Browse...

OK Apply Cancel Help

Figure D.2 Chemkin import step 2

2) Patch method:

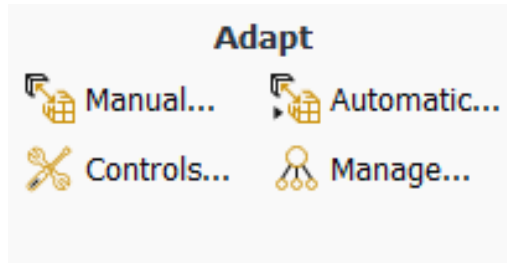


Figure D.3 Patch step 1

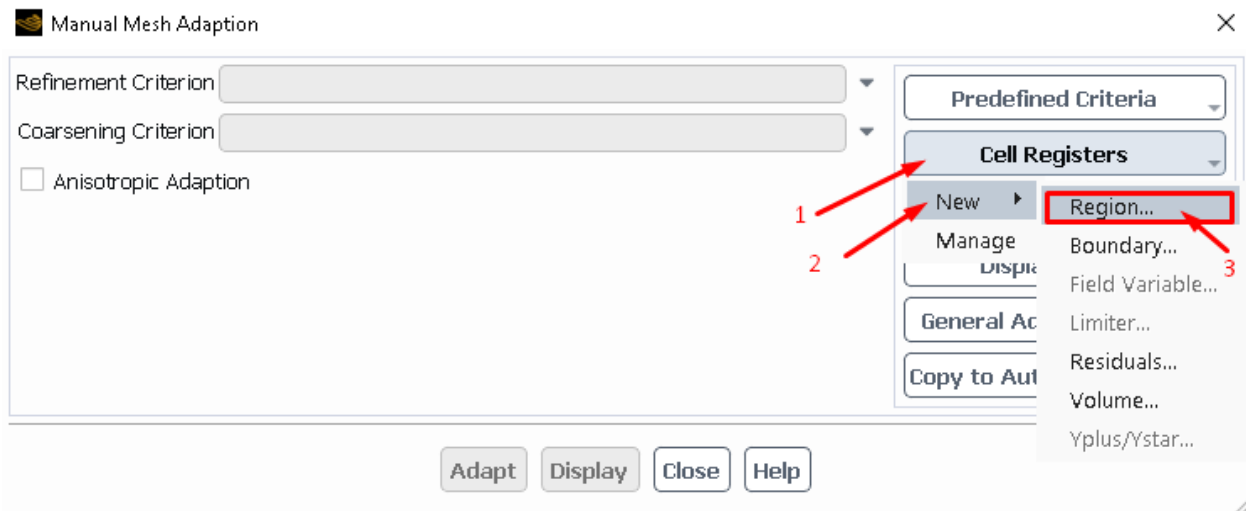


Figure D.4 Patch step 2

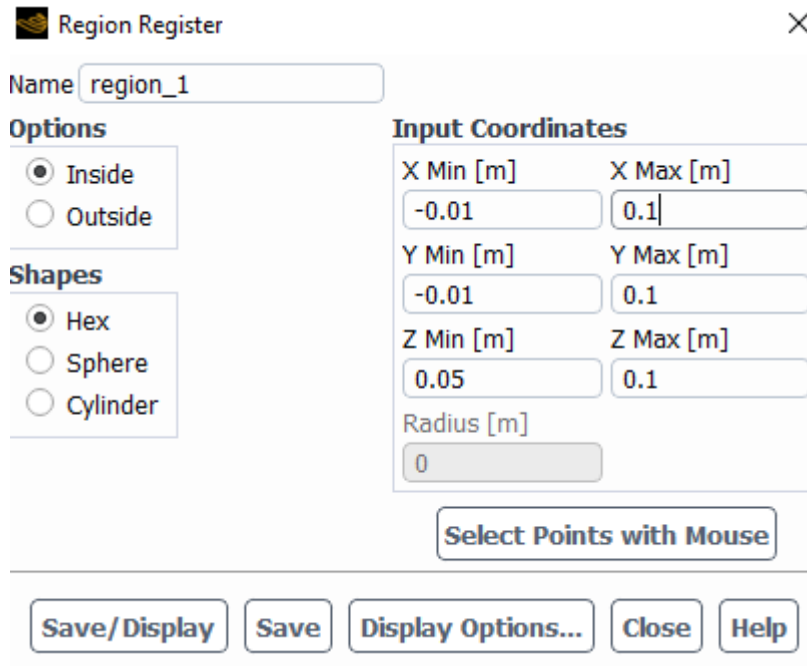


Figure D.5 Patch step 3

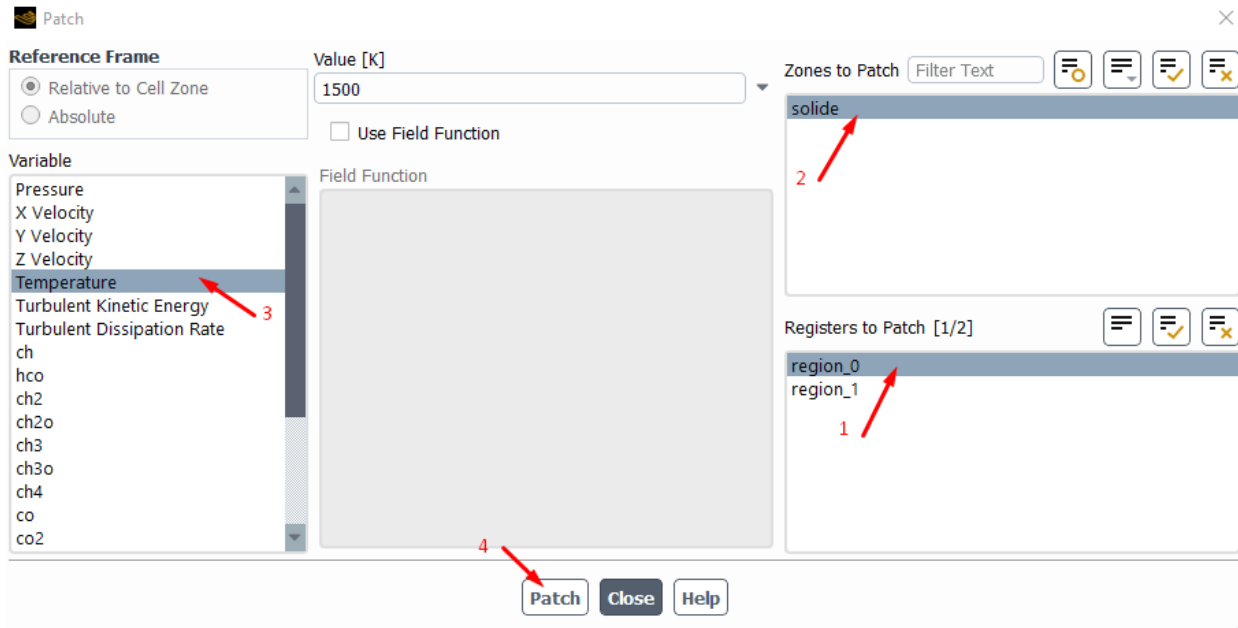


Figure D.6 Patch step 4

REFERENCES:

- [1] O. Deutschmann, A. D'Anna, A. Sarofim, and H. A. Michelsen, "Hydrogen Combustion: Fundamentals and Applications," Butterworth-Heinemann, 2012.
- [2] J. M. Ogden and S. M. Steinbugler, "The hydrogen economy," *Chem. Eng. Prog.*, vol. 99, no. 7, pp. 24–32, 2003.
- [3] C. Liu and S. Han, "Hydrogen energy: development, utilization, and sustainability," *Energy Procedia*, vol. 88, pp. 1–6, 2016.
- [4] M. J. Zelina, R. M. Luecke, and S. M. Seltzer, "CO₂ emissions from commercial aviation, 2018," *Transportation Research Part D: Transport and Environment*, vol. 81, pp. 1–13, 2020.
- [5] H. A. Dawood and A. T. A. Mohammed, "The use of methane in aircraft engines," in *Advances in Aircraft and Spacecraft Science*, InTech, 2012, pp. 1–16.
- [6] P. W. Teare and M. A. Widdowson, "Combustion characteristics of aviation kerosene and gas turbine fuels," *Combust. Sci. Technol.*, vol. 177, no. 7, pp. 1191–1220, 2005.
- [7] A. H. Lefebvre and D. G. McDonell, "The role of fuel chemistry in soot formation," *Prog. Energy Combust. Sci.*, vol. 21, no. 3, pp. 229–273, 1995.
- [8] L. Goumri-Said, M. P. Heap, and A. M. A. Mohamed, "Hydrogen addition to enhance combustion characteristics and reduce nitrogen oxides emissions in natural gas fired engines—a review," *Renewable and Sustainable Energy Reviews*, vol. 69, pp. 835–854, 2017.
- [9] M. G. Mostafa, "3D Simulation of Jet-A Combustion in a Model Aircraft Engine Combustion Chamber," *Int. J. Aero. Eng.*, vol. 2017, pp. 1–14, 2017.
- [10] A. F. Hegazy, "Combustion Fundamentals," in *Clean Combustion Technologies*, Springer, 2013, pp. 1–28.
- [11] M. J. Moran and H. N. Shapiro, "Fundamentals of Engineering Thermodynamics," Wiley, 2018.
- [12] R. Schlogl, "Fritz Haber and Carl Bosch - The Story of Two Men Who Changed the World," *Angewandte Chemie International Edition*, vol. 50, no. 48, pp. 11200–11207, 2011.
- [13] Y. Liu, C. L. Haslam, and Y. Zhang, "Numerical Simulation of Gaseous Fuel Combustion," in *Gaseous Combustion*, Springer, 2019, pp. 1–19.
- [14] A. Trounev, "Large Eddy Simulation of Turbulent Combustion," *Progress in Energy and Combustion Science*, vol. 30, no. 3, pp. 329–366, 2004.

REFERENCES

- [15] J. O. Smith and N. Peters, Introduction to Chemical Engineering Thermodynamics, 7th ed.
- [16] S. R. Turns, An Introduction to Combustion: Concepts and Applications, 3rd ed.
- [17] I. Glassman, Combustion, 3rd ed.
- [18] S. R. Turns, Thermodynamics: Concepts and Applications, Cambridge University Press, 2000.
- [19] "4 Stages of combustion in CI engine," Retrieved from <https://www.enggstudy.com/stages-of-combustion-in-ci-engine/> [Accessed: June 14, 2023].
- [20] J. M. Smith, H. C. Van Ness, and M. M. Abbott, Introduction to Chemical Engineering Thermodynamics, 7th ed.
- [21] N. J. Tro, Chemistry: A Molecular Approach, 3rd ed.
- [22] P. Atkins and J. de Paula, Physical Chemistry, 8th ed.
- [23] I. N. Levine, Physical Chemistry, 6th ed.
- [24] R. Chang, Physical Chemistry for the Biosciences.
- [25] J. G. Smith and G. J. Denton, Modern Physical Organic Chemistry, University Science Books, 2018.
- [26] "Damköhler numbers," Retrieved from https://en.wikipedia.org/wiki/Damk%C3%B6hler_numbers [Accessed: June 14, 2023].
- [27] M. A. Hossain, "Design of a High Intensity Turbulent Combustion System."
- [28] H. W. R. Dembinski, "Flow measurements using combustion image velocimetry in diesel engines," KTH Machine Design.
- [29] M. Bidabadi, H. B. Dizaji, F. F. Dizaji, and S. A. Mostafavi, "A parametric study of Icypodium dust flame."
- [30] W. L. Masterton, C. N. Hurley, and E. J. Neth, Chemistry: Principles and Reactions.
- [31] ChemSpider, Retrieved from http://www.chemspider.com/Chemical-Structure.762.html?rid=44c540f7-6470-4ac5-92f3-0d82adfa108c&page_num=0 [Accessed: June 14, 2023].
- [32] United States Environmental Protection Agency (EPA), "Drinking Water Contaminants - Standards and Regulations," Retrieved from <https://www.epa.gov/dwstandardsregulations/drinking-water-contaminants-standards-and-regulations> [Accessed: June 14, 2023].
- [33] National Institute of Standards and Technology (NIST), "Hydrogen, H₂," Retrieved from <https://webbook.nist.gov/cgi/cbook.cgi?ID=C1333740> [Accessed: June 14, 2023].

REFERENCES

- [34] Periodic Table, s.v. Hydrogen – Thermal Conductivity, Retrieved from <https://www.periodic-table.org/Hydrogen-thermal-conductivity/> [Accessed: June 14, 2023].
- [35] Convertunits, "Molecular weight of Methane," Retrieved from <https://www.convertunits.com/molarmass/Methane> [Accessed: June 14, 2023].
- [36] Material Properties, "Methane – Density – Heat Capacity – Thermal Conductivity," Retrieved from <https://material-properties.org/methane-density-heat-capacity-thermal-conductivity/> [Accessed: June 14, 2023].
- [37] National Center for Biotechnology Information (NCBI), "Kerosene," Retrieved from <https://pubchem.ncbi.nlm.nih.gov/compound/Kerosene> [Accessed: June 14, 2023].
- [38] SAE International, "Aerospace Recommended Practice ARP866A - Conversion Factors and Tables, Properties of Aircraft Fuels," Retrieved from <https://www.sae.org/standards/content/arp866a/> [Accessed: June 14, 2023].
- [39] International Labour Organization, "Kerosene," Retrieved from https://www.ilo.org/dyn/icsc/showcard.display?p_lang=en&p_card_id=0663&p_version=2 [Accessed: June 14, 2023].
- [40] Wikipedia, "Kerosene," Retrieved from <https://en.wikipedia.org/wiki/Kerosene> [Accessed: June 14, 2023].
- [41] National Institute for Occupational Safety and Health (NIOSH), "NIOSH Pocket Guide to Chemical Hazards - Kerosene," Retrieved from <https://www.cdc.gov/niosh/npg/npgd0368.html> [Accessed: June 14, 2023].
- [42] U.S. Environmental Protection Agency (EPA), "AP-42, Compilation of Air Pollutant Emission Factors - Chapter 1: External Combustion Sources."
- [43] T.-S. Wang, "Thermophysics Characterization of Kerosene Combustion," Journal of Thermophysics and Heat Transfer, vol. 15, no. 2, pp. 140-147, 2001.
- [44] University of California, Davis (UC Davis), "Heat of Vaporization," Retrieved from [https://chem.libretexts.org/Courses/University_of_California_Davis/UCD_Chem_124A%3AKauzlarich/Winter_2014_\(Kauzlarich\)/Lab_Workbook/Experiment_1%3ACalorimetry/2.Heat_of_Vaporization](https://chem.libretexts.org/Courses/University_of_California_Davis/UCD_Chem_124A%3AKauzlarich/Winter_2014_(Kauzlarich)/Lab_Workbook/Experiment_1%3ACalorimetry/2.Heat_of_Vaporization) [Accessed: June 14, 2023].
- [45] Engineering Toolbox, "Specific Heat Capacity of Kerosene."
- [46] Engineering Toolbox, "Thermal Conductivity of Liquids."
- [47] SES Hydrogen, "H2 Safety #1: Understanding hydrogen. Physical and chemical properties of the fuel of the future - Ses Hydrogen," Retrieved from <https://seshydrogen.com/en/safety-of-hydrogen->

REFERENCES

- [systems/#:~:text=The%20standard%20auto%2Dignition%20temperature,compared%20to%20long%20molecule%20hydrocarbons](#) [Accessed: June 14, 2023].
- [48] United States Environmental Protection Agency (EPA), Health & Environmental Research Online (HERO), Retrieved from https://hero.epa.gov/hero/index.cfm/reference/details/reference_id/6087635#:~:text=It%20appears%20that%20the%20normally,lie%20below%20600%C2%B0C [Accessed: June 14, 2023].
- [49] R. Amirante, E. Distaso, P. Tamburrano, and R. Reitz, "Laminar flame speed correlations for methane, ethane, propane and their mixtures, and natural gas and gasoline for peak-ignition engine simulations."
- [50] A. Mariani, B. Morrone, and A. Unich, "A Review of Hydrogen-Hydrogen-Natural Gas Blend Fuels in Internal Combustion Engines."
- [51] National Institute of Standards and Technology (NIST), "Methane," Retrieved from <https://webbook.nist.gov/cgi/cbook.cgi?ID=C74828> [Accessed: June 14, 2023].
- [52] National Institute of Standards and Technology (NIST), "Hydrogen, H₂," Retrieved from <https://webbook.nist.gov/cgi/cbook.cgi?ID=C1333740> [Accessed: June 14, 2023].
- [53] A. E. Azzouz and L. Aliouat, "Simulation de la combustion turbulente dans une chambre de combustion tubulaire pour le mélange kérosène/air et méthane/air," Blida Saad Dahleb University, 2022.
- [54] Chemtalk, "Enthalpy of Reaction, Formation, and Combustion."
- [55] M. Yu, K. Zheng, L. Zheng, T. Chu, and P. Guo, "Effects of hydrogen addition on propagation characteristics of premixed methane/air flames."
- [56] P. Xiao, H. Wu, Z. Wang, S. Zhang, C.-F. Lee, Z. Wang, and F. Liu, "Experimental and kinetic investigation on the effects of hydrogen additive on laminar premixed methanol–air flames," *International Journal of Hydrogen Energy*.
- [57] Q. Li, G. Hu, S. Liao, Q. Cheng, C. Zhang, and C. Yuan, "Kinetic Effects of Hydrogen Addition on the Thermal Characteristics of Methane–Air Premixed Flames," *Energy and Fuel*.
- [58] C. Mandilas, M. P. Ormsby, C. G. W. Sheppard, and R. Woolley, "Effects of hydrogen addition on laminar and turbulent premixed methane and iso-octane–air flames," *Proceedings of the Combustion Institute*.
- [59] Y. Wang, X. Zhang, and Y. Li, "Hydrogen-air premixed combustion in turbulence," *International Journal of Hydrogen Energy*.
- [60] S. Ouchene, N. Ghandour, "Simulation Numérique D'écoulements Hypersoniques en Hors-equilibre Thermochimique Derrière Une Onde de Choc Intense", 2015.

REFERENCES

- [61] M. G. Mostafa, "3D Simulation Of Jet-A Combustion In A Model Aircraft Engine Combustion Chamber," North Carolina Agricultural and Technical State University, 2012.
- [62] D. D. Toporov, "Combustion of Pulverised Coal in a Mixture of Oxygen and Recycled Flue Gas."
- [63] University of Washington, "12.4 Standard, RNG, and Realizable k-epsilon Models Theory," 2006.
- [64] N. Fatchurrohman and S. T. Chia, "Performance of hybrid nano-micro reinforced mg metal matrix composites brake calliper: simulation approach," IOP Conference Series: Materials Science and Engineering.
- [65] A. Abou-Taouk et al., "Four-step global reaction mechanism for CFD simulations of flexi-fuel burners for gas turbines."
- [66] B. Lewis and G. von Elbe, "Combustion, Flames, and Explosions of Gases."
- [67] J. Warnatz, U. Maas, and R. W. Dibble, "Combustion: Physical and Chemical Fundamentals, Modeling and Simulation, Experiments, Pollutant Formation."
- [68] "A study on the effects of air preheat on the combustion and heat transfer characteristics of Bunsen flames" by Zhang, et al. (2017)
- [69] B. Zouhri, "Large Scale Hydrogen Production," Hydrogen Energy, 2019.
- [70] "What's The Difference Between FEM, FDM, and FVM?," MachineDesign, 2016. [Online]. Available: <https://www.machinedesign.com/3d-printing-cad/fea-and-simulation/article/21832072/whats-the-difference-between-fem-fdm-and-fvm>. [Accessed: June 25, 2023].